Technische Universität München
TUM School of Medicine and Health

Hemodynamic-vascular influences on blood-oxygenation-level-dependent functional connectivity (BOLD-FC) in resting-state functional Magnetic Resonance Imaging (rs-fMRI)

Sebastian Constantin Schneider

Vollständiger Abdruck der von der TUM School of Medicine and Health der Technischen Universität München zur Erlangung eines

Doctor of Philosophy (Ph.D.)

genehmigten Dissertation.

Vorsitz: Prof. Dr. Susanne Kossatz

Betreuer*in: Priv.-Doz. Dr. Christian Sorg

Prüfer*innen der Dissertation:

1. Prof. Dr. Christine Preibisch
2. Prof. Dr. Simon Jacob

Die Dissertation wurde am 12.10.2023 bei der TUM School of Medicine and Health der Technischen Universität München eingereicht und durch die TUM School of Medicine and Health am 09.01.2024 angenommen.

Abstract

While resting-state blood-oxygenation-level-dependent functional connectivity (BOLD-FC), has been a widely used method to measure organization and functioning of neural activity, non-neural influences on the BOLD signal and its derived measures have increasingly been recognized in the past years. As these potentially confound the proposed proxy function of BOLD-FC measures for synchronized neural activity, the influence of some distinct hemodynamic-vascular parameters has been studied before. However, it is still poorly understood how these parameters influence BOLD-FC both mechanistically and to which extent, when compared among each other. I therefore thoroughly analyzed multi-parametric MRI data from a human fMRI study, combined with a simulation study of BOLD-FC, to examine the relative influence of different hemodynamic-vascular parameters on BOLD-FC and provide potential causal explanations for underlying mechanisms of BOLD-FC impairments.

The study sample comprised 28 patients with asymptomatic internal carotid artery stenosis (ICAS), and 27 age-matched healthy controls (total sample size = 55). Patients with asymptomatic ICAS have a largely preserved neuronal functioning, but suffer from impaired hemodynamic-vascular processes due the stenosis. I investigated the influence of several distinct local and systemic hemodynamic-vascular parameters on BOLD-FC. In detail, the local hemodynamic-vascular parameters capillary transit time heterogeneity (CTH) and cerebral blood volume (CBV) were derived from dynamic susceptibility contrast (DSC) MRI, and cerebral blood flow (CBF) from pseudo-continuous arterial spin labeling (pCASL). Systemic hemodynamic-vascular parameters time-to-peak (TTP) and BOLD lag were derived from DSC and rs-functional MRI, respectively.

For Project 1, I focused on examining the impact of local hemodynamic-vascular alterations on BOLD-FC and its potential mechanisms. We specifically hypothesized CTH to constitute a promising parameter, matching local blood flow temporal response characteristics previously found to impact simulated BOLD-FC. I, therefore, analyzed how BOLD-FC between homotopic VOIs is affected by differences in CTH, CBF and relative CBV (rCBV). In addition, we investigated the impact of locally delayed blood flow response on BOLD-FC with simulations. I found that increasing differences in CTH, but also CBF, lead to reduced homotopic BOLD-FC – with a more pronounced effect for ICAS patients. This was in-line with the simulation results, which also showed reduced BOLD-FC with an increasing unilaterally delayed blood flow response.

For Project 2, I compared the relative of influence of local, CTH, CBF and rCBV, hemodynamic-vascular parameters to the influence of systemic, TTP and BOLD lag, parameters on homotopic BOLD-FC. To this end, I constructed three different, but nested, linear-mixed model (LMM) regression models, considering firstly only the participants' BOLD-FC averages, secondly, I added the local parameters, and thirdly, I constructed a model comprising both local and system parameters as well as the BOLD-FC averages. Based on this, I found that systemic parameters exert an about two-times lager influence on BOLD-FC as compared to the local parameters. Thereby, the total variation in BOLD-FC explained with the full model was 40.7%, with hemodynamic-vascular parameters accounting for about 20%.

For Project 3, I extended the analysis beyond the homotopic BOLD-FC examined for Projects 1 and 2, namely heterotopic (between non-homotopic areas on different hemispheres) and intrahemispheric (between areas on the same hemisphere) BOLD-FC. I did so by introducing three types of connectivities (FC-types) in the regression analysis, which allowed to identify changes in mean BOLD-FC and slopes for non-homotopic BOLD-FC. I found that ICAS patients had lower average homotopic BOLD-FC as compared to the healthy controls, but showed largely identical heterotopic and intrahemispheric BOLD-FC. Furthermore, both local and systemic parameters had significantly less influence on heterotopic and intrahemispheric BOLD-FC as compared to homotopic BOLD-FC.

Overall, I could show that firstly, local hemodynamic-vascular parameters, in particular aspects of local blood flow timing, have a complex and partially non-linear influence on BOLD-FC, leading to FC reductions, which is in line with simulation results. Secondly, especially systemic parameters associated with delayed blood arrival have a stronger influence on BOLD-FC, as compared to the local parameters. Lastly, especially homotopic BOLD-FC is particularly vulnerable to hemodynamic-vascular differences between brain regions, as compared to heterotopic and intrahemispheric BOLD-FC. Conclusively, my thesis provides further evidence that the canonical interpretation of BOLD-FC as a proxy measure for synchronized neural activity does not hold in all circumstances and especially not in patient cohorts with suspected hemodynamic-vascular disorders.

Zusammenfassung

Die Analyse von funktioneller Konnektivität im Ruhezustand auf Grundlage von MRT Signalen, die von der Blutsauerstoffsättigung beeinflusst werden (blood-oxygenation-level-dependent functional connectivity, BOLD-FC) ist eine weit verbreitete Methode, um auf die Organisation und Funktion neuronaler Aktivität zurück zu schließen. Dabei wird das BOLD Signal als Marker für die, durch Magnetresonanztomographie (MRT) nicht direkt erfassbare, neuronale Aktivität verwendet. Ermöglicht wird dies durch den Prozess der neurovaskulären Kopplung (neurovascular coupling, NVC), welcher die Sauerstoffversorgung des Gehirns durch Anpassung des Blutflusses an die unterliegende neuronale Aktivität reguliert. Jedoch wurde in den vergangenen Jahren zunehmend erkannt, dass auch nicht-neuronale Einflüsse auf diese Blutsauerstoffsättigung einwirken und somit das abgeleitete Signal beeinflussen. Damit schwächen diese Einflüsse auch die Annahme, dass korrelierte Fluktuationen des BOLD Signals, d.h. die funktionelle Konnektivität, als Stellvertreter für synchronisierte neuronale Aktivität verwendet werden können. Deswegen wurden die Auswirkungen einzelner nicht-neuronaler hämodynamisch-vaskulärer Einflüsse auf die funktionelle Konnektivität bereits untersucht. Jedoch ist nach wie vor unzureichend verstanden, wie und in welchem Ausmaß diese Parameter funktionelle Konnektivität im Vergleich zueinander beeinflussen. Um diese Aspekte zu untersuchen, habe ich eine ausführliche Analyse multi-parametrischer MRT Daten durchgeführt, welche mit einer Simulationsstudie kombiniert wurde. Dabei hatte ich das Ziel, die relativen Einflüsse verschiedener hämodynamisch-vaskulärer Parameter auf die MRT-basierte funktionelle Konnektivität zu untersuchen und mögliche kausale Erklärungen für veränderte funktioneller Konnektivität zu finden.

Die Studienstichprobe umfasste 28 Patienten mit einer asymptomatischen Stenose der internen Karotisarterie (internal carotid artery stenosis, ICAS) und 27 gesunde Kontrollteilnehmer des gleichen Alters (Gesamtstichprobe = 55 Personen). Als Folge der Stenose weisen ICAS-Patienten Beeinträchtigungen bei bestimmten zerebralen hämodynamisch-vaskulären Prozessen auf; Beeinträchtigungen neuronaler Prozesse sind jedoch nicht vorhanden. Die für diese Arbeit untersuchten lokalen hämodynamisch-vaskulären Parametern umfassten dabei zum einen die Heterogenität der kapillaren Transitzeiten roter Blutkörperchen (capillary transit time heterogeneity, CTH) und das zerebrale Blutvolumen (cerebral blood volume, CBV), welche durch Kontrastmittelbildgebung gewonnen wurden (dynamic susceptibility contrast, DSC). Als weiterer lokaler Parameter wurde zudem auch der zerebrale Blutfluss (cerebral blood flow, CBF) verwendet,

welcher durch magnetische Markierung des Blutwassers als intrinsischem Tracer gewonnen wurde (pseudo-continuous arterial spin labeling , pCASL). Als systemischer Parameter wurde die Zeit bis zur Ankunft der maximalen Konzentration des Kontrastmittels (time-to-peak, TTP) und die zeitliche Verzögerung des BOLD Signal (BOLD lag) verwendet, welche aus der DSC MRT und dem funktionellen MRT im Ruhezustand gewonnen wurden.

Für mein erstes Projekt untersuchte ich die Auswirkungen lokaler hämodynamisch-vaskulärer Veränderungen auf die funktionelle Konnektivität, sowie deren potentielle Mechanismen. Angestoßen wurde diese Untersuchung durch vorherige Simulationsergebnisse, welche negative Auswirkungen von Verzögerungen im lokalen Blutfluss auf die funktionelle Konnektivität fanden. Aufgrund theoretischer Überlegungen nahmen wir an, dass der Parameter CTH als Proxy für die zuvor simulierte zeitliche Verzögerung und Verbreiterung in der Antwort des lokalen Blutflusses auf die neuronale Aktivität verwendet werden kann. Gegenstand der Untersuchung war deswegen, inwiefern die BOLD-FC zwischen homotopen Gehirnregionen durch Differenzen in CTH, CBF und des relativen CBV (rCBV) beeinflusst wird. Zusätzlich ergänzten wir meine empirische Untersuchung mit Simulationen, welche den Einfluss von Verzögerungen in der zeitlichen Reaktion des lokalen Blutflusses auf funktionelle Konnektivität nochmals genauer beleuchteten. Dabei konnte ich zeigen, dass zunehmende Seitenunterschiede sowohl in CTH als auch in CBF zu zunehmend verringerter funktioneller Konnektivität führten, wobei ICAS-Patienten stärker davon betroffen waren als gesunde Kontrollpersonen. Dies stimmte mit den Simulationsergebnissen überein, welche ebenfalls eine reduzierte funktionelle Konnektivität mit zunehmender verzögerter einseitiger Blutflussreaktion zeigten.

Für mein zweites Projekt verglich ich die relativen Einflüsse der zuvor verwendeten lokalen Parameter, CTH, CBF und rCBV, mit denen der systemischen Parameter, TTP und BOLD lag, auf die mittels BOLD Signalen gemessene funktionelle Konnektivität. Dafür verglich ich drei gestaffelte Regressionsmodelle im Hinblick auf ihre Eignung Varianz in den Daten zu erklären (linear-mixed model, LMM). Dabei umfasste das erste Modell lediglich Alter und Gruppenzugehörigkeit der Probanden, das zweite enthielt zusätzlich die lokalen hämodynamisch-vaskulären Parameter und das dritte darüber hinaus die systemischen Parameter. Dabei stellte sich heraus, dass der Einfluss der systemischen Parameter auf die BOLD-FC ungefähr doppelt so groß ist wie der Einfluss der lokalen Parameter. Insgesamt konnte das vollständige Modell 40,7 % der gesamten BOLD-FC-Varianz aufklären, wobei ungefähr 20 % durch hämodynamisch-vaskuläre Parameter erklärt werden konnte.

Für mein drittes Projekt erweiterte ich meine Analyse über die zuvor verwendete homotope funktionelle Konnektivität hinaus, und zwar sowohl auf die heterotope (zwischen nicht-homotopen Regionen auf verschiedenen Hemisphären) als auch die intrahemisphärische (zwischen Regionen auf der gleichen Hemisphäre) funktionelle Konnektivität. Dafür führte ich einen weiteren Faktor in das Regressionsmodel ein, welcher die drei verschiedenen Konnektivitätstypen umfasste. Dabei stelle ich fest, dass ICAS-Patienten, verglichen mit den gesunden Kontrollen, zwar durchschnittlich eine verringerte homotope BOLD-FC aufwiesen, jedoch keine Unterschiede für heterotope und intrahemisphärische funktionelle Konnektivität zeigten. Darüber hinaus wiesen, verglichen mit homotoper funktioneller Konnektivität, sowohl lokale als auch systemische hämodynamisch-vaskuläre Parameter einen signifikant geringeren Einfluss auf heterotope und intrahemisphärische funktionelle Konnektivität auf.

Insgesamt konnte ich zeigen, dass erstens, lokale hämodynamisch-vaskuläre Parameter, speziell zeitliche Aspekte des lokalen Blutflusses, einen komplexen und nicht-linearen Einfluss auf funktionelle Konnektivität ausüben, was im Einklang steht mit dezidierten Simulationsergebnissen. Zweitens, konnte ich feststellen, dass insbesondere systemische hämodynamisch-vaskuläre Parameter, die mit einem verzögerten Eintreffen des Blutes assoziiert sind, im Vergleich zu lokalen Parametern einen stärkeren Einfluss auf die funktionelle Konnektivität haben. Schließlich konnte ich belegen, dass speziell die homotope funktionelle Konnektivität, im Vergleich zu heterotoper und intrahemisphärischer funktioneller Konnektivität, anfällig ist für regionale hämodynamisch-vaskuläre Unterschiede.

Zusammenfassend bietet meine Arbeit weitere Evidenz dafür, dass die kanonische Interpretation von funktioneller Konnektivität als Maß für synchronisierte neuronale Aktivität nicht unter allen Umständen hält, insbesondere nicht in Patientengruppen mit vermuteten hämodynamisch-vaskulären Beeinträchtigungen.

Table of Contents

List of Tables

List of Figures

Abbreviations

ASL – arterial spin labeling

BOLD – blood oxygenation level dependent

BOLD-FC – BOLD-functional connectivity

BOLD-TC – BOLD signal time course

CBF – cerebral blood flow

CBV – cerebral blood volume

$CMRO_2$ – cerebral metabolic rate of oxygen

CTH – capillary transit time heterogeneity

DSC – dynamic susceptibility contrast

fMRI – functional magnetic resonance imaging

ICAS – internal carotid artery stenosis

LMM – linear-mixed model

MRI – magnetic resonance imaging

pCASL – pseudo-continuous ASL

rCBV – relative cerebral blood volume

rs-fMRI – resting state fMRI

SSS – superior sagittal sinus

TTP – time to peak

VOI – volume of interest

δS_{BOLD} – percentage peak-to-peak BOLD amplitude

1. Introduction

1.1 Resting-state functional Magnetic Resonance Imaging (rs-fMRI) in Systems Neuroscience

The concept of resting-state functional Magnetic Resonance Imaging (rs-fMRI) was first introduced in a seminal paper by Bharat Biswal and colleagues in 1995 (Biswal et al., 1995). Participants in that study underwent blood oxygenation level sensitive echo-planar imaging (EPI) scans while once performing both a motor-task, tapping their fingers, and once in a "resting-state", i.e., with the instruction to not consciously perform any motor-, cognitive- or language task (basically to rest and not fall asleep). In their analysis, Biswal and colleagues then selected brain regions active during the motor-task and, after low-pass (< 0.08Hz) filtering them, correlated their time courses obtained during rest with the time-courses of all other brain regions. As a result, they could show that the same regions exhibiting elevated co-activity during the motor-task, e.g., primary motor areas, also expressed correlated EPI time-courses during the resting-state. They concluded that these correlations between anatomically separated but functionally related brain regions are in line with the concept of functional connectivity (FC), defined as "as the temporal correlation of a neurophysiological index measured in different brain areas" (Biswal et al., 1995; Friston et al., 1993), and that "the low frequency fluctuation[s] of blood flow and oxygenation" (Biswal et al., 1995) therefore contain meaningful neurophysiological information (Biswal et al., 1995). This was a major breakthrough in the field of fMRI, which then solely relied on meticulously planned and conducted task-based scans and experiments to obtain such neurophysiological information in humans.

The fundamental practice of rs-fMRI, consisting of a) obtaining fMRI images from participants at rest, i.e., lying quietly in the scanner with no task, b) selecting a brain region- or volume-of-interest (ROI/VOI), c) extracting its low frequency fluctuations and then d) obtaining correlations with other brain regions, i.e., calculating FC, has been a major tool of Systems Neuroscience ever since, as evident by the ever increasing use in both animal and human research (see **Fig. 1**).

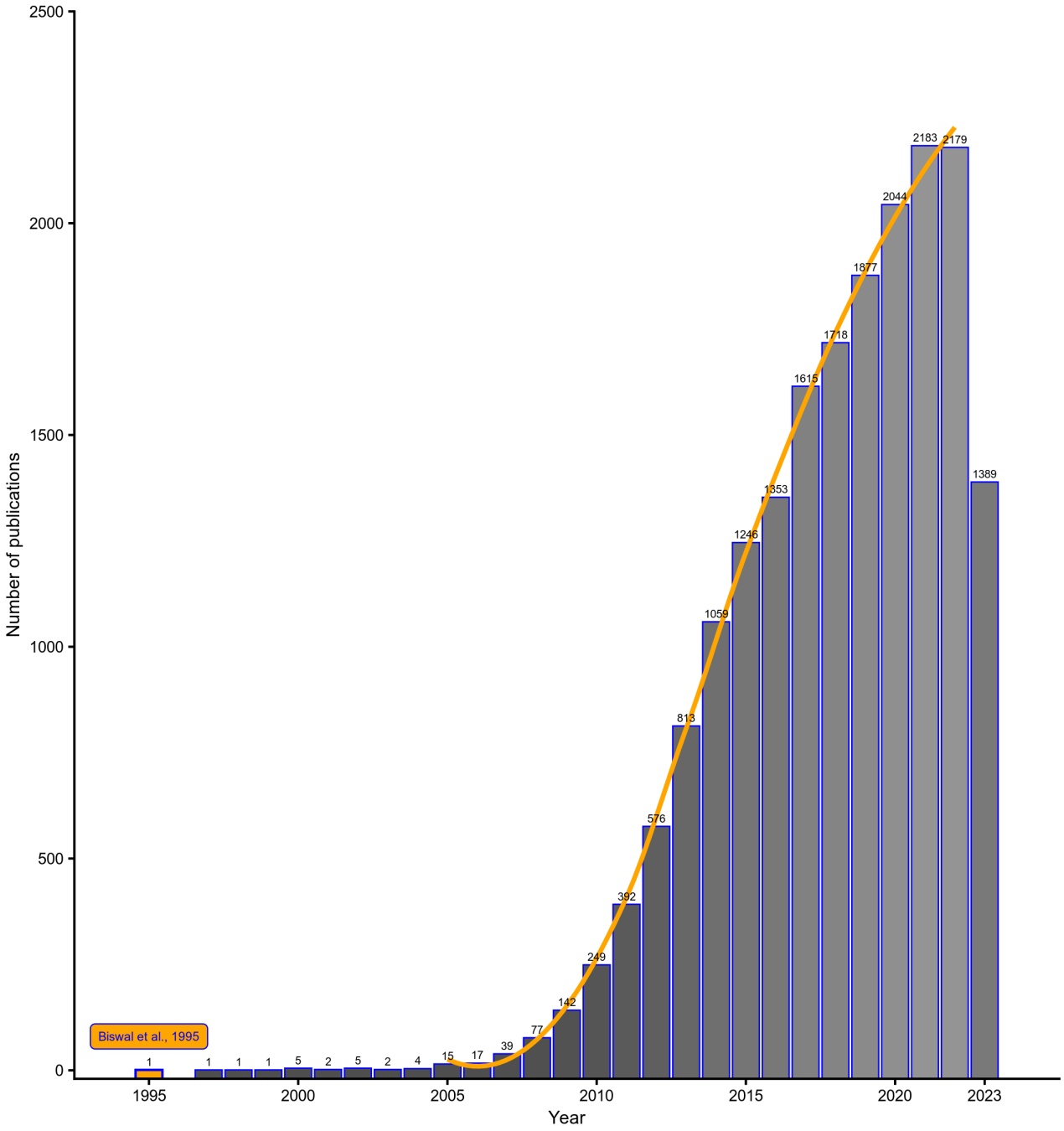

Figure 1. Yearly publications regarding resting-state functional connectivity.

Results were obtained with PubMed using the search term "resting state functional connectivity fMRI". One entry from 1993 was excluded for this figure, as it was wrongfully labeled, i.e. not containing research related to rs-fMRI or FC. The seminal rs-fMRI paper by Biswal and colleagues from 1995 is highlighted in orange. From the year 2005 on a steady increase in publications per year can be observed, which plateaus after the year 2020.

While the basic methodology as first described by Biswal and colleagues (Biswal et al., 1995) and built the fundament of rs-fMRI studies, numerous methodological advances and analysis techniques have since been implemented. For one, methodological advances have been made in

the area of image acquisition. While the initial studies had to rely on a restricted number of slices, poor spatial and temporal resolution, much research has now lead to largely increased spatial (J. Goense et al., 2016) and temporal resolution (Preibisch et al., 2015; Risk et al., 2021), leading to a more accurate recording of the ongoing neurophysiological information. However, the most important improvements concerned the preprocessing of acquired images. While the initial study of Biswal and colleagues (Biswal et al., 1995) merely performed low-pass filtering, rs-fMRI data preprocessing now contains a litany of procedures, such as correcting for head motion, slice-acquisition-time differences, correcting for physiological parameters, band-pass filtering, smoothing, normalization to a common template and much more (Esteban et al., 2019; Weissenbacher et al., 2009). Furthermore, analysis techniques for rs-fMRI data made advances, spawning new possibilities such as analyzing the spectral components of regional time courses or applying independent component analysis (ICA) to rs-fMRI datasets, instead of ROI-based FC estimates (H. Lv et al., 2018; Power et al., 2014).

One of the most notable and impactful findings using rs-fMRI however was the discovery that intrinsic brain activity at rest can be organized in different, independent networks, the so called resting-state networks (RSN)(Fox et al., 2005; Fox & Raichle, 2007; M. D. Greicius et al., 2003; Raichle et al., 2001). These networks comprise anatomically separated regions, which, however, are functionally connected, as shown by their co-activation not only during specific tasks or activities, but also during spontaneous fluctuations at rest. Depending on the specific parcellation, these RSNs can be broadly categorized into primary sensory and motor networks, task-active networks related to cognitive or emotional processes and task-negative networks, e.g., the widely known default-mode network (DMN) (Fox et al., 2005; Thomas Yeo et al., 2011). The study of these networks has given crucial insights into the brains large-scale organization and has, therefore, also been used to gain insight into the potential aberrations underlying various brain-related disorders such as Alzheimer's Disease (AD) or schizophrenia (SCZ) (Brandl et al., 2019; M. D. Greicius et al., 2004; Manoliu et al., 2014; Sorg et al., 2007).

But not only has the rs-fMRI methodology advanced, significant improvements have also been made since its inception towards understanding the physiological basis of rs-fMRI. For one, it has been robustly shown that the FC as indicated by rs-fMRI can also be found in resting-state electrophysiological studies, implying that the rs-fMRI-based FC indeed captures spontaneous

neural activity (Hiltunen et al., 2014; Hipp & Siegel, 2015; Nir et al., 2007; Schölvinck et al., 2013). Second, not only its accordance with directly measured neural activity has been demonstrated, but also its agreement with the underlying anatomical brain structure could be established (Honey et al., 2009; Johnston et al., 2008; Van Den Heuvel et al., 2009; Vincent et al., 2007). Overall these advances provided further necessary background, strengthening the interpretation of rs-fMRI-based FC containing meaningful neurophysiological information about the brains neural activity.

1.2 Rs-fMRI of grey matter: blood-oxygenation-level-dependent (BOLD) signal

The initial study of Biswal and colleagues already reported much weaker rs-fMRI signal fluctuations in white matter (WM) than grey matter (GM) and characterized the rs-fMRI signal as "low frequency fluctuation[s] of blood flow and oxygenation" which can be imaged with EPI scans (Biswal et al., 1995). This blood oxygenation-based signal was then only described and coined blood-oxygenation-level-dependent (BOLD) contrast for the first time a mere 5 years ago by Seiji Ogawa and colleagues in 1990 (Ogawa, Lee, Kay, et al., 1990). This now seminal report by Ogawa and colleagues demonstrated that the blood deoxyhemoglobin level can be imaged and used as a naturally occurring contrast agent to map blood oxygenation changes due to neural activity in rats (Ogawa, Lee, Kay, et al., 1990; Ogawa, Lee, Nayak, et al., 1990; Ogawa & Lee, 1990). This was possible due to the paramagnetic properties of deoxyhemoglobin, in contrast to the diamagnetic properties of oxygenated hemoglobin, causing a magnetic susceptibility effect in the blood and surrounding tissue, detectable by gradient-echo images (Ogawa, Lee, Kay, et al., 1990; Ogawa, Lee, Nayak, et al., 1990; Ogawa & Lee, 1990).

Subsequently, it was demonstrated that this contrast could be used in human fMRI as well, which was reported by Ogawa and colleagues as well as two other independent groups just another two years later in 1992 (Bandettini et al., 1992; Kwong et al., 1992; Ogawa et al., 1992). Presenting volunteer participants a blocked visual stimulation or instructions to tap their fingers, the groups found a matching blocked change in BOLD signal in the respective targeted functionally relevant brain regions, i.e., the primary visual as well as motor and sensory cortical GM. These seminal articles were the first to report the use of the BOLD signal in human fMRI to produce a functional brain map via non-invasive means. While then being conducted in a now classical task-based BOLD fMRI setting, these studies paved the way to use the BOLD signal in a resting-state fMRI setting as

done so only a few years later by Biswal and colleagues (Biswal et al., 1995). Overall this breakthrough discovery opened up the opportunity to “map human mental operations” via non-invasive neuroimaging means, as Ogawa and colleagues stated in their report (Ogawa et al., 1992).

The BOLD signal change observed in fMRI is caused by a change in the relaxation time of the transverse magnetization, T2, specifically the effective relaxation time, T2*, of hydrogen protons in the underlying tissue water, which is caused by local field homogeneities depending on the concentration of de-oxygenated hemoglobin, as already stated in the earliest reports (Ogawa, Lee, Kay, et al., 1990; Ogawa, Lee, Nayak, et al., 1990; Ogawa & Lee, 1990).

The physical principle of nuclear magnetic resonance depends on magnetic properties of hydrogen nuclei (protons). Protons possess a magnetic moment, termed spin that tends to align with the static magnetic field of MRI scanners, which results in a longitudinal magnetization (Buxton, 2013; Uludag et al., 2015). This longitudinal magnetization can be manipulated by radio frequency (RF) pulses, spatially encoded by magnetic field gradients and recorded for generating MR images. These radio frequency (RF) pulses, tilt the longitudinal magnetization out of its alignment with the static magnetic field to a transverse plane, generating transverse magnetization, which, by losing phase coherence among the precessing spins, decays exponentially with the transverse relaxation time T2. The rotating transverse magnetization induces an oscillating electric current in a receiving coil, which decays over time (free induction decay signal, FID) (Buxton, 2013). For fMRI, the emitted energy is usually measured at an echo time (TE), where the echo signal can either be generated via gradients (i.e., gradient echo) or appropriate RF pulses (i.e., spin echoes). Due to naturally occurring local field inhomogeneities in the tissue, the observed transverse magnetization decay is faster than the intrinsic T2 relaxation time in a perfectly homogenous magnet field, which is called T2* (see Buxton, 2013; Uludag et al., 2015 for a comprehensive overview).

In the context of BOLD fMRI, deoxygenated hemoglobin causes additional localized magnetic field inhomogeneities in and around the tissue of venous blood vessel, as deoxygenated hemoglobin is paramagnetic and alters the magnetic susceptibility of the blood (Buxton, 2013; Ogawa, Lee, Kay, et al., 1990; Ogawa, Lee, Nayak, et al., 1990; Ogawa & Lee, 1990). This leads to variable changes in the T2* of brain tissue, depending on the local concentration of deoxygenated hemoglobin (Buxton, 2013). In other words, reading the BOLD signal at the same TE for two regions, the region with less deoxygenated hemoglobin, i.e., less field inhomogeneities, will have a stronger signal, as

the transverse magnetization has not decayed as much, due to its longer T2*. This is the fundamental physical basis of the blood-oxygenation-level-dependent, i.e. BOLD, signal.

From a physiological point of view, the fluctuating levels of blood oxygenation leading to the BOLD signal changes are caused by a transient oversupply of arterial oxygenated blood to regions of increased neural activity, a process which is called functional hyperemia (Drew, 2019; Logothetis & Wandell, 2004; Nippert et al., 2018). As a result the venous concentration of oxygenated hemoglobin increases adjacent to regions of neuronal activity, leading to BOLD signal increases (Ogawa, Lee, Kay, et al., 1990). The BOLD signal is therefore primarily arising from the venous system (Ogawa et al., 1993; Ogawa, Lee, Kay, et al., 1990; Yu et al., 2016), as arterial blood is usually fully saturated with oxygen, leaving no room for large variations in deoxyhemoglobin content. While the ultimate reason for this vast increase in blood flow and thus oversupply of oxygenated blood is still unclear (Drew, 2022), it constitutes the physiological basis for the BOLD signal.

The process orchestrating this interplay between increased neural activity, metabolic demands and blood delivery has been termed neurovascular coupling (NVC) (Lecrux et al., 2019). As part of that process, a multitude of different cells, such as excitatory neurons, inhibitory neurons or astrocytes act on local arterioles via the release of vasoactive mediators such as adenosine (Ado), nitric oxide (NO), somatostatin (SOM) (Lecrux et al., 2019; Nippert et al., 2018). As a summary of all processes, a local hyperpolarization of pre-capillary endothelial cells is initiated, which retrogradely spreads up the vascular tree, leading to a consequent relaxation of vessel-lining smooth muscle cells as well as pericytes causing vasodilation and thus increased blood flow to the area in need (Drew, 2019). While this process enables measuring local neural activity via the proxy of blood oxygenation, i.e., BOLD signal, it also inherently limits the potential spatial resolution of BOLD signal-based measures, as vasodilation spreads up from the initial site of activity (Hillmann 2014) and consequently affects larger regions with increased blood flow and thus changed deoxyhemoglobin concentration.

As the BOLD signal merely conveys proxy information about the originally desired underlying neural activity, much research has also gone into uncovering the neural origins. The discovery that the BOLD response is most strongly linked to the local field potential (LFP) in both sedated and awake primates was one of the key observations in that regard (J. B. M. Goense & Logothetis,

2008; Logothetis et al., 2001). The LFP is associated with post-synaptic potentials and signals local neural information integration and computation rather than spiking activity, i.e., action potentials, of local neurons (Burns et al., 2010; Hall et al., 2016). One further key observation has been the strong link between the BOLD signal and high frequency components of both the LFP and importantly also directly recorded human neural activity, electroencephalography (EEG) and electrocorticography (ECOG), in the range of gamma oscillations (commonly 30-80 Hz) (X. Huang et al., 2019; Khursheed et al., 2011; Mulert et al., 2010). The BOLD signal therefore largely constitutes a valid proxy signal to local neural information processing in both animals and humans.

The aforementioned associations and backgrounds for the BOLD signal, however, mostly apply to recordings from GM. The difference between BOLD signal changes between GM and WM was already observed in the first human (resting-state) BOLD studies (Biswal et al., 1995; Ogawa et al., 1992) and has since been studies in more detail, showing that it arises from the different vascular physiology, e.g., capillary density, and neural activity, e.g. fewer post synaptic potentials in WM (Gawryluk et al., 2014). Thus, WM has been mostly neglected in BOLD fMRI studies, but more recent studies have started to provide further insight into the basis of BOLD signal in WM and related measures (Guo et al., 2022; Y. Huang et al., 2023; Özbay et al., 2018).

1.3 Rs-fMRI across patient populations

With the breakthrough of BOLD fMRI in human neuroimaging studies, which offered the opportunity to “image mental operations” (Ogawa et al., 1992), BOLD fMRI was already championed early on to replace the then standard positron-emission-topography (PET) to image various neuropsychiatric and neurological disorders (Rajagopalan et al., 1995). Already very early on, task-based BOLD fMRI was used to image alterations in schizophrenia (SCZ), Alzheimer's Disease (AD), obsessive-compulsive disorder (OCD) or stroke, lauding its non-invasive as well as fast, save and relative ease of use, while simultaneously calling for more refinement of the method and practices (Rajagopalan et al., 1995).

The introduction of rs-fMRI, as described above, can confidently be presented as such a called-for refinement. While task-based BOLD fMRI already brought along several advantages over PET studies, rs-fMRI had the further advantage of not needing an explicit task, while also cutting down the overall scan length, making it even more accessible. This allowed fMRI of patient populations

for which cognitive or motor tasks were hard or even impossible to carry out, such as drug addiction, multiple sclerosis (MS) or AD. Thus, alteration in BOLD-fMRI-based functional connectivity (BOLD-FC) were already reported in the early days of rs-fMRI. Since then rs-fMRI BOLD-FC alterations have been firmly established in a plethora of different disorders such as AD, depression, SC, generalized anxiety disoder (GAD), autism spectrum disorder (ASD), bipolar disoder (BP), Parkinsons' disease (PD) or also chronic pain patients (Claeys et al., 2022; Du et al., 2018; Gotts et al., 2019; M. Greicius, 2008; M. D. Greicius et al., 2004; Kolesar et al., 2019; S.-J. Li et al., 2000; L. Lin et al., 2018; Lowe et al., 2002; Pfannmöller & Lotze, 2019; Ragland et al., 2007; Sorg et al., 2007; Tessitore et al., 2019; Wilcox et al., 2019).

In-line with the canonical interpretation that takes BOLD signal changes as a proxy for neural activity, these BOLD-FC aberrations are most commonly interpreted in terms of neural alterations or impairments (e.g. Sorg et al., 2007).

1.4 Non-neural influences on the BOLD signal and derived BOLD-FC

However, parallel to the widespread use of rs-fMRI in patient studies, non-neural influences on the BOLD signal have been investigated as well, such as cardiac or respiratory related contributions (Birn et al., 2008; C. Chang et al., 2009; Glover et al., 2000). Since then non-neuronal influences on the BOLD signal have been studied in much more detail, with evidence strongly pointing to a BOLD model, which is critically shaped by both local neurally-evoked and non-neural oxygenation fluctuations (Das et al., 2021; Drew, 2019).

For one, strong contributions from alterations in local hemodynamic-vascular parameters, such as NVC impairments, leading to changes in baseline cerebral blood flow (CBF) or blood volume (CBV), have been shown to shape the BOLD signal and influence derived measures such as BOLD-FC (Archila-Meléndez et al., 2020; Chu et al., 2018; Cohen et al., 2002; Liang et al., 2013). For example, a simulation study could demonstrate BOLD-FC aberrations following unilaterally impaired hemodynamic-vascular responses to neural activity. While response amplitude impairments of blood inflow led to simple linear effects on BOLD-FC, response timing impairments, i.e., a delayed and broadened blood inflow, had complex and non-linear effects (Archila-Meléndez et al., 2020). This is line with earlier observations of a BOLD signal amplitude and timing dependence on baseline CBF level (Cohen et al., 2002). Consequently, the BOLD signal derived FC strength in healthy adults has been reported to be associated with baseline CBF (Jann et al., 2015),

with the association depending on the composition of the regionally underlying tissue and level of baseline CBF (Chu et al., 2018). A further source of local non-neural contributions are fluctuations in oxygen beyond the process of NVC, e.g., as induced by vasomotion. These constitute intrinsic periodic vessel dilations, which are present even in the absence of neural activity, causing the local oxygenation level to fluctuate on a timescale of several seconds (~0.1Hz for humans) (Das et al., 2021; Lu et al., 2019; Noordmans et al., 2018; Rayshubskiy et al., 2014; Winder et al., 2017) and by that also affect resting-state BOLD-FC (Das et al., 2021).

Second, not only local hemodynamic-vascular parameters, but also systemic macrovascular ones, have been shown to influence the BOLD signal. For example, there has been ample evidence that systemic body-wide blood oxygenation changes are part of the cerebral BOLD signal, as indicated by rs-fMRI-based BOLD lags (Y. Li et al., 2018; Tong et al., 2012; Tong & Frederick, 2014). Furthermore, such systemic hemodynamic-vascular effects have also been reported to be incorporated into the WM BOLD signal (Guo et al., 2022; Özbay et al., 2018). Systemic hemodynamic-vascular regulation likewise seems to follow the organization in networks akin to RSN, thereby merging with the neural activity derived BOLD signal (Bright et al., 2020). These systemic parameters such as the BOLD lag have likewise been shown to impact BOLD-FC in healthy adults and to explain substantial portions of BOLD-FC variability across regions of the DMN (Erdoğan et al., 2016), to cause spurious BOLD correlations (Tong et al., 2015) and to artificially boost rs-fMRI BOLD-FC replicability by introducing a consistent non-neural component (Wanger et al., 2022).

These factors overall lead to the repeatedly observed phenomenon of the BOLD signal exhibiting a much lower coupling to neural activity at rest, as compared to a task based fMRI setting (Drew, 2019; Jaime et al., 2019; Lu et al., 2019; Winder et al., 2017), implying larger contributions of non-neural sources of oxygenation fluctuations.

Overall this leads to the conclusion that the BOLD signal and derived FC, especially when derived from rs-fMRI, is a composite signal, which currently cannot easily be delineated into its neural or hemodynamic-vascular components in a regular rs-fMRI experiment. However, these hemodynamic-vascular factors are rarely considered, especially those caused by NVC alterations (Tsvetanov et al., 2021), leading to potentially wrong conclusions with regard to the underlying participant group or phenomena associated with rs-fMRI BOLD-FC.

1.5 Consequences for rs-fMRI BOLD-FC studies in populations with hemodynamic-vascular alterations

While BOLD-FC is already shaped by hemodynamic-vascular factors in healthy adults, the influence is furthermore amplified in conditions of altered hemodynamic-vascular properties, such as in certain patient populations. In such samples larger alterations in either the non-neural component part of the BOLD signal or, even worse, in both non-neural and neural components of the signal can be expected. This majorly complicates the interpretation of potential BOLD-FC aberrations as a proxy for underlying neural activity aberrations.

For example, alterations in local NVC, baseline physiology, vascular properties or systemic perfusion have been demonstrated in cerebral vascular disorders such as ICAS or stroke (Dirnagl, 2012; Göttler et al., 2020; Göttler, Kaczmarz, et al., 2019; Kaczmarz et al., 2021; Viticchi et al., 2021; L. Wang et al., 2021; Zou et al., 2022), neurodegenerative disorders such as dementia (Soto-Rojas et al., 2021; Yu et al., 2020; Zlokovic, 2011), neuropsychiatric disorders such SCZ (Bazzari & Bazzari, 2022; Hoirisch-Clapauch et al., 2014; Katsel et al., 2017; Najjar et al., 2017; Shalev et al., 2009), neurological disorders such as mulitple sclerosis (MS) (Merlini et al., 2012; VanGilder et al., 2011) or even healthy aging (Ances et al., 2009; De Vis et al., 2015; Preibisch et al., 2011; Tsvetanov et al., 2021; West et al., 2019). These can impact the BOLD-signal beyond influences from a potentially altered neural activity, leading to BOLD-FC aberrations not grounded in altered brain functioning. For example, local alterations in baseline CBF in AD patients have been found to explain up to 12% of BOLD-FC variability in the DMN (Göttler, Preibisch, et al., 2019), to cause spurious BOLD-FC differences between mild traumatic brain injury (mTBI) patients and healthy controls (Champagne et al., 2020) and between elderly and younger adults (Champagne et al., 2022). Such results are also in line with previous simulations showing the impact of altered local hemodynamic-vascular factors on BOLD-FC, even if only one brain region is affected (Archila-Meléndez et al., 2020). Systemic perfusion changes, as indicated by BOLD lag, have likewise been found to alter BOLD-FC of the DMN in Moyamoya disease (Jahanian et al., 2018), to cause BOLD-FC aberrations after stroke (Siegel et al., 2016), or even cause the complete disappearance of BOLD-FC (Christen et al., 2015).

Thus, the interpretation of BOLD-FC aberrations as “neural activity aberrations” is potentially confounded and the impact of hemodynamic-vascular factors on the BOLD-signal and consequently BOLD-FC is commonly underestimated and often neglected (Lu et al., 2019;

Tsvetanov et al., 2021). Estimating BOLD-FC, especially at rest, from a sample with suspected or unknown hemodynamic-vascular alterations, therefore runs the risk of getting a flawed neurophysiological index (Biswal et al., 1995; Friston et al., 1993), as BOLD-FC estimations are not necessarily indicative of the underlying neural activity.

As evident from the studies summarized above, influences of several hemodynamic-vascular factors – whether local or systemic – on BOLD-FC have been already been studied, however, investigations comparing different factors with regard to their influence on BOLD-FC are scarce, particularly in humans. The effort of quantifying several distinct hemodynamic-vascular parameters alongside BOLD-FC within a single imaging session is one of the main reasons behind that. Even fewer attempted to further combine those with a simulation framework to gain additional insight into causal mechanisms.
However, to the best of my knowledge no study has so far combined a multi-parametric human fMRI study with BOLD-FC simulations to compare influences of different hemodynamic-vascular parameters and to provide causal explanations for underlying mechanisms of BOLD-FC aberrations due to hemodynamic-vascular impairments.

1.6 Study design

Given the crucial yet widely ignored influence of hemodynamic-vascular factors on BOLD-FC, this thesis is focused on thoroughly investigating their interplay. The experimental design is based on the well-founded assumption that both local and systemic hemodynamic-vascular factors influence regional BOLD signals, which is supported by empirical data and simulation results (Archila-Meléndez et al., 2020; Drew, 2019). Underlying differences in these factors consequently lead to regionally different BOLD signals, which in turn affect the derived BOLD-FC between the respective areas. Therefore, to optimally study the isolated influence of those hemodynamic-vascular factors, other aspects of the regions from which BOLD signals are derived, should be controlled for, i.e., be as identical as possible. Critically, such circumstances can be found for homotopic brain regions, i.e., “mirror-regions” on the left and right hemispheres (Mancuso et al., 2019). Homotopic brain regions have repeatedly been shown to exhibit synchronous metabolic and neural activity (Duffy et al., 1996; Lee et al., 2008; Nir et al., 2008), as well as having strong structural connectivity (Johnston et al., 2008; Van Den Heuvel et al., 2009) and a coherent vascular geometry and activity (Mateo et al., 2017), due to the brains’ symmetrical architecture, resulting in strong BOLD-FC

(Johnston et al., 2008; Mancuso et al., 2019; Stark et al., 2008). Using homotopic brain regions, therefore, allows to assess the effect of certain hemodynamic-vascular factors on BOLD-FC, while controlling for other metabolic, vascular and neural region properties.

To test these assumptions, I combined data from a human multi-parametric fMRI study, providing 5 different hemodynamic-vascular parameters, with simulations of BOLD-FC under impaired NVC conditions. The studied sample consisted of asymptomatic patients with unilateral internal carotid artery stenosis (ICAS) and age-matched healthy controls, which have previously been studied in detail (Göttler et al., 2020; Göttler, Kaczmarz, et al., 2019; Kaczmarz et al., 2021). ICAS is a cerebrovascular disorder where the main feeding artery, the internal carotid, is partially occluded by an atherosclerotic plaque, constricting blood flow to the ipsilateral hemisphere (Malhotra et al., 2017). This lead to pronounced hemodynamic-vascular impairments in my patient sample, specifically ipsilateral to the stenosis and within individual watershed areas (Göttler et al., 2020; Göttler, Kaczmarz, et al., 2019; Kaczmarz et al., 2021). Comparisons with healthy controls, however, showed preserved oxygen metabolism (CMRO2), which was slightly elevated contralateral to the stenosis (Göttler, Kaczmarz, et al., 2019; Kaczmarz et al., 2021). Neurocognitive functioning of the patients was likewise largely maintained, with the exception of subtle visual attention deficits (Göttler et al., 2020), indicative of intact neural functioning in line with the intact oxygen metabolism. Unilateral ICAS therefore constitutes and ideal lesion model of impaired hemodynamic-vascular functioning, critically limited to one hemisphere, while exhibiting preserved neural functioning. Based on these existing data, the impact of selected local and systemic hemodynamic-vascular parameters on BOLD-FC could be studied, specifically between well-controlled homotopic regions on the left and right hemispheres. For Project 1, I considered the capillary transit time heterogeneity (CTH), baseline CBF and regional CBV (rCBV) as the local hemodynamic-vascular parameters, and for Projects 2 and 3, I additionally considered time-to-peak (TTP) and BOLD lag as systemic hemodynamic-vascular parameters.

In detail, I examined the influence of differences among the chosen hemodynamic-vascular parameters between volumes-of-interests (VOIs) on the respective BOLD-FC, which was limited to homotopic VOI pairs for Projects 1 and 2. This approach allowed me to assess BOLD-FC between brain regions in dependence of region-wise differences among the non-neural component of the BOLD signal. In order to test these dependencies, I employed a specific regression approach, namely a linear mixed-model (LMM), allowing for both fixed group-average effects, ICAS and healthy controls, as well as random individual variations for the estimated effects (i.e., intercepts

and slopes) among the participants. Chosen outcome of the models was homotopic BOLD-FC with the respective hemodynamic-vascular VOI differences being the main predictors. Additional control variables such as group, ICAS or healthy controls, and participant age or sex were also included. For Project 3 the analysis was extended to also cover BOLD-FC between non-homotopic VOI pairs, namely crosshemispheric heterotopic pairs and intrahemispheric VOI pairs, which was implemented as a further model variable.

The empirical analysis of Project 1 was supplemented with BOLD-FC simulations to gain further insight into the mechanisms underlying BOLD-FC aberrations caused by local hemodynamic-vascular alterations. The simulations relied on a biophysical NVC framework supported by empirical work (Archila-Meléndez et al., 2020) and allowed for dynamic alterations of NVC parameters in response to a synthetic neural activity input to create BOLD signal time courses. This allows to generate both, a reference BOLD signal, simulated from "healthy" NVC parameters and several target BOLD time courses based on "impaired" or altered NVC parameters. Similarly, the simulation framework had previously been used to demonstrate both local blood flow amplitude and response timing effects on BOLD-FC (Archila-Meléndez et al., 2020).

1.7 Hemodynamic-vascular MRI

For all Projects, previously collected hemodynamic-vascular MRI data was used from the aforementioned ICAS patients and healthy controls sample (Göttler et al., 2020; Göttler, Kaczmarz, et al., 2019; Kaczmarz et al., 2021). Parameters CTH, rCBV and TTP were derived from dynamic susceptibility contrast (DSC) MRI data. DSC MRI is a contrast-agent based technique, relying on the passage of a bolus of a paramagnetic gadolinium containing tracer through the brain to provide voxel-wise estimates of cerebral hemodynamic properties (Boxerman et al., 2020), such as CBV. CBV is an indicator of the overall blood volume in the underlying tissue, indicated in milliliters blood per 100g of tissue, and can be derived from the DSC MRI gadolinium bolus concentration-time curve (Boxerman et al., 2020; Hedderich et al., 2019; Kluge et al., 2016). While absolute CBV quantification is quite demanding, robust measures of relative CBV (rCBV) can be obtained by standardizing CBV values to normal appearing white matter (NAWM) (Hedderich et al., 2019; Kluge et al., 2016). TTP is a further DSC MRI derived measure and indicates the arrival time of maximal gadolinium contrast agent concentration and is an indicator for cerebral perfusion timing and delay in seconds (Wouters et al., 2017). CTH represents the transit time distribution of red blood cells passing through the capillaries in seconds (Jespersen & Østergaard, 2012). While it can be directly

observed for animals, it is accessible for human MRI studies as well, by parametric modeling of the DSC MRI data (Mouridsen et al., 2014). CTH has previously been demonstrated to be impaired in neurodegenerative as well as symptomatic vascular brain diseases (Madsen et al., 2022; Mundiyanapurath et al., 2016; Nielsen et al., 2020; Østergaard, Aamand, et al., 2013; Østergaard et al., 2016; Østergaard, Jespersen, et al., 2013; Potreck et al., 2019) and was also found to be altered in the aforementioned sample of ICAS patients, who exhibited increased CTH values, i.e., less homogeneous baseline capillary blood flow on the hemispheres ipsilateral to their stenosis (Kaczmarz et al., 2021).

To derive a quantitative index for baseline cerebral perfusion, CBF, pseudo-continuous arterial spin labeling was employed (pCASL) as a further MRI measurement. At its core, arterial spin labeling uses arterial blood as an endogenous tracer to derive cerebral perfusion information. To this end, blood water in the brain feeding arteries is magnetically labeled before entering the brain tissue, where it then leads to a MRI signal change which can be read-out after an appropriate post label delay (PLD) (Alsop et al., 2015). PCASL constitutes a refinement of the arterial spin labeling, which increase signal-to-noise ratio and labeling efficiency (Petcharunpaisan, 2010). The derived CBF is indicated in milliliters of blood per 100 gram brain tissue per minute.

Lastly, the collected BOLD rs-fMRI data was used to derive the BOLD lag as indicator of cerebral perfusion timing. While TTP is an established contrast agent based indicator of systemic cerebral perfusion times, derived from the aforementioned DSC MRI, BOLD lag constitutes a more novel approach to mapping systemic cerebral blood arrival times, directly derived from rs-fMRI data (Amemiya et al., 2020; Aso et al., 2019; Fitzgerald et al., 2021; Khalil et al., 2017, 2020; Kroll et al., 2017; Y. Lv et al., 2013; Nishida et al., 2019; Tanrıtanır et al., 2020; Tong et al., 2012, 2017; Tong, Yao, et al., 2019; Tong & Frederick, 2014). The time lags are derived via cross-correlation of a suitable reference BOLD time course, e.g., from the superior sagittal sinus (SSS) or the average GM signal, with BOLD signals from all other brain voxels. By that a relative time delay is obtained for each voxel with respect to the reference time course BOLD lag has been shown to be in good accordance with the arrival time of fresh oxygenated blood at the respective region (Fitzgerald et al., 2021; Tong et al., 2017; Tong, Yao, et al., 2019; Yao et al., 2019) and was used for assessing hemodynamic-vascular impairments (Amemiya et al., 2014, 2022; Khalil et al., 2020; Y. Lv et al., 2013).

1.8 Projects and Hypotheses

The results of both Project 1 and 2 have previously been published (Schneider et al., 2022, 2023 respectively) and the respective publications were adapted for this thesis (see beginning of chapters 2, Project 1, and 3, Project 2, for detailed information about adapted chapters and citation).

For Project 1 (Schneider et al., 2022), we hypothesized that the capillary transit time heterogeneity (CTH) constitutes a promising imaging parameter that may serve as a proxy for simulated local blood flow response timings, likewise leading to impaired BOLD-FC. We specifically proposed that CTH represents a NVC microvascular blood flow timing parameter, comparable to simulated blood flow response timing effects, leading to BOLD-FC aberrations in cases of timing mismatch between brain regions. To test this hypothesis, I first examined the relationship between homotopic BOLD-FC and homotopic differences in CTH, while controlling for simultaneous differences in baseline CBF and rCBV, in the described LMM regression approach. We then examined the proposed indication of CTH with regard to the simulated NVC response timing effects by using the previously established BOLD signal simulations (Archila-Meléndez et al., 2020).

For Project 2 (Schneider et al., 2023), I extended the scope of Project 1 by including further factors, specifically comparing systemic vs. local hemodynamic-vascular parameters. To this end, I additionally included the TTP and BOLD lag parameter maps in the LMM analysis. I specifically expected the systemic parameters to have a larger impact as compared to the local parameters, following previous reports of large-scale BOLD-FC aberrations in samples with strong systemic perfusion delays (Christen et al., 2015; Jahanian et al., 2018; Siegel et al., 2016). I examined this in an approach akin to Project 1, estimating the impact of both local and systemic hemodynamic-vascular parameters on BOLD-FC in one model. In addition I compared explained BOLD-FC variance between regression models either containing only the local parameters or both local and systemic.

For Project 3 I finally extended the analysis beyond the well-controlled homotopic regions to BOLD-FC between heterotopic and intrahemispheric regions. While homotopic BOLD-FC is ideal for investing the influence of unilateral hemodynamic-vascular impairment and as a standalone measure has been successfully used to differentiate types of dementia (Cheung et al., 2021), in

meta-analytic approaches to reveal intrinsic brain properties (Mancuso et al., 2019) or to show age- and sex-related changes regarding integration and segregation of homotopic areas (Zuo et al., 2010), it is seldom used as a standalone measure in rs-fMRI studies. These commonly investigate BOLD-FC between a vast set of regions, i.e., homo- and heterotopic as well as intrahemispheric BOLD-FC. To be able to draw conclusions regarding the impact of hemodynamic-vascular effects on more commonly used BOLD-FC measures, I therefore extended the regression based approach, to also include a differentiation between homotopic, heterotopic or intrahemispheric regions. I hypothesized that the impact of hemodynamic-vascular differences should generally be reduced for heterotopic and intrahemispheric BOLD-FC. This follows from the observation that non-homotopic regions differ more in the various criteria, I initially strived to control for, e.g. metabolic and neural activity, WM connectivity or vascular geometry and activity. These are expected to lead to already substantially different regional BOLD-signal time courses, even before the influence of hemodynamic-vascular factors, diminishing their impact on the already reduced BOLD-FC.

2. Project 1: Combined simulation and empirical study of local hemodynamic-vascular influences on BOLD-FC

Results of this Project have previously been published as an original research article in NeuroImage, 255, in 2022, (Schneider et al., 2022), with chapters 2.1 to 2.3 of this thesis adapted from this publication:

Schneider, S. C., Archila-Meléndez, M. E., Göttler, J., Kaczmarz, S., Zott, B., Priller, J., Kallmayer, M., Zimmer, C., Sorg, C., & Preibisch, C. (2022). Resting-state BOLD functional connectivity depends on the heterogeneity of capillary transit times in the human brain A combined lesion and simulation study about the influence of blood flow response timing. NeuroImage, 255, 119208. https://doi.org/10.1016/j.neuroimage.2022.119208

2.1 Methods of Project 1

This Project has three parts. First, I performed an empirical study in patients with ICAS and healthy controls regarding the impact of CTH on BOLD-FC (see methods section 2.1.1.). Second, we studied – in a simulation study – the impact of CBF response timing on BOLD-FC (see methods section 2.1.2). The third part of the Project regards a potential link between CTH and CBF response timing and their effects on BOLD-FC (see methods section 2.1.3.) that is further scrutinized in the second half of the discussion.

2.1.1 Empirical study: CTH and BOLD-FC

I analyzed multi-parametric hemodynamic MRI data, namely BOLD-fMRI, arterial spin labeling (ASL) and dynamic susceptibility contrast (DSC) MRI, from asymptomatic ICAS patients and age-matched healthy controls. From my subject cohort, analyses regarding hemodynamic impairments in ICAS have been published previously (Göttler et al., 2020; Göttler, Kaczmarz, et al., 2019; Kaczmarz et al., 2021). Here, I derived BOLD-FC from BOLD-fMRI data and investigated its relation to hemodynamic alterations, in particular changes in CTH.

2.1.1.1 Participants

From an existing sample of 29 ICAS patients and 30 age-matched controls, which were analyzed previously (Göttler et al., 2020; Göttler, Kaczmarz, et al., 2019; Kaczmarz et al., 2018, 2021), I

included data from 28 ICAS patients (11 females) and 27 healthy controls (15 females), from whom all necessary data are available and of sufficient quality, leading to an overall sample size of 55 participants. Median age of participants from both groups was 71 years (age range: 52–84 years; mean age: 70.1 years; no significant group differences). The asymptomatic ICAS patients had an unilateral, high-grade stenosis of the extracranial internal carotid artery (11 with left-sided stenosis; each stenosis was > 70% as defined by (NASCET SC, 1991). All participants underwent extensive medical testing to exclude neurological, psychiatric and chronic kidney diseases, which constituted exclusion criteria along with incidental MRI findings hinting at brain lesions (e.g. stroke). The study was approved by the medical ethical board of the Klinikum rechts der Isar; for a detailed description of the overall sample characteristics see **Table 1**. Participants provided written informed consent to all conducted examinations.

Table 1. Summary of participant characteristics for Project 1.

Parameter	**Control (N=27)**	**ICAS (N=28)**	***p***
Age [years]: mean (SD)	70.1 (4.9)	70.1 (7.1)	0.99
Sex – female: N (%)	15 (55.6%)	11 (39.3%)	0.23
Side of Stenosis – left: N (%)	-	11 (39.3%)	
Stenotic degree [%] (NASCET)	-	0.8 (0.1)	
BMI: mean (SD)	27.1 (4.2)	26.3 (4.9)	0.52
Smoking [packs per year]: mean (SD)	8.4 (14.4)	15.3 (22.1)	0.17
Fazekas: mean (SD)	0.9 (0.9)	1.5 (0.8)	**0.02**
PAOD: N (%)	3 (11.1%)	8 (28.6%)	0.11
Hypertension: N (%)	15 (55.6%)	22 (78.6%)	0.07
Diabetes: N (%)	2 (7.4%)	7 (25.9%)	0.07
Statins: N (%)	5 (18.5%)	20 (71.4%)	**< 0.001**
Antiplatelets: N (%)	5 (18.5%)	25 (89.3%)	**< 0.001**
Antihypertensives: N (%)	11 (40.7%)	19 (67.9%)	0.25
Antidiabetics: N (%)	2 (7.4%)	4 (14.3%)	0.25
MMSE: mean (SD)	28.7 (1.4)	28.2 (2.4)	0.39
TMT-A: mean (SD)	41.8 (13.2)	49.7 (23.4)	0.13
TMT-B: mean (SD)	103.2 (39.3)	139.5 (63.7)	**0.02**
BDI: mean (SD)	8.4 (5.2)	9.9 (9.8)	0.51
STAI: mean (SD)	34.9 (10.1)	38.6 (10.7)	0.22

Note: Variables are represented by either mean and standard deviation (SD) or absolute number N and fraction in percent. Two-sample t-tests were used for group comparisons in age, mean pack-years, BP, BMI, MMSE, TMT-A/B, BDI,

STAI, and LBT; Chi-squared test for remaining group comparisons. Bold print indicates significant group differences $p < 0.05$. Abbreviations: BMI, body mass index; PAOD, peripheral artery occlusive disease; CHD, coronary heart disease; BP, blood pressure; MMSE, mini mental state exam; TMT-A/B, trail making test-A/B; LBT, line bisection test; BDI, Beck's depression inventory; STAI, state trait anxiety inventory.

2.1.1.2 MRI acquisition, BOLD signal preprocessing and calculation of hemodynamic parameter maps

MRI acquisition: All MR imaging was conducted using a 3T Philips Ingenia MR-Scanner (Philips Healthcare, Best, The Netherlands) and a 32-channel head coil. Brain parcellation and lesion detection was derived from anatomical MRI data, namely T1-weighted magnetization prepared rapid gradient echo (MPRAGE; TE = 4 ms, TR = 9 ms, α = 8°, TI = 1000 ms, shot interval = 2300 ms, SENSE AP/RL 1.5/2.0, 170 slices, matrix size = 240x238, voxel size = 1x1x1 mm^3) and T2-weighted fluid attenuated inversion recovery (FLAIR; TE = 289 ms, TR = 4800 ms, inversion delay = 1650 ms, TSE factor = 167, 163 slices, matrix size = 224x224, voxel size = 1.12 mm^3 isotropic). BOLD-TCs and BOLD-FC were derived from T2*-weighted multiband echo planar imaging (EPI) time series (TE = 30 ms, TR = 1.2 s, α = 70°, multiband factor 2, SENSE factor 2, 38 slices, matrix size = 192x192, voxel size = 3x3x3 mm^3, 500 dynamic scans, scan duration 10 min). Baseline CBF was derived from pseudo-continuous arterial spin labeling (pCASL) acquisitions (post label delay (PLD) = 2000 ms, label duration = 1800 ms, 16 slices). To maximize the number of eligible subjects as well as data quality, I included for each subject the highest quality CBF map from pCASL data that were acquired for sequence comparisons (Kaczmarz et al., 2016). For the majority of 40 subjects, a 3D gradient spin echo (GRASE) readout with 4 background suppression (BGS) pulses, TE/TR/α = 7.4 ms/ 4377 ms/90°, turbo spin echo factor 19, EPI factor 7, voxel size = 2.75x2.75x6 mm^3 was employed. For the remaining subjects, sequences with a 2D EPI readout and similar acquisition parameters were used, with either 4 BGS pulses (6 subjects), 2 BGS pulses (7 subjects), or no BGS (2 subjects). Lastly, CTH and rCBV were derived from DSC MRI (80 single-shot EPI volumes, TE = 30 ms, TR = 1513 ms, α = 60°, 26 slices, voxel size = 2.0x2.0x3.5 mm^3, bolus injection of Gd-Dota, concentration 0.5 mmol/ml, dose 0.1 mmol/kg, at least 7.5 mmol per subject).

BOLD signal preprocessing: Preprocessing of BOLD fMRI and anatomical MRI data was done with the Data Processing Assistant for Resting-State fMRI advanced edition (DPARSFA) toolbox V5.0_200401 (Yan, C.G. & Zang, Y.F., 2010) and SPM12 (v7771; Wellcome Trust Centre for

Neuroimaging, UCL, London, UK) using MATLAB (R2019b; MathWorks, Natick, MA, USA). This minimal preprocessing approach included realignment of the EPI time series data, manual reorientation of all images along the anterior-posterior commissure (AC-PC), cropping of the anatomical data, spatial co-registration of anatomical and fMRI data, brain extraction and Diffeomorphic Anatomical Registration Through Exponentiated Lie Algebra (DARTEL) segmentation of the anatomical images (Ashburner, 2007), nuisance covariate regression including six motion parameters and a linear trend regressor, smoothing with a 6 mm Full Width at Half Maximum (FWHM) Gaussian kernel and applying a temporal bandpass filter from 0.01 to 0.1 Hz.

NVC parameter map calculation: CTH, rCBV and CBF parameter maps were calculated with custom MATLAB programs (R2016b; MathWorks, Natick, MA, USA). Spatial coregistration and segmentation were performed with SPM12 (Wellcome Trust Centre for Neuroimaging, UCL, London, UK) as previously described in detail (Kaczmarz et al., 2021).

Preprocessing of DSC data comprised correction for motion and slice timing effects. CTH and rCBV parameter maps were then derived from relative concentration time curves that were calculated from the time course signal *S*(t) according to $C(t) \propto \Delta R_2(t) = -\ln\left(\frac{S(t)}{S(0)}\right)/TE$ (Østergaard et al., 1999).

Calculation of CTH parameter maps employed parametric modeling of *C*(t) (Jespersen & Østergaard, 2012; Mouridsen et al., 2014). To achieve model-based estimation of the tissue residue function *R(t),* a gamma variate function with parameters α and β is employed to parametrize the probability density distribution $h(\tau)$ of capillary transit times τ (across a capillary bed of parallel capillaries)

$$h(\tau;\alpha,\beta) = \frac{-dR}{d} = \frac{-1}{\beta^{\alpha}\Gamma(\alpha)}\tau^{\alpha-1}e^{-\tau/\beta}. \quad [1]$$

Parameter estimation is then performed by an expectation–maximization-type algorithm, which permits inclusion of prior information (Mouridsen et al., 2006). Using the parametrization according to Eq. [1], CTH is determined as the standard deviation of the capillary transit time distribution ($\sigma = \sqrt{\alpha}\beta$) in seconds, with larger values indicating a larger heterogeneity. The vascular mean transit time (MTT) can be obtained as $\mu = \alpha\beta$.

For CBV calculation, leakage correction of the concentration time curve *C(t)* was performed as described previously (Kluge et al., 2016). Relative CBV was then calculated by integrating the

leakage corrected concentration time curve (Hedderich et al., 2019; Kluge et al., 2016). Resulting rCBV maps were re-referenced to normal appearing white matter (NAWM) with CBV=2.5% (Leenders, 1994).

Quantitative baseline CBF maps were derived from the pCASL data following recommendations outlined in the ISMRM perfusion study group consensus paper (Alsop et al., 2015). In short, the label and control images were motion corrected separately, differences averaged after pairwise subtraction, and CBF calculated according to Eq. [1] from (Alsop et al., 2015) with M_0 being used for normalization. The resulting CBF maps were smoothed using a 5 mm isotropic Gaussian kernel.

2.1.1.3 BOLD-FC, CTH, baseline CBF, and rCBV in homotopic left-right region pairs

For the presented analysis, I focused on pairwise homotopic BOLD-FC, as correlated BOLD signal fluctuations between homotopic left-right volumes-of-interest (VOIs) are unlikely to be affected by incoherent vascular geometry, blood arrival times, vasomotion, and neural activity (Drew et al., 2020). Those factors have been shown to be largely comparable due to both the brain's symmetrical anatomy and cross-hemispheric fiber connectivity (see Drew et al., 2020 for a comprehensive review). Furthermore, functional connectivity between homotopic VOIs provides relatively strongest BOLD-FC values compared to within-hemisphere or non-homotopic across hemisphere VOI pairs, likely due to supporting pairwise homotopic structural connectivity (Drew et al., 2020). Thus, homotopic pairwise BOLD-FC is an excellent paradigm for analyzing the impact of one-sided NVC alterations on BOLD-FC.

VOI Selection: To obtain left-right pairwise homotopic BOLD-FC, I used the Atlas of Intrinsic Connectivity of Homotopic Areas (AICHA) (Joliot et al., 2015). The AICHA was derived from resting-state BOLD-FC of a large sample of healthy participants (N = 281), with the parcellation algorithm being explicitly weighted towards the homotopic organization of the brain and its functional separation, resulting in an atlas being ideally suited for BOLD fMRI analyses of homotopic areas. It provides overall 384 anatomically labeled VOIs, which can be separated in 192 cross-hemispheric VOI pairs, covering cortical and subcortical grey matter areas of the forebrain.

BOLD-FC Analysis: All analyses involving pairwise BOLD-FC and NVC parameter maps were performed in the individual participants' native space. To this end, I adapted the AICHA to each individual's native anatomy via a non-linear transformation using the reverse flow fields that I

obtained by MNI normalization of the individual anatomical MRI data (T1-weighted MPRAGE). The AICHA atlas was then resliced to match the resolution of the functional MRI data used in my study. To ensure maximum overlap with the individual participants' brain anatomy, the atlas was masked with a grey matter (GM) mask derived from the individual participants' segmented MPRAGE data ($p_{GM} > 0.3$, resliced to fMRI resolution). To this end, individual GM probability maps were obtained by segmenting each subject's MPRAGE data with SPM12 (Wellcome Trust Centre for Neuroimaging, UCL, London, UK) using default settings. For each participant, VOI-average BOLD-TCs were then extracted from all 384 VOIs and correlated using Pearson's correlation between the left and right homotopic areas. Correlation coefficients were then Fisher-r-to-z transformed to obtain 192 pairwise BOLD-FC values for each participant.

NVC Parameter Analysis: Similarly, differences in CTH, baseline CBF and rCBV parameter values were extracted from these homotopic VOI pairs. The AICHA atlas, already in subject-space, was resliced to the respective parameter maps and subsequently masked by an accordingly resliced GM mask. For each VOI, the underlying metric was then extracted, and the differences in parameter values calculated between pairwise homotopic VOIs by subtracting the right from the left sided VOI value. In particular, ΔCTH [sec] = $CTH_{VOI\text{-}Left} - CTH_{VOI\text{-}Right}$, ΔCBF [ml/100g/min] = $CBF_{VOI\text{-}Left} - CBF_{VOI\text{-}Right}$, and ΔrCBV [pp (percentage points)] = $rCBV_{VOI\text{-}Left}t - rCBV_{VOI\text{-}Right}$. A difference of '0' means that the two homotopic areas exhibit no difference in the respective parameter values. Differences with negative or positive values reflect higher right-sided or higher left-sided parameter values, respectively, indicating an imbalance between right and left homotopic cortical areas.

As both rs-fMRI and hemodynamic MRI parameter maps did not cover the whole brain, some VOIs included either no or only very few voxels, which was enhanced by GM masking. I therefore excluded all VOIs with fewer than 10 voxels in the fMRI resolution (3x3x3 mm^3). The VOI-extracted NVC parameter differences were consequently z-standardized across all VOIs and subjects. After exclusion of VOIs based on voxel number, some VOI-average CTH, baseline CBF and rCBV parameters values still constituted outliers, i.e., implausible physiological values (e.g., due to imaging artifacts or partial volume effects with CSF). I, therefore, also excluded VOI pair differences with z-values below -2.56 and above 2.56, respectively, (i.e., 1% of extreme differences, including 99% of observations) for each parameter to remove excessive physiologically implausible

differences. In total, 1844 observations were excluded (1325 due to low voxel counts, 519 due to z-score outliers), retaining 8716 observations.

2.1.1.4 Statistical testing of empirical BOLD-FC analyses

Group differences in BOLD-FC & NVC parameters: To test for significant group differences in pairwise BOLD-FC and NVC parameters, I computed the mean BOLD-FC as well as the mean absolute CTH, baseline CBF and rCBV differences, i.e., |ΔCTH|, |ΔCBF|, and |ΔrCBV|, for each participant across all VOI pairs. These mean values were then compared between groups using Welch's t-test. One-sample t-tests were used to test for each group separately if mean pairwise NVC parameter differences were significantly different from zero. In order to explore potential regional effects, I examined how BOLD-FC, |ΔCTH|, |ΔCBF| and |ΔrCBV| differed between the groups across 54 VOI pairs that were derived from the AICHA (Joliot et al., 2015) by merging subregions of cortical and subcortical areas, e.g., in the Thalamus, where the regions N_Thalamus-1,-2,-3 were merged to N_Thalamus, for each participant. Merging was performed to simplify the analysis by reducing the number of VOIs. In addition, I examined if the ICAS patients' mean BOLD-FC, |ΔCTH|, |ΔCBF| and |ΔrCBV| depend on the degree of stenosis by means of a correlation analysis.

Influence of NVC parameters on BOLD-FC: To examine the influence of NVC parameters, especially of CTH, on BOLD-FC between homotopic brain regions, I regressed the influence of z-standardized pairwise NVC differences, i.e., |ΔCTH|, |ΔCBF|, and |ΔrCBV|, on pairwise BOLD-FC. I did so by means of a linear-mixed model (LMM) approach to account for the influence of multiple NVC parameters and the factor group, i.e., ICAS patients versus healthy controls, as well as to control for the participants' age and corresponding interactions, e.g., between age and influence of |ΔCTH|. In an additional model, I further controlled for sex differences. The LMM also allowed for assessing the full complexity of a potential association by capturing the between-subject variance with regard to the group effects.

Using z-standardized regressors was necessary to enable comparison of regression effects because the effect sizes of predictors on BOLD-FC are determined by their absolute values. In this case, a difference of 1 would constitute a large difference for CTH, but only a small difference for CBF. Thus, z-standardization ensured an identical scale and range for all included parameters since a

change of 1 always indicates a change of 1 standard deviation (σ) even though σ_{CTH} =2.47 sec and σ_{CBF} = 5.73 ml/100g/min differed numerically.

Concretely, the LMM approach was performed by use of the lme4 package (Bates et al., 2015) for R (R Core Team, 2020) within Rstudio (RStudio Team, 2019). I opted for a random-coefficient model with pairwise BOLD-FC as dependent variable and |ΔCTH|, |ΔCBF|, and |ΔrCBV| as primary regressors. Adding |ΔCBF| and |ΔrCBV| as regressors in to the model allowed me to assess the specific impact of |ΔCTH| on BOLD-FC, independent of differences in baseline CBF and rCBV. In addition, I used these regressors to study the impact of CBF and rCBV on BOLD-FC, respectively. Further regressors were the participants' age and group affiliation. Age was centered on the overall median (71 years). For each of the pairwise NVC parameter differences, I further controlled for interactions with age and group affiliation. Deviations from the overall average effects among participants were controlled by including the intercepts and slopes of |ΔCTH|, |ΔCBF|, and |ΔrCBV| as random effects. The model's degrees of freedom and *p*-values were estimated via the Tests in Linear Mixed Effects Models (lmerTest) package (Kuznetsova et al., 2017) using Satterthwaite's method.

2.1.2 Theoretical considerations regarding the link between CTH and CBF response timing – a preliminary approximation

Beyond the impact of CTH on BOLD-FC, we were interested in a potential link between CTH and CBF response timing. Therefore, I outline some theoretical considerations about such a link and, in particular, similarities regarding the impact of CTH and CBF response timing on BOLD-FC, respectively.

To better understand the impact of timing aspects of CBF responses on BOLD-FC, we employed a recently proposed simulation framework (Archila-Melendez et al., 2020). Critically, with respect to CBF, an increase in the characteristic time constant τ_f of the gamma variate function used to model the CBF response results in an increasingly delayed and broadened CBF response function with a peak at $t = 2 \cdot \tau_f$, a diminishing amplitude, and a constant area under the curve (for more details see **Fig. 2** and section 2.1.3.). Critically, this behavior resembles aspects of CTH. In particular, the distribution *h* of capillary transit times $h(\tau)$ is also modelled by a gamma variate function (see Eq. (1)) to facilitate CTH measurement by parametric modeling of DSC MRI (Mouridsen et al., 2014). This similarity between CBF response function and distribution of capillary transit times $h(\tau)$ is at the core of our idea that CTH might represent critical aspects of CBF response timing, and might

therefore serve as kind of an zero-order approximation. In the following, I want to clarify this similarity between CBF response and CTH in more detail.

By means of a vascular model (Jespersen & Østergaard, 2012; Mouridsen et al., 2014), the probability density function of capillary transit times $h(\tau)$ can be parametrized by a gamma variate function with shape parameters α and β (see Eq. (1)). According to tracer kinetic theories, $h(\tau)$ corresponds to the slope of the residue function $R(t)$, which describes the washout of an intravascular tracer (Østergaard et al., 1996, 1999) and is thus related to the vascular mean transit time ($MTT = \int_{-\infty}^{\infty} \tau h(\tau)\, d\tau / \int_{-\infty}^{\infty} h(\tau)\, d\tau$) and via the central volume theorem also to CBV and CBF, i.e., MTT = CBV/CBF. Using the parametrization in Eq. (1), MTT and CTH are obtained as the mean ($\mu = \alpha\beta$) and standard deviation ($\sigma = \sqrt{\alpha}\,\beta$) of $h(\tau)$, respectively (Jespersen & Østergaard, 2012). While an increase in MTT could also be accomplished by a homogenous increase in capillary transit times and could thus be used as a proxy for a merely delayed CBF response, an increase in CTH necessarily implies a broadening as well as a delay in CBF (see Eq. (6) in Østergaard et al., 1999). This correspondence in response nature and distribution model thus supports the idea that the characteristic time constant τ_f in our simulation model resembles important aspects of measured CTH.

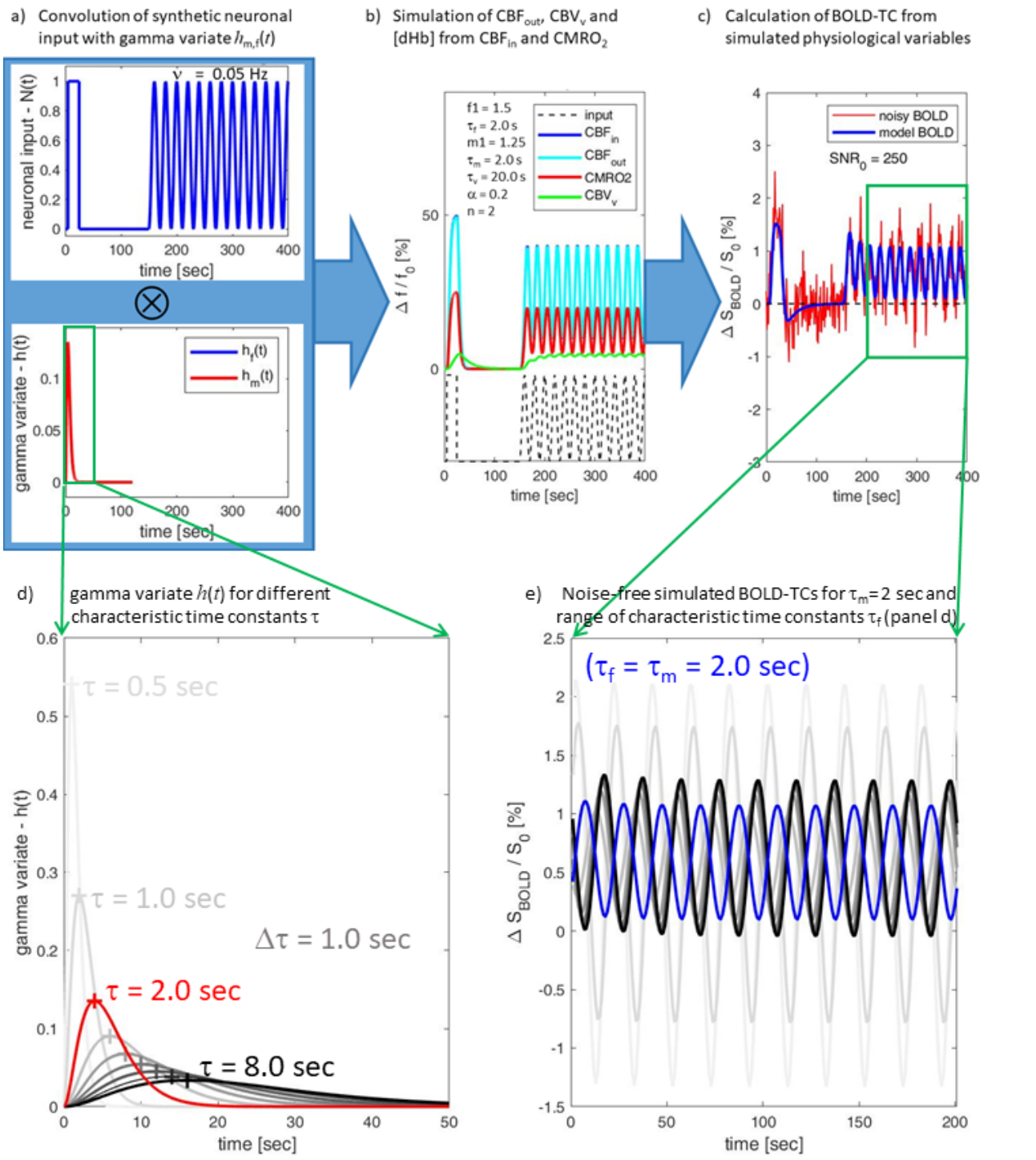

Figure 2. Illustration of the BOLD signal time course (BOLD-TC) simulation process for the reference BOLD-TC (seed) (a-c) together with gamma variate response functions h(t) (d) and BOLD-TCs for a range of characteristic time constants τf of blood flow response (e).

(a) A purely sinusoidal input signal $N(t)$ with a frequency of 0.05 Hz is coupled to an initial boxcar portion (top) and convoluted with gamma variate functions $h_f(t)$ and $h_m(t)$ (bottom; note that both functions are overlapping). (b) This yields independent normalized inputs $f_{in}(t)$ (CBFin) and $m(t)$ (CMRO2), which were used to simulate blood flow out of the tissue ($CBF_{out} \approx CBF_{in}$), venous CBV ($CBV_v$) and deoxyhemoglobin content [dHb] assuming a slow CBV response (τ_v = 20.0 sec). (c) The resulting BOLD-TC (blue) with a temporal resolution of TR = 1000 ms is complemented with random

white noise to yield a noisy BOLD-TC (red) with SNR_0 = 250. The signal portion used for BOLD-FC calculations is marked by a green frame. (d) Gamma variate response functions h(t) and (e) BOLD-TCs for a range of characteristic time constants τ_f of blood flow response. (d) The $h(t)$ with τ = 2.0 sec (corresponding to the condition in panel (a)) is highlighted in red. The remaining curves range between τ = 0.5 sec and [1.0, … , 8.0] sec with $\Delta\tau$ = 1 sec. Note that $h(t)$ peaks at t = 2·τ and the amplitude decreases such that the area under the curve remains constant. The BOLD-TCs in panel (e) were simulated for the range of characteristic time constants τ_f as shown in panel (d)) and τ_m = 2.0 sec. Note that the colors are matched to panel (d) but the BOLD-TC with τ_f = 2.0 sec (corresponding to the condition in panel (c)) is highlighted in blue.

2.1.3 Simulation study: CBF response timing and BOLD-FC modeling

In order to systematically explore the dependence of BOLD-FC on CBF response timing (i.e., varying τ_f), BOLD-FC was calculated between a selected reference seed BOLD-TC (with supposedly 'healthy' parameter settings) and a range of target BOLD-TCs (with supposedly 'impaired' parameter settings). The constellation of 'healthy' and 'impaired' BOLD-TCs corresponds to the situation in my empirical analysis of pairwise homotopic BOLD-FC in ICAS patients, where BOLD-TCs from the healthy contralateral side are correlated with potentially impaired BOLD-TCs extracted from homotopic VOIs ipsilateral to the stenosis. In addition, we explicitly explored the BOLD-TCs' amplitudes and their temporal delays (lags) with respect to the selected reference seed BOLD-TC. The simulated BOLD-TCs are referred to as BOLD responses because in our simulation model they are elicited by purely sinusoidal synthetic neuronal input signals at different frequencies in the infra-slow frequency spectrum below 0.1Hz. All described calculations and simulations were implemented and performed using MATLAB (R2019b; MathWorks, Natick, MA, USA).

BOLD-TC signal model: Details of our model have been described recently(Archila-Meléndez et al., 2020). Importantly, it allows for independent modeling of CBF and CMRO2 responses to neuronal activity, with respect to amplitudes as well as timing characteristics. Our implementation in Simulink and MATLAB (R2019b; MathWorks, Natick, MA, USA) is similar to the one proposed by (Simon & Buxton, 2015), which is based on a modified balloon model (Buxton et al., 1998; Obata et al., 2004), critically extended for including extra- and intravascular BOLD signal contributions according to (Obata et al., 2004). With respect to nomenclature, we stick to previous conventions and express changes in dynamic variables relative to baseline values (see **Table 2**).

Table 2. Summary of dynamic model parameters following (Archila-Meléndez et al., 2020; Blockley et al., 2009; Buxton et al., 2004; Simon & Buxton, 2015). Default settings employed for simulation of the reference seed BOLD-TC are accentuated by bold print.

Parameter	Description	Value
$N(t)$	input intrinsic neuronal activity at time t	dynamic [0 – 1]
$m(t)$	ratio of $CMRO_2$ to baseline at time t	dynamic
$m1$	$CMRO_2$ 'response' amplitude	**1.25**
$f_{in}(t)$	ratio of CBF inflow to baseline at time t	dynamic
$f1$	CBF 'response' amplitude	**1.5**
$f_{out}(t)$	ratio of CBF outflow at time t to baseline	dynamic
$q(t)$	ratio of deoxyhemoglobin quantity at time t to baseline	dynamic
$v(t)$	ratio of venous CBV at time t to baseline	dynamic
$h_{f,m}(t)$	convolution kernel relating CBF and $CMRO_2$ to neuronal input	variable
$H_{f,m}$	scaling parameter for CBF and $CMRO_2$ convolution kernels	variable
τ_m	characteristic time constants for $CMRO_2$	**2 sec**
τ_f	characteristic time constants for CBF:	
	reference seed BOLD-TC	**2 sec**
	target BOLD-TCs	[0.5 – 8.0] sec
α_v	exponent describing steady state venous flow–volume coupling	**0.2**
τ_v	characteristic time constants for venous CBV response	**20 sec**
v_0	frequency offset of a fully deoxygenated blood vessel at 3 T	80.6 sec^{-1}
r_0	slope defining the dependence of the R_2* on blood oxygenation at 3T	178 sec^{-1}
ξ	intrinsic ratio of blood to tissue signals at rest at 3T	0.24
τ_0	transit time for blood through venous compartment	0.75 sec
z	shape parameter for CBF and $CMRO_2$ convolution kernels	3

In short, dynamic changes in normalized blood flow, $f_{in}(t)$, and oxygen consumption, $m(t)$, are modeled as linear responses to a prescribed neuronal input $\mathrm{N}(t)$ by convolution of $\mathrm{N}(t)$ with scaled gamma distributions $h_{f,m}(t)$, which are defined independently for flow (f) and metabolic (m) input functions, respectively (Archila-Meléndez et al., 2020)

$$f_{\mathrm{in}}(t) = N(t) * h_f(t) \tag{2}$$

$$m(t) = N(t) * h_m(t) \tag{3}$$

with

$$h_{f,m}(t) = H_{f,m} \frac{1}{\tau_{f,m}(z-1)!} \left(\frac{t}{\tau_{f,m}} \right)^{(z-1)} e^{-t/\tau_{f,m}}. \quad (4)$$

The shape parameter *z*, scaling parameters $H_{f,m}$, and characteristic time constants $\tau_{f,m}$ take distinct values for flow (*f*) and metabolic (*m*) input functions, respectively (see **Table 2**). From both flow, $f_{in}(t)$, and oxygen consumption, $m(t)$, inputs, a system of coupled differential equations is used to derive relative changes in deoxyhemoglobin content, $q(t)$, and venous blood volume, $v(t)$ (see Eqs. [6]-[10] in Archila-Meléndez et al., 2020). Based on $q(t)$ and $v(t)$, BOLD signal changes relative to baseline are calculated accounting for extra- and intravascular signal contributions (see Eq. [5] in Archila-Meléndez et al., 2020). The simulation process is illustrated in **Figure 2** and employed parameters and their settings as summarized in **Table 2**.

Figure 2 demonstrates that the employed simulation model is capable of simulating a wide range of NVC-behaviors that have been observed in empirical studies. On the one hand, the initial block stimulus (**Fig. 2a**, top, left) causes a strong and prolonged CBV response that causes a distinct BOLD signal undershoot (**Fig. 2c**, left), on the other hand, the infra-slow oscillatory neuronal input (**Fig. 2a**, top, right) induces hardly recognizable CBV oscillations in the steady state (**Fig. 2b**, right) but distinct BOLD signal oscillations (**Fig. 2c**, right – green framed portion between 200 and 400 sec; see Archila-Meléndez et al., 2020 for a detailed discussion). **Figure 2d** illustrates the behavior of $h_{f,m}(t)$: With increasing characteristic time constant $\tau_{f,m}$, the peak is not only delayed but the curve broadens and the amplitude is reduced in a way that the area under the curve remains constant. **Figure 2e** finally shows BOLD-TCs that were simulated with different τ_f (as shown in **Fig. 2d**) at τ_m = 2.0 sec. It can clearly be seen that a change in τ_f influences amplitude as well as phase of the resulting BOLD-TC signals presented in **Figure 2e**.

Matrix representation of BOLD-TCs in the (τ_f, v) parameter space: BOLD-TCs were simulated across a 16x10 matrix, where the characteristic time constant τ_f of the CBF response was systematically varied in 16 steps ($\Delta\tau_f$ = 0.5 sec) with τ_f = [0.5,…, 8.0] sec for a range of ten purely sinusoidal input functions $N(t)$ with frequencies ν between 0.01 Hz and 0.1 Hz ($\Delta\nu$ = 0.01 Hz). The same input parameters and settings were used as described in (Archila-Meléndez et al., 2020) for 'Scenario 2 – CMRO2 and CBF delays' at slower CBV response (see **Table 2**). The neuronal input functions $N(t)$ were coupled to a boxcar portion similar to previous work (Archila-Meléndez et al., 2020). This

allows direct comparisons between outputs of the BOLD signal model for an ultra-slow (boxcar) stimulus and the oscillatory inputs at different frequencies that are separated by a low-level constant baseline.

Matrix representations of BOLD-TC amplitudes and lags: Next, matrices of BOLD-TCs across the (τ_f, ν) parameter space were analyzed with respect to both BOLD signal peak-to-peak amplitudes δS_{BOLD} and temporal shifts (i.e., lags) of the simulated BOLD-TCs with respect to the reference seed BOLD-TCs with τ_f = 2.0 sec at each of ten purely sinusoidal input functions $N(t)$. This information helps to understand the CBF timing effects on BOLD-FC. Concerning BOLD-TC amplitude, δS_{BOLD} was calculated as the percentage difference between the maximum and minimum signal in the purely oscillatory 'resting' fMRI portions of the simulated BOLD-TCs (last 200 sec). Concerning BOLD-TC lags, temporal shifts of the simulated BOLD signal with respect to the reference seed BOLD-TC (τ_f = τ_f = 2.0 sec) were obtained by cross-correlation (Matlab function 'xcorr') from noise-free simulated BOLD-TCs, normalized by the period length of the input oscillatory signal (T_p = [100, …., 10] sec) and reduced to a unique range of [-0.5, …., 0.5].

Matrix representations of BOLD-FC: Finally, based on the matrix representation of BOLD-TCs across the (τ_f, ν) parameter space, we studied the dependence of BOLD-FC on the characteristic time constant τ_f of the CBF response as well as on the frequency of the sinusoidal neuronal input signals $N(t)$. To this end, we performed Pearson's correlations between the reference seed BOLD-TC (τ_f = 2.0 sec) and the range of target BOLD-TCs (τ_f = [0.5,…, 8.0] sec) at each of the 10 input frequencies ν = [0.01, …, 0.1] Hz. The seed and target BOLD-TCs were complemented with random white noise to achieve a signal to noise ratio (SNR) of 250. For each pair of investigated parameter values, correlations were performed for BOLD-TCs complemented by 16x16 different random white-noise realizations. For display, matrices of Pearson's correlation coefficients were Fisher-r-to-z transformed to z-values. In this work, we did not consider the influence of different noise levels and sampling frequency (i.e., repetition times) because decreasing SNR and temporal resolution have been shown to simply deteriorate the simulated BOLD-FC overall (Archila-Meléndez et al., 2020).

This matrix of pairwise BOLD-FC between 'healthy' and 'impaired' regions provides us with predictions of altered BOLD-FC as a function of altered local CBF response timing at different neuronal input frequencies ν. These predictions were applied to interpret how pairwise homotopic

BOLD-FC of patients with unilateral carotid artery stenosis and healthy controls depends on the heterogeneity of local capillary transit times, which we assume to reflect local CBF response variability in terms of response timing.

2.2 Results of Project 1

2.2.1 Empirical results regarding the dependence of homotopic pairwise BOLD-FC on CTH

Distribution of BOLD-FC and NVC parameter values and their group differences: AICHA VOIs and NVC parameter maps are shown in **Figure 3a-d** for a selected slice of an asymptomatic ICAS patient with a right-sided stenosis. The distribution of homotopic pairwise BOLD-FC, as well as pairwise ΔCTH, ΔCBF, and ΔrCBV are depicted in **Figure 3e-h** for both asymptomatic ICAS patients and healthy controls across 192 region pairs, approximating normal distributions in all cases. As these distributions suggest marked group differences, I conducted an additional group comparison analysis for individually averaged outcomes, i.e., BOLD-FC, |ΔCTH|, |ΔCBF| and |ΔrCBV|, respectively. At $p < 0.05$, Welch's t-testing revealed comparable BOLD-FC and |ΔrCBV| for ICAS patients and controls, but significantly larger side differences for |ΔCTH| and |ΔCBF| in patients **(Fig. 3i-l**). Albeit ICAS patients exhibited stronger side differences, significant pairwise differences between homotopic areas were detected for both the patients and healthy controls in all three NVC parameters, namely |ΔCTH|, |ΔCBF|, and |ΔrCBV| (group-wise one-sample t-tests at $p < 0.05$; control group, $p < 0.0001$; ICAS group, $p < 0.0001$).

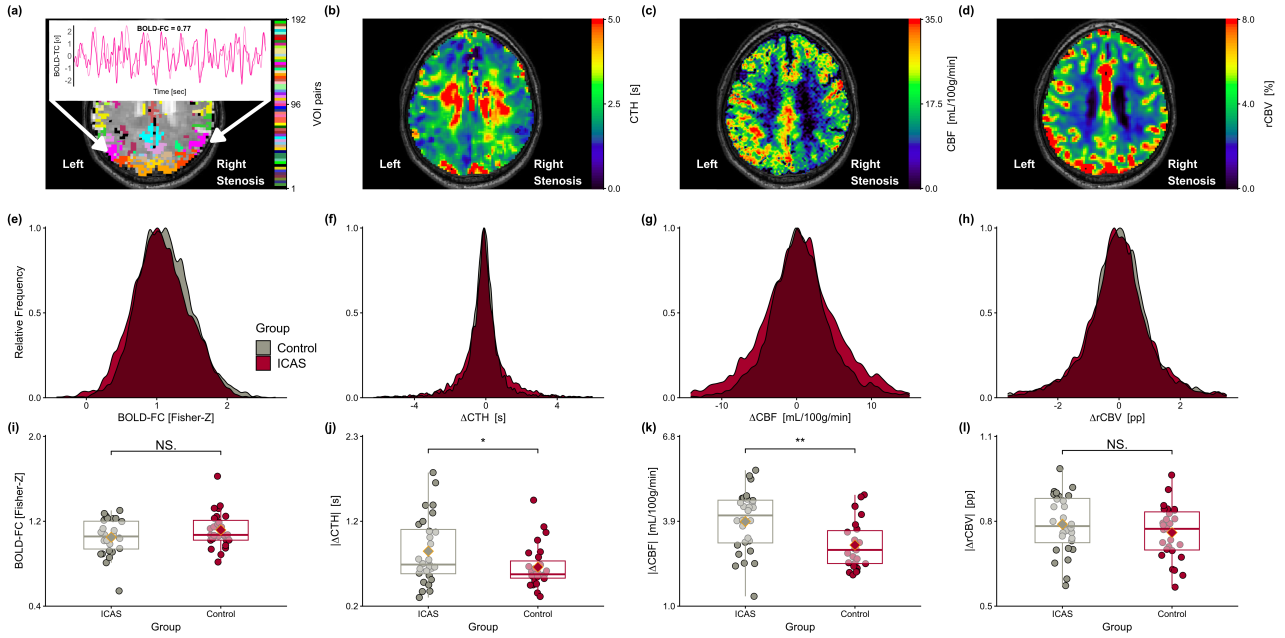

Figure 3. AICHA VOIs (a), exemplary NVC parameter maps of one ICAS patient (b-d), sample distributions (e-h) and group differences (i-l) in BOLD-FC and NVC parameters.

(a) Brain parcellation according to the AICHA atlas with an insert depicting two exemplary BOLD-TCs of homotopic regions, whose Pearson's correlation reflects homotopic BOLD-FC, (b-d) exemplary parameter maps of CTH (b), CBF (c) and rCBV (d) for a selected slice of an ICAS patient with a right-sided stenosis. (e-h) Frequency distributions of BOLD-FC (e) between pairwise homotopic VOIs and corresponding ΔCTH (f), ΔCBF (g) and ΔrCBV (h) across all VOI pairs of asymptomatic ICAS patients and healthy controls. Relative frequency of measured values are indicated in grey for healthy controls and in bright red for ICAS patients. Dark red color indicates overlap between groups. (i-l) Paired scatterplots of BOLD-FC (i) as well as |ΔCTH| (j), |ΔCBF| (k) and |ΔrCBV| (l) between pairwise homotopic VOIs averaged across 192 VOI pairs for each participant. In each panel, one dot represents one participants' average value, where red indicates ICAS patients and black healthy control participants. Thick horizontal bars indicate median values for each group, upper and lower borders of the square indicate the 75% (third quartile) and 25% (first quartile) percentile, respectively. Vertical lines indicate the 1.5 times interquartile range (between first and third quartile). Orange dots indicate the respective group mean. Global group differences regarding the respective variables were examined with Welch's t-test, significant group differences are indicated with asterisks (* for $p < 0.05$, ** for $p < 0.01$), non-significant differences with NS. Abbreviations: AICHA, Atlas of Intrinsic Connectivity of Homotopic Areas; BOLD-FC, blood oxygenation level dependent functional connectivity; CBF, cerebral blood flow; CTH, capillary transit time heterogeneity; rCBV, relative cerebral blood volume; ICAS, internal carotid artery stenosis; NVC, neuro-vascular coupling; VOI, volume of interest.

Regional Analysis: With regard to regional differences across brain regions, an additional analysis identified specific regions with group differences for BOLD-FC, |ΔCTH|, |ΔCBF| and |ΔrCBV|, respectively, such as fusiform sulcus or supramarginal gyrus (see **Fig. 4**). Regions with significant differences in |ΔCTH| and |ΔCBF| partially overlapped but to a lesser degree with BOLD-FC. To

allow a better assessment of anatomic localization, regions showing significant differences (at $p < 0.05$ uncorrected) are shown as color overlay in **Figure 5**. Furthermore, I found a weak but significant correlation between |ΔCBF| and the degree of stenosis in ICAS patients (see **Fig. 6**).

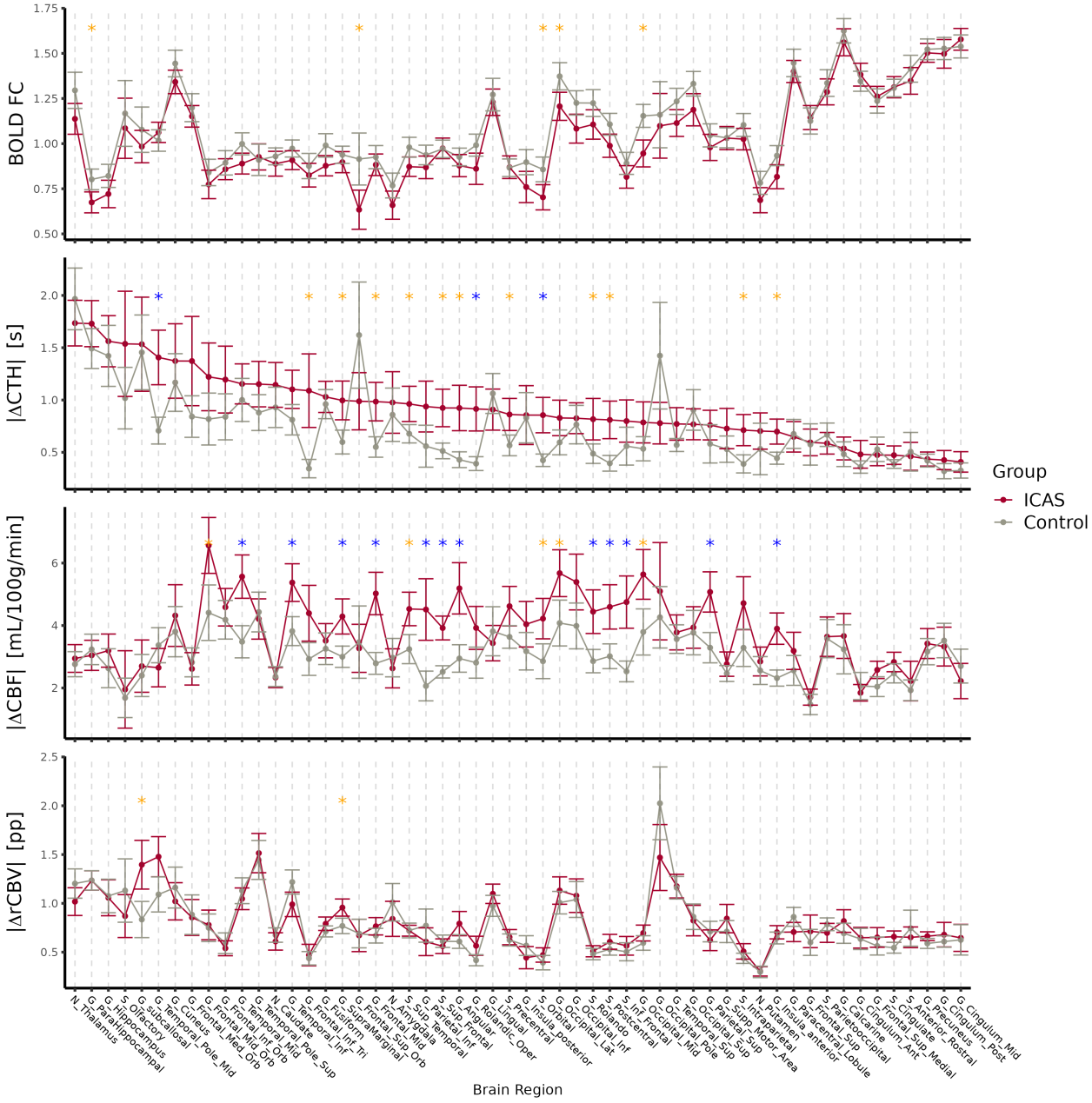

Figure 4. Mean BOLD-FC (top, |ΔCTH| (2nd row), |ΔCBF| (3rd row) and |ΔrCBV| (bottom) across 54 homotopic VOI pairs for each group.

Error-bars indicate the 84% confidence interval (mean between groups is significantly different if error-bars do not overlap). Significant differences at p < 0.05 are indicated by an asterisk (FDR-corrected - blue; uncorrected – orange).

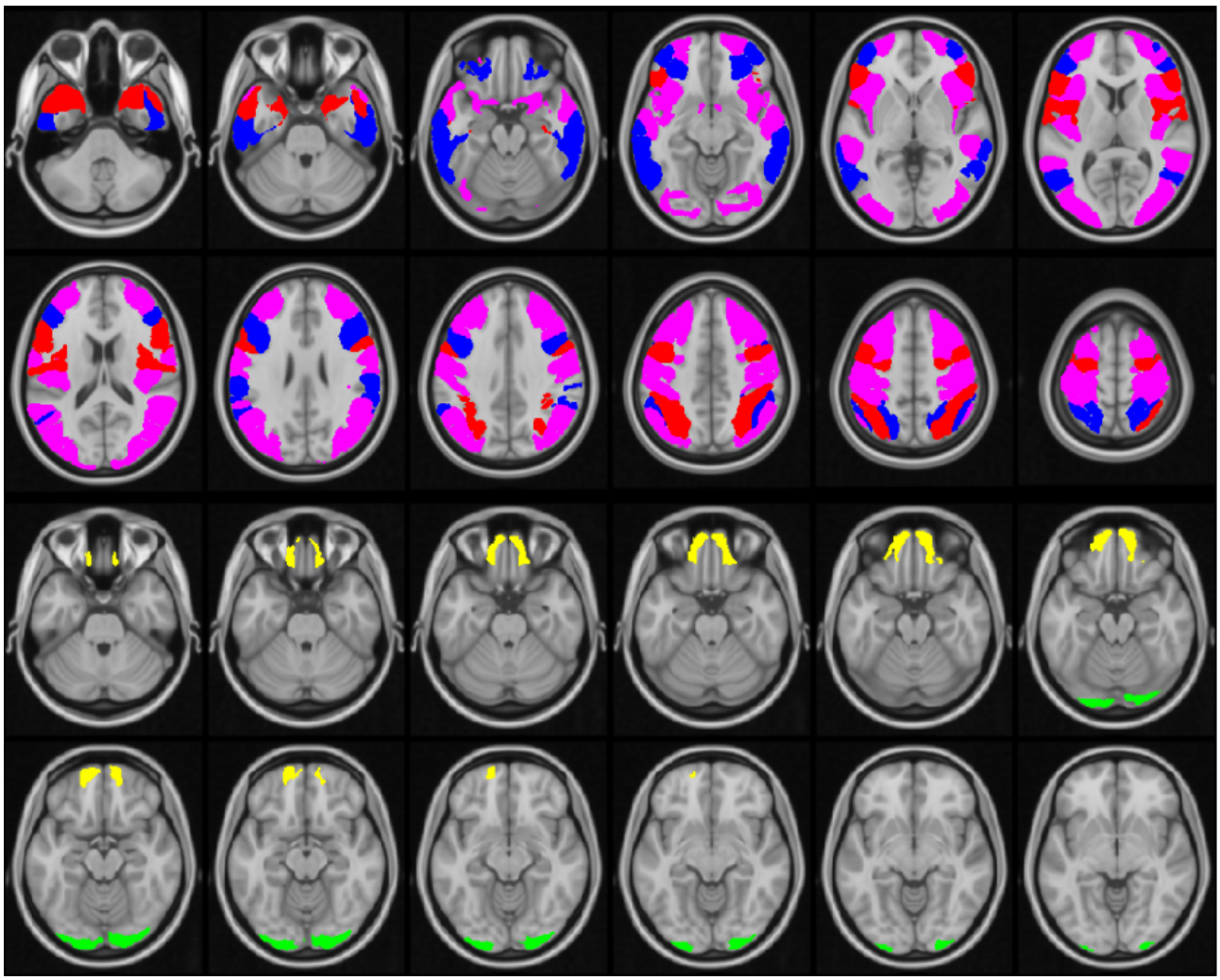

Figure 5. Parameter group differences.

The top panel shows brain regions in which ICAS patients exhibit significantly larger ($p < 0.05$) |ΔCTH| (red), |ΔCBF| (blue) or both (purple) than healthy controls. The bottom panel shows regions with high variance in |ΔCTH| and |ΔCBV|, namely the occipital pole (green) and the superior orbitofrontal gyrus (yellow).

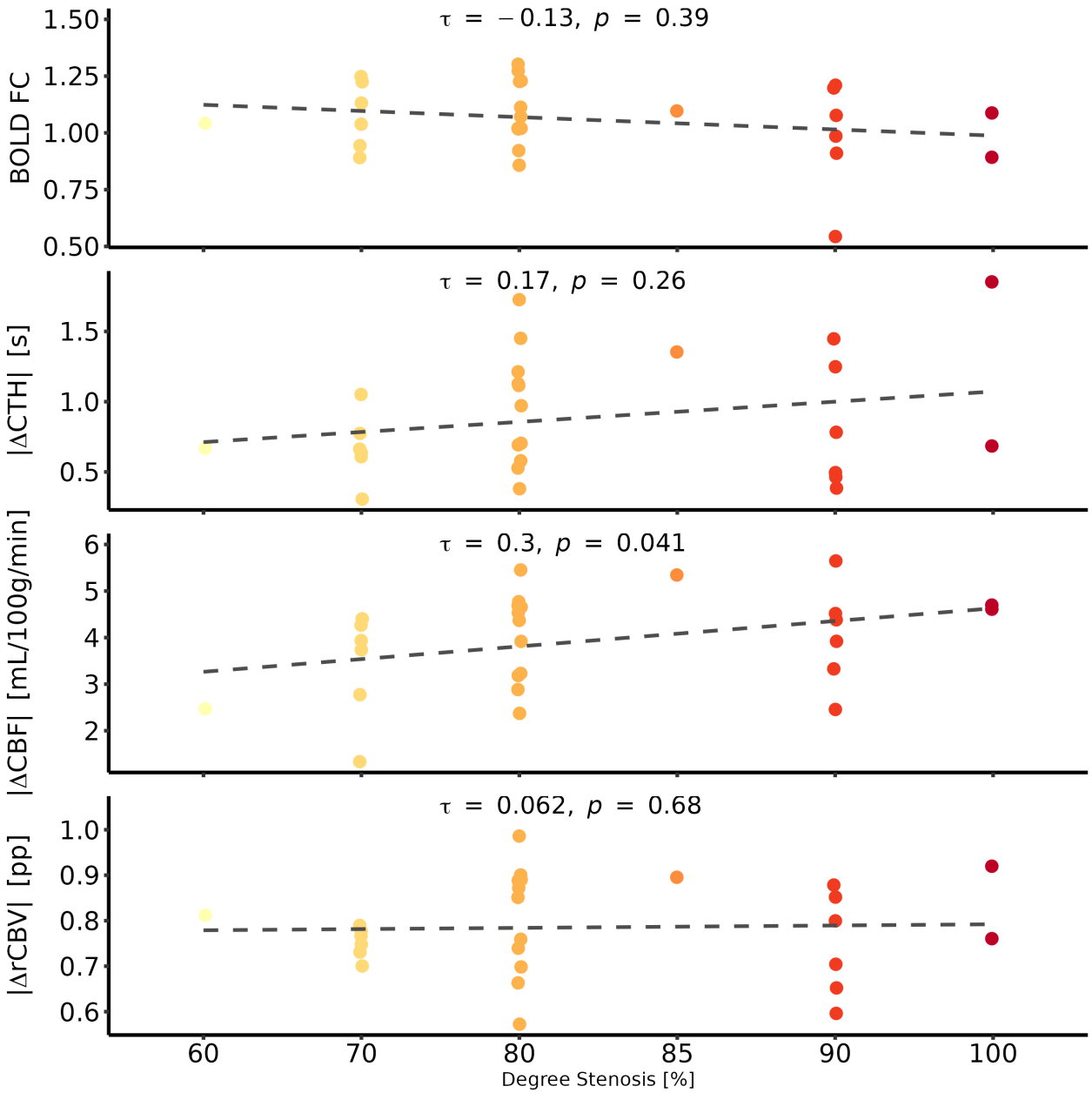

Figure 6. Correlation with stenotic degree.

Correlation of average BOLD-FC (top), |ΔCTH| (2nd row), |ΔCBF| (3rd row) and |ΔrCBV| (bottom) with degree of stenosis in ICAS patients.

Influence of CTH and further NVC parameters on BOLD-FC: To test our hypothesis that CTH influences BOLD-FC, I performed a LMM analysis with pairwise BOLD-FC as dependent variable and pairwise |ΔCTH| as independent variable of interest. I further included |ΔCBF| and |ΔrCBV| as independent variables in order to both control for their effects on BOLD-FC and to study their influence on BOLD-FC. In addition, age was included to control for systemic age-related deviations. With regard to random effects, the slope of |ΔrCBV| had to be excluded because its variation

among participants was close to zero, thus prohibiting a model fit (singular fit). Overall 8716 observations were included in the model, distributed across the 55 participants. Results are summarized in **Table 3** and **Figure 7**.

(i) *BOLD-FC*, i.e., pairwise BOLD-FC without differences in hemodynamic parameters between homotopic VOI pairs, was at z = 1.16 (corresponding to Pearson's r = 0.82; 95% CI: 1.11 to 1.21) across participants, indicating high levels of homotopic functional connectivity. The two groups, ICAS patients and healthy controls, did not significantly deviate from this average in terms of group difference.

(ii) *Significant group-wise, fixed effects of NVC parameters on BOLD-FC* were found for both |ΔCTH| and |ΔCBF| across both groups. More specifically, BOLD-FC decreased with increasing |ΔCTH| and |ΔCBF|.

a) For |ΔCTH|, BOLD-FC was estimated to decrease on average by -0.12 (95% CI: -0.15 to -0.09; -10% from baseline) per 1 σ of |ΔCTH| (i.e., 2.47 sec) between homotopic VOIs. This effect was significantly different between both groups, as demonstrated by a significant interaction of CTH and group (see **Fig. 7a** and **Table 3** – Group [ICAS]:|ΔCTH|). Quantitatively, the decrease was significantly stronger for ICAS patients (-0.16; 95% CI: -0.19 to -0.13; -14% from baseline) than for the control group (-0.08; 95% CI: -0.11 to -0.05; -7% from baseline). These effects were only slightly altered by age for female participants (for details see **Table 4** & Results – *Influence of sex differences*). The effect of |ΔCTH| on BOLD-FC was furthermore dependent on the participants' baseline BOLD-FC. More specifically, higher baseline values indicated stronger BOLD-FC decrease with |ΔCTH| (r = -0.51).

b) For |ΔCBF|, BOLD-FC was estimated to decrease on average by -0.05 (95% CI: -0.08 to -0.03; -4% from baseline) per 1 σ of |ΔCBF| (i.e., 5.72 ml/100g/min; see **Fig. 7b and Table 3** –|ΔCBF|). While there were no group specific effects of |ΔCBF|, age had a small but significant interacting influence, i.e., the decrease was slightly stronger in participants older than the median age of 71 years (an additional -0.01 per year; see **Table 3** – cAge:|ΔCBF|) and vice versa for participants younger than median age. This effect was stronger for participants in the control group (additional -0.01, i.e. -0.02 per year) and almost vanished for the ICAS patients (additional +0.01, i.e., 0 per year; see **Table 3** – Group [ICAS]:cAge:|ΔCBF|). Comparison of overall effect sizes of |ΔCTH| and |ΔCBF| revealed that the BOLD-FC reduction due to increases in |ΔCTH| were significantly stronger than the ones caused

by baseline CBF (Welch's t-test of participants estimated individual slopes; t = -3.1, $p < 0.05$).

c) For |ΔrCBV|, I did not found any effect on BOLD-FC (see **Fig. 7c**).

d) Regarding model explanatory power, the estimated R^2 value for the model was 0.23 (based on (Nakagawa et al., 2017; Nakagawa & Schielzeth, 2013) when accounting for the variation of participants among the estimated group based effects of hemodynamic parameters.

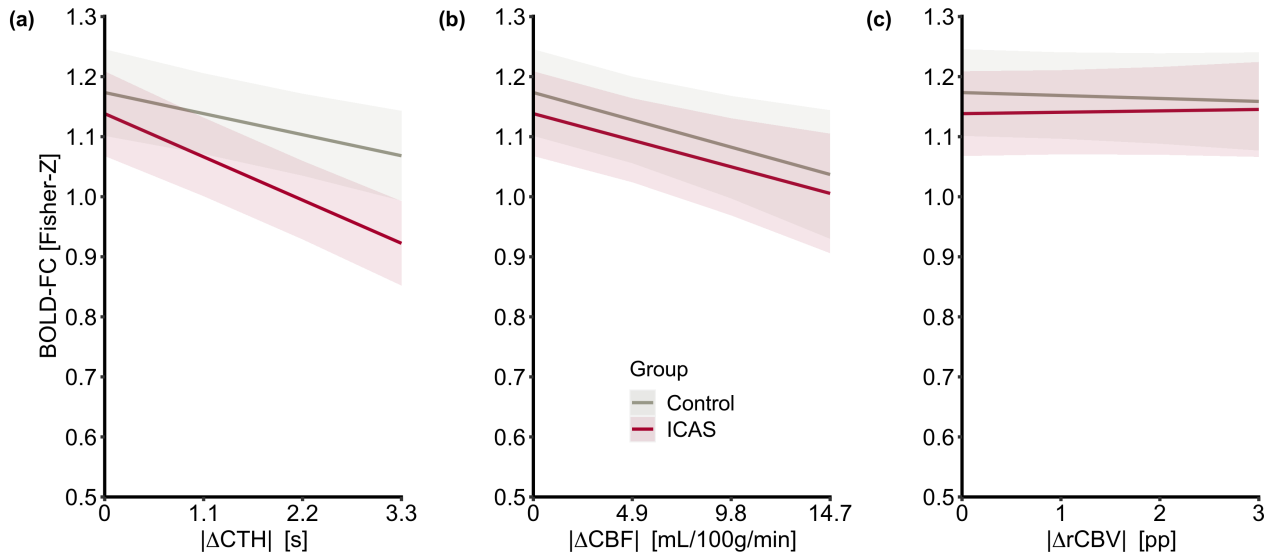

Figure 7. Group effects of NVC parameters on BOLD-FC.

Slopes indicate predicted changes in BOLD-FC (y-axis) with increasing |ΔCTH| (a), |ΔCBF| (b) and |ΔrCBV| (c) between pairwise VOIs for ICAS patients (red) and controls (black). The group-wise intercepts indicate the individually estimated baseline BOLD-FC for VOI pairs without difference in the respective NVC metric. Shaded areas indicate the 95% confidence interval of the predicted values. Range of presented absolute parameter differences, i.e. |X| have been adapted to be comparable to Project 2 based on parameter difference standard deviation ($\sigma_{CTH\ -\ Project\ 1}$ = 2.47s & $\sigma_{CTH\ -\ Project\ 2}$ = 1.1s, $\sigma_{CBF\ -\ Project\ 1}$ = 5.72 ml/100g/min & $\sigma_{CBF\ -\ Project\ 2}$ = 4.9 5.72 ml/100g/min, $\sigma_{rCBV\ -\ Project\ 1}$ = 1.4 pp. & $\sigma_{rCBV\ -\ Project\ 2}$ = 1 pp.). Abbreviations: BOLD-FC, blood oxygenation level dependent functional connectivity; CBF, cerebral blood flow; CTH, capillary transit time heterogeneity; rCBV, relative cerebral blood volume; ICAS, internal carotid artery stenosis; NVC, neuro-vascular coupling; VOI, volume of interest.

Random effects: On an individual, random effects level (see **Table 3** for an overview), participants exhibited some variance among the estimated fixed effects, exhibiting different baseline BOLD-FC values and being more or less affected by differences in NVC parameters. In detail, ~68.2% (1 standard deviation) of participants had an estimated baseline pairwise BOLD-FC between 0.98 and 1.34. Similarly, 68.2% had their pairwise BOLD-FC decreased between -0.20 and -0.05 for each 1 σ

or 2.47 seconds difference in CTH and averaged between -0.13 and 0.02 BOLD-FC change for each 1 σ or 5.72 ml/100g/min difference in CBF.

Table 3. Summary of fixed and random effects for LMM analysis.

Predictors	**Estimates**	**CI**	**Statistic**	***p***
(Intercept)	1.16	1.11– 1.21	44.91	**<0.001**
Group [ICAS]	-0.02	-0.07 – 0.03	-0.68	0.5
Age	0	-0.01 – 0.01	0.85	0.4
|ΔCTH|	-0.12	-0.15 – -0.09	-7.67	**<0.001**
|ΔCBF|	-0.05	-0.08 – -0.03	-4.03	**<0.001**
|ΔrCBV|	0	-0.02 – 0.01	-0.23	0.82
Age:|ΔCTH|	0	-0.00 – 0.01	1.58	0.12
Age:|ΔCBF|	-0.01	-0.01 – -0.00	-2.2	**0.03**
Age:|ΔrCBV|	0		-1.24	0.22
Group [ICAS]:Age	-0.01	-0.02 – 0.00	-1.38	0.17
Group [ICAS]:|ΔCTH|	-0.04	-0.07 – -0.01	-2.64	**0.01**
Group [ICAS]:|ΔCBF|	0	-0.02 – 0.03	0.05	0.96
Group [ICAS]:|ΔrCBV|	0.01	-0.01 – 0.02	0.64	0.53
Group [ICAS]:Age:|ΔCTH|	0	-0.01 – 0.00	-0.79	0.43
Group [ICAS]:Age:|ΔCBF|	0.01	0.00 – 0.01	2.51	**0.01**
Group [ICAS]:Age:|ΔrCBV|	0		0.2	0.84
Random Effects (Participants)				
σ^2	0.12			
$SD_{Intercept}$	0.18			
$SD_{\|\Delta CTH\|}$	0.07			
$SD_{\|\Delta CBF\|}$	0.07			
Corr.	-0.51			
	-0.16	0.66		
ICC	0.21			
$N_{Participant}$	55			
Observations	8716			

Note: Under predictors the variables incorporated in the model are listed. Categorical variables were deviation coded (Group: ICAS = 1, Controls = -1). Age was centered on the median age in the sample (participants with a median age equal 0 in the coding). The intercept estimate describes average BOLD-FC when all other predictor variables are 0, i.e. for all included participants of median age. Estimates for other variables indicate the estimated change in BOLD-FC

should the predictor value increase by 1 σ (e.g. a decrease of BOLD-FC by -0.12 for every 2.47 seconds CTH difference between the respective VOIs). Interactions between participant group and predictors are indicated by a colon, with the respective Group in square brackets. Confidence intervals for the estimates are indicated by CI. If no CI is indicated this means that the effect was always smaller than 0.001. The test statistic is derived from a one-sample t-test, against the null-hypothesis that the estimate does not differ significantly from 0. Effects for the healthy control group are identical to those of ICAS patients, except being reversed in polarity (Group coding for healthy participants = -1).

Influence of sex differences: In an additional model, I further controlled for sex differences (see **Table 4**), as effects of sex have been reported on parts of the NVC processes (Duque et al., 2017) and in particular on CBF (Alisch et al., 2021; Daniel et al., 1989). While I did not find a major impact of sex on the main outcomes, sex indeed moderated the association between age and the impact of |ΔCTH| on BOLD-FC. In particular, the CTH effect decreased minimally (on a level of the 3rd decimal) with increasing age for female participants but remained unaffected by age for male participants. This could be in-line with findings of a vanishing influence of sex on CBF with increasing age (Aanerud et al., 2017), given my sample of rather older adults.

Table 4. Summary of linear mixed model, LMM, analysis including sex.

Predictors	**Estimates**	**CI**	**Statistic**	***p***
Intercept	1.15	1.10 – 1.20	43.79	**<0.001**
Group [ICAS]	-0.03	-0.08 – 0.03	-0.96	0.34
Age	0	-0.00 – 0.01	1.02	0.31
Sex [Male]	0.05	-0.01 – 0.10	1.75	0.08
|ΔCTH|	-0.12	-0.15 – -0.09	-8.04	**<0.001**
|ΔCBF|	-0.05	-0.08 – -0.03	-3.92	**<0.001**
|ΔrCBV|	0	-0.02 – 0.02	-0.12	0.91
Age:|ΔCTH|	0.01	0.00 – 0.01	2.04	**0.05**
Age:|ΔCBF|	0	-0.01 – -0.00	-2.02	**0.05**
Age:|ΔrCBV|	0	-0.00 – 0.00	-1.48	0.14
Sex [Male]:|ΔCTH|	-0.03	-0.06 – 0.00	-1.81	0.08
Sex [Male]:|ΔCBF|	0	-0.02 – 0.03	0.25	0.81
Sex [Male]:|ΔrCBV|	-0.01	-0.03 – 0.01	-1.1	0.27
Sex [Male]:cAge	0	-0.01 – 0.01	0.1	0.92
Age:Sex [Male]:|ΔCTH|	-0.01	-0.01 – -0.00	-2.87	**0.00**
Age:Sex [Male]:|ΔCBF|	0	-0.00 – 0.01	0.94	0.35
Age:Sex [Male]:|ΔrCBV|	0	-0.00 – 0.01	1.9	0.06

Group [ICAS]:Age	-0.01	-0.01 – 0.00	-1.19	0.24
Group [ICAS]:Sex [Male]	0.04	-0.02 – 0.09	1.37	0.18
Group [ICAS]:|ΔCTH|	-0.04	-0.07 – -0.01	-2.94	**0.01**
Group [ICAS]:|ΔCBF|	0	-0.03 – 0.03	-0.01	0.99
Group [ICAS]:|ΔrCBV|	0.01	-0.01 – 0.02	0.98	0.33
Group [ICAS]:Age:|ΔCTH|	0	-0.01 – 0.00	-0.6	0.55
Group [ICAS]:Age:|ΔCBF|	0.01	0.00 – 0.01	2.44	**0.02**
Group [ICAS]:Age:|ΔrCBV|	0	-0.00 – 0.00	-0.02	0.98
Group [ICAS]:Sex [Male]*|ΔCTH|	0	-0.03 – 0.03	-0.06	0.95
Group [ICAS]:Sex [Male]:|ΔCBF|	-0.01	-0.04 – 0.02	-0.75	0.46
Group [ICAS]:Sex [Male]:|ΔrCBV|	0	-0.02 – 0.02	0.06	0.95
Group [ICAS]:Age:Sex [Male]	0	-0.01 – 0.01	0.1	0.92
Group [ICAS]:Age:Sex [Male]:|ΔCTH|	0	-0.00 – 0.01	0.56	0.58
Group [ICAS]:Age:Sex [Male]:|ΔCBF|	0	-0.01 – -0.00	-1.98	**0.05**
Group [ICAS]:Age:Sex [Male]:|ΔrCBV|	0	-0.00 – 0.00	-0.08	0.94
Random Effects (Participants)				
σ^2	0.12			
$SD_{Intercept}$	0.18			
$SD_{\|\Delta CTH\|}$	0.06			
$SD_{\|\Delta CBF\|}$	0.07			
Corr.	-0.55			
	-0.19	0.89		
ICC	0.21			
$N_{Participant}$	55			
Observations	8716			

Note: Under predictors the variables incorporated in the model are listed. Categorical variables were deviation coded (Group: ICAS = 1, Controls = -1; Sex: Male = 1, Female = -1). Age was centered on the median age in the sample (participants with a median age equal 0 in the coding). The intercept estimate describes average BOLD-FC when all other predictor variables are 0, i.e. for all included participants of median age. Estimates for other variables indicate the estimated change in BOLD-FC should the predictor value increase by 1 σ (e.g. a decrease of BOLD-FC by -0.12 for every 2.47 seconds CTH difference between the respective VOIs). Interactions between participant group and predictors are indicated by a colon, with the respective Group in square brackets. Confidence intervals for the estimates are indicated by CI. If no CI is indicated this means that the effect was always smaller than 0.001. The test statistic is derived from a one-sample t-test, against the null-hypothesis that the estimate does not differ significantly from 0. Effects for the healthy control group are identical to those of ICAS patients, except being reversed in polarity

(Group coding for healthy participants = -1) and vice versa for female participants (Group coding for female participants = -1).

2.2.2 Simulation results regarding the influence of CBF response timing on pairwise BOLD-FC

In order to facilitate understanding of how BOLD-FC depends on CBF response timing, results of BOLD-FC simulations are presented together with analyses of BOLD-TC characteristics. **Figure 2e** illustrates the relation for a neuronal input frequency of ν = 0.05 Hz. Compared to the healthy reference BOLD-TC simulated with τ_f = 2.0 sec (depicted in blue), faster CBF responses (τ_f < 2.0 sec, depicted in light grey) elicit higher BOLD signal changes and the periodic BOLD-TC signal is shifted to the left, corresponding to negative temporal lags. Slower CBF responses (τ_f > 2.0 sec, depicted in dark grey) on the other hand, cause positive temporal lags (i.e., signal shifts to the right) and less pronounced influence on ΔS_{BOLD}. Simulation results for the whole range of 16 characteristic CBF time constants (τ_f = [1.0,…, 8.0] sec, vertical axis) and ten neuronal input frequencies (ν = [0.01,…, 0.1] Hz, horizontal axis) are summarized via color-coded BOLD-TC amplitudes (**Fig. 8a**), temporal lags (**Fig. 8b**), and finally BOLD-FC (**Fig. 8c**) together with corresponding p-values (**Fig. 8d**).

Significantly positive BOLD-FC is observed in the lower left quarter of **Figure 8c**, where τ_f (for each investigated frequency), ranges around the healthy reference value (τ_f = 2.0 sec, framed in yellow). For the lowest investigated frequency (ν = 0.01 Hz), positive BOLD-FC values range up to τ_f = 5.5 sec, though with vanishing statistical significance (**Fig. 8d**). With increasing neuronal input frequency, the range of positive BOLD-FC drastically narrows to τ_f = [1.0, …, 2.5] sec at ν = 0.06 Hz, while at ν= 0.07 Hz and above, p-values indicate that correlations are no longer significant (**Fig. 8d**). Significantly positive BOLD-FC goes along with BOLD signal amplitudes similar to the reference (framed in yellow, **Fig. 8a**) and small positive or negative temporal lags compared to the reference (framed in yellow, **Fig. 8b**).

Significantly negative BOLD-FC is observed for longer characteristic time constants, being separated from the realm of positive BOLD-FC by a transition zone of vanishing BOLD-FC (**Fig. 8c**). The location of this transition zone is frequency dependent, it occurs at τ_f = 6.0 sec for ν = 0.01 Hz and drops to τ_f = 3.0 sec for ν = 0.07 Hz. At 0.07 Hz and above, negative BOLD-FC is hardly significant (**Fig. 8d**). Significantly negative BOLD-FC goes along with BOLD signal amplitudes rather higher than the reference (framed in yellow, **Fig. 8a**) and large positive temporal lags compared to the

reference (framed in yellow, **Fig. 8b**). Weakly significant negative BOLD-FC could also occur for very fast CBF responses (τ_f = 0.5 sec) at high neuronal input frequencies (ν = 0.09 Hz).

Together with information on timing aspects of the CBF response as obtained by the empirical analysis of multi-parametric MRI data, these BOLD-FC matrices can be used to interpret and explain empirical BOLD-FC results.

Together with information on timing aspects of the CBF response as obtained by the empirical analysis of multi-parametric MRI data, these BOLD-FC matrices can be used to interpret and explain empirical BOLD-FC results.

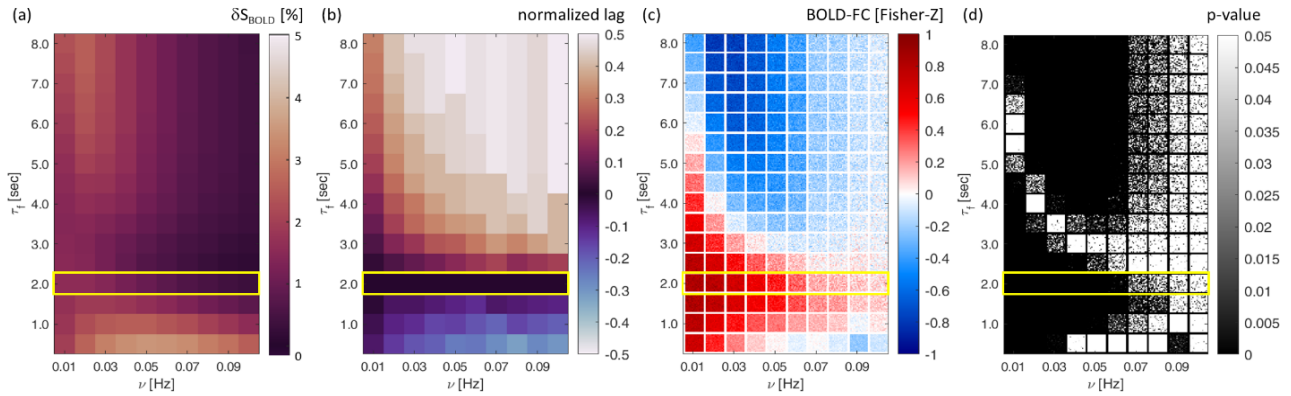

Figure 8. Matrix representations of BOLD-TC peak-to-peak amplitudes (a), normalized temporal lags (b), BOLD-FC (c) and corresponding p-values (d) across the range of investigated CBF characteristic time constants τf and neuronal input frequencies ν.

(a) Peak-to-peak amplitudes and (b) normalized temporal lags were determined from noise free resting state portions of the simulated BOLD-TCs (last 200sec) yielding one value per simulated (τ_f, ν) scenario. At each neuronal input frequency, the temporal lags between the respective reference BOLD-TC (framed in yellow at τ_f = 2.0 sec) and the target BOLD-TCs with τ_f = [0.5 … 8.0] sec were determined via cross correlation and normalized by the period of the neuronal input frequency, resulting in normalized lags between -0.5 and 0.5. (c) BOLD-FC and (d) p-values values at each neuronal input frequency were obtained by calculating Z-transformed Pearson's correlation coefficients between the resting portions (last 200 sec) of the selected reference seed BOLD-TC (framed in yellow at τ_f = 2.0 sec) and the target BOLD-TCs across the entire range of BOLD-TCs with τ_f = [0.5 … 8.0] sec. Insignificant correlations (at $p < 0.05$) appear white in panel (d). Individual squares in panels (c) and (d) appear noisy because the seed and target BOLD-TCs were complemented with random white noise prior to BOLD-FC calculation achieving SNR_0 = 250 in the baseline portions of the signal. 16x16 different random white-noise realizations were used for each pair of investigated parameter values, constituting the individual squares in panels (c) and (d). Abbreviations: δS_{BOLD}: percentage peak-to-peak BOLD amplitude.

2.3 Interim discussion of Project 1

In order to test the hypothesis that capillary transit time heterogeneity, CTH, influences BOLD-FC and may serve as an indicator for broadened and delayed CBF responses, I used a combined empirical and theoretical approach. (i) My empirical analysis of multi-parametric hemodynamic MRI data of asymptomatic high-grade unilateral ICAS patients and healthy controls demonstrates significant reductions of BOLD-FC with increasing CTH differences between homotopic brain areas that were significantly more pronounced in ICAS patients. Crucially, due to largely preserved neuronal functioning in asymptomatic ICAS, ,my results demonstrate that CTH differences between homotopic brain areas can explain BOLD-FC reductions independent from changes in neuronal activity. (ii) The theoretical simulation-based approach revealed that an increase in the characteristic time constant τ_f of blood flow responses induces delays and broadening of the CBF response, which in turn is associated with significant changes in BOLD-FC, including sign shifts from positive to negative. (iii) Linking empirical and theoretical findings, simulation results of BOLD-FC variability as a function of CBF response timing variability fit my empirical findings of CTH impact on BOLD-FC, suggesting that CTH may serve as an indicator of CBF response timing.

This is the first study demonstrating local CTH impacts on BOLD-FC in humans. Furthermore, results support the interpretation of CTH as a surrogate marker of local perfusion temporal response characteristics. In summary, results suggest that perfusion response delay and broadening impact on BOLD-FC independently from neuronal changes.

2.3.1. Empirical findings reveal NVC impact on BOLD-FC

2.3.1.1 CTH and its impact on BOLD-FC

I observed that BOLD-FC is significantly predicted by CTH differences between homotopic cortical VOI pairs. Specifically, BOLD-FC correlations between homotopic brain regions' BOLD-TCs decreased when |ΔCTH| increased (**Fig. 7a**). Moreover, the observed effect was both significantly stronger in patients with ICAS than healthy controls and independent of age.

Physiologically, CTH describes the distribution of red blood cell capillary transit times, where an increase in CTH corresponds to a broadening of this distribution (Jespersen & Østergaard, 2012). Based on relations between distributions of relative flow rates and capillary transit times (Østergaard et al., 1999), we assume that such broadening necessarily also causes a delayed CBF response, which lead us to propose CTH as a marker for τ_f (see rationale in section '*2.1.2*

Theoretical considerations regarding the link between CTH and CBF response'). In previous simulation studies, it has already been demonstrated that CTH influences CBF and BOLD responses in brain activation studies (Angleys et al., 2018; Rasmussen et al., 2015), yielding results consistent with experimental findings in small animal studies (Rasmussen et al., 2015). The influence of CTH on BOLD-FC has not yet been examined in human rs-fMRI studies so far but CTH increases have been demonstrated in neurodegenerative and vascular diseases, which are known to suffer from impaired cerebral oxygen supply (Mundiyanapurath et al., 2016; Nielsen et al., 2020; Potreck et al., 2019; Schneider et al., 2022). Furthermore, there is some evidence that CTH eventually impedes cerebral oxygen supply in neurodegenerative and vascular diseases (Arsava et al., 2018; Østergaard, Aamand, et al., 2013; Østergaard et al., 2016; Østergaard, Jespersen, et al., 2013).

In our patients with asymptomatic ICAS, elevated CTH in the hemisphere ipsilateral to the stenosis is not accompanied by alterations in oxygen extraction fraction (OEF) (Kaczmarz et al., 2021; Figures 3 & 4). Furthermore, CBF and CMRO2 ipsilateral to the stenosis are comparable to healthy controls, while contralateral values are significantly higher in ICAS patients (Göttler et al., 2020; see Figure 3 of Göttler, Kaczmarz, et al., 2019). In the healthy subjects of our study cohort, we did not find general hemispheric CTH differences, in line with their overall intact perfusion status (Kaczmarz et al., 2021), but detailed regional analysis revealed that CTH differences between homotopic regions nevertheless exist across the brain – even though to a lesser degree than in asymptomatic ICAS patients (**Fig. 3f**, **j**; see **Fig. 4 & 5** for detailed regional analysis). Accordingly, the CTH effect on BOLD-FC for the healthy participant group might be underestimated, explaining the significant interaction between group and |ΔCTH| on BOLD-FC. Nevertheless, systematic group differences in the relation between |ΔCTH| and BOLD-FC exist, possibly due to intact compensatory mechanisms in the healthy vascular-hemodynamic system. Cerebrovascular reactivity could be a potential candidate for such a mechanism, as impaired CVR has also been shown in our cohort of asymptomatic ICAS patients (Kaczmarz et al., 2021). Interestingly, CVR is not only reduced ipsilateral to the stenosis compared to the unaffected contralateral side, but also bilaterally compared to healthy controls (see Figure 3 in Kaczmarz et al., 2021). Since an intact CVR is necessary for healthy blood flow responses to increased neuronal activity (De Vis et al., 2015; D'Esposito et al., 2003; Lewis et al., 2020; Mark et al., 2015; van Niftrik et al., 2019), weak physiological differences in CTH might be compensated by an intact CVR.

The question of which possible hemodynamic and physiological processes might underpin the effect of CTH increases on BOLD-FC decreases will be discussed below using our simulation results for interpretation.

2.3.1.2 Baseline perfusion, namely CBF and rCBV, and its impact on BOLD-FC.

Reductions in BOLD-FC were also related to increasing cross-hemispheric differences in local baseline CBF (**Fig. 7b**) but not to differences in rCBV (**Fig. 7c**). In contrast to CTH, there were no ICAS group specific effects of |ΔCBF| on BOLD-FC, but age had a small and significant effect. In my cohort of asymptomatic ICAS patients, increases in |ΔCBF| and |ΔrCBV| correspond to reduced CBF and increased CBV ipsilateral to the stenosis (see Figure 3 in Kaczmarz et al., 2021). The ICAS patients' average |ΔCBF|, but not |ΔCTH| and |ΔrCBV|, increased weakly but significantly with the degree of stenosis (**Fig. 6**). Since hemodynamic impairments strongly depend on the individual vascular anatomy, mainly collateralization across the circle of Willis (Kaczmarz et al., 2018; Richter et al., 2017), this weak dependence fits my expectation. In ICAS patients, reductions in microvascular perfusion (i.e., baseline CBF) and accompanying, compensatory increases in rCBV ipsilateral to the stenosis (Kaczmarz et al., 2021) are supposed to result from a reduced cerebral perfusion pressure (Powers, 1987; Schroeder, 1988). While the healthy controls do not show global baseline CBF and rCBV differences between hemispheres (Kaczmarz et al., 2021), my regional analysis still revealed small but significant pairwise differences for baseline CBF (**Fig. 3g,k**) and rCBV (**Fig. 3h,l**), albeit to a significantly lower degree as compared to ICAS patients (see **Fig. 4 & 5** for a detailed regional analysis).

Concerning the significant influence of baseline CBF on BOLD-FC, my result is in line with several previous findings. For example, BOLD-FC was found to be significantly correlated with regional baseline CBF in functional brain network hubs (Liang et al., 2013) and coupled to regional baseline CBF (Z. Li et al., 2012). Using a scaling approach, first proposed by Qiu et al. (2017), Champagne et al. (2020) demonstrated recently that accounting for regional differences in baseline CBF reduced the difference in BOLD-FC patterns observed between patients with mild traumatic brain injury and healthy controls.

Concerning the relatively stronger |ΔCTH| than |ΔCBF| effect on BOLD-FC, my results suggest a link among previously separate findings. In patients with Alzheimer's disease, not only aberrant CTH has been demonstrated (Nielsen et al., 2020; Østergaard, Aamand, et al., 2013), but also an impact of reduced baseline CBF on BOLD-FC (Göttler, Preibisch, et al., 2019). In ICAS patients, I

similarly found aberrant CTH and impact of reduced baseline CBF on BOLD-FC but also increased rCBV (see Figure 3 in Kaczmarz et al., 2021). Thus, I suggest more generally, that brain disorders of subtle but chronic hypo-perfusion, which are likely accompanied by chronic compensatory vasodilation, are at higher risk for CTH alterations. Based on our results of relatively smaller effects of |ΔCBF] compared to |ΔCTH|, the relevance of CTH alterations seems to be higher for BOLD-FC, than the influence of baseline perfusion. This might be explained by an inherently larger extent of CTH changes than those of baseline CBF and compensatory rCBV changes. This explanation is inspired by our finding in asymptomatic ICAS patients, namely that CTH increases ipsilateral to the stenoses are much more widespread than those of baseline CBF and rCBV, which are rather restricted to vascular border zone areas (Kaczmarz et al., 2021). In any case, the simultaneous and strongly correlated impact of both CTH and baseline CBF on BOLD-FC accords with an inherent link between these variables (Jespersen & Østergaard, 2012).

Finally, the small moderating effect of age on the influence of CBF, with stronger effects in healthy older subjects, could hint at a loss of compensatory factors countering the detrimental effects of CBF differences with progressing age. Given the widespread impact of age on various hemodynamic-vascular processes and thus NVC (Beishon et al., 2021), a larger moderating effect could be expected in a sample with a larger age range. The negligible effect of age among ICAS patients on the other hand, fits with my assumption of already depleted compensatory factors.

2.3.2 Simulations reveal CBF timing impact on BOLD-FC

Our simulations of BOLD-FC across a range of characteristic time constants τ_f demonstrate the dependency of BOLD-FC on delayed and broadened CBF responses. For a purely sinusoidal neuronal input of 0.05 Hz, we found diminished BOLD-FC for characteristic CBF time constants deviating more than a second from the healthy reference at τ_f = 2 sec. Regarding slower CBF responses, BOLD-FC is already clearly reduced for τ_f = 2.5 sec, turning largely insignificant for τ_f = 3.0 sec, and finally getting negative for τ_f > 3.0 sec (see **Fig. 8c & d**). This behavior can be well explained by an increasingly positive lag with increasing τ_f, where bright colors in **Figure 8b** indicate that the target BOLD-TCs for τ_f > 6.5 sec are almost in opposite phase to the reference BOLD-TC (at τ_f = 2.0 sec).

The result of diminished BOLD-FC fits with our empirical results as well as with a number of rs-fMRI studies that demonstrated decreased rs-fMRI-based BOLD functional connectivity in patients with vascular diseases including ICAS (Avirame et al., 2015; T.-Y. Chang et al., 2016; Cheng et al., 2012;

C.-J. Lin et al., 2014; T. Wang et al., 2017), but also in neurodegenerative diseases, depression and schizophrenia (Brandl et al., 2019; Manoliu et al., 2014; Zhou et al., 2010; Zhou & Seeley, 2014). All these disorders have also been associated with perfusion deficits (Göttler et al., 2020; Göttler, Preibisch, et al., 2019; Kaczmarz et al., 2021; Katsel et al., 2017; Love & Miners, 2016). In addition and highly interestingly, negative BOLD-FC has been observed in a range of different brain disorders from Alzheimer's disease or Frontotemporal Dementia (Nuttall et al., 2016; Zhou et al., 2010) to schizophrenia (Damaraju et al., 2014; Manoliu et al., 2014), all of which have been associated with significant perfusion deficits (Katsel et al., 2017; Love & Miners, 2016). Typically, negative BOLD-FC has been explained by potential effects of either global signal changes (C. Chang et al., 2016; Schölvinck et al., 2010; Turchi et al., 2018) or problematic pre-processing of rs-fMRI data with respect to the global grey matter BOLD signal such as global signal regression (Liu et al., 2017; Murphy & Fox, 2017; Power et al., 2012; Siegel et al., 2014). However, our simulation results shed new light on that issue, offering effects of impaired neurovascular coupling, such as local perfusion delays, as a possible explanatory mechanism for the emergence of negative BOLD-FC. Thus moving the field forward in the understanding of a phenomenon that has proven challenging and has thus been largely ignored so far.

Exploring the frequency dependence of BOLD-FC, we performed simulations for neuronal inputs between 0.01 Hz and 0.1 Hz (**Fig. 8**). Again, observed BOLD-FC changes at different input frequencies ν can be explained by the interplay of changing peak-to-peak amplitudes (**Fig. 8a**) and temporal lags/phase shifts (**Fig. 8b**). Areas of diminished BOLD-FC (in the (τ_f, ν) parameter space) either overlap with areas of low to vanishing BOLD-TC amplitudes (see **Fig. 8a**) or coincide with relevant lags (see **Fig. 8b**). Strong positive BOLD-FC (**Fig. 8c**) is observed where high peak-to-peak amplitudes coincide with temporal lags around zero, indicating that the BOLD-TCs of seed and target regions are in phase. Significantly negative BOLD-FC values are observed in parts of the parameter space, where the BOLD-TCs are shifted by about half a period where the BOLD-TCs in the seed and target region are roughly in opposite phase. Remarkably, the area with low and diminished BOLD-FC in the parameter space extends with increasing input frequency and shrinks with decreasing input frequency, compared to the middle input frequency of 0.05Hz (see **Fig. 8c**). This finding implies a filter effect of NVC, in a sense that low frequency neuronal input (< 0.05 Hz) appears more likely to produce positive BOLD-FC than high frequency neuronal input (> 0.05 Hz). This simulation-based finding fits very well with a recent experimental observation (Siegel et al., 2016). In a cohort of patients with subacute stroke, the authors found a decrease of BOLD signal

power with frequency in non-lesioned brain areas that exhibited significant lags in the BOLD signal. Interestingly, brain areas without and with lag, respectively, showed comparable BOLD signal power between 0.01 and 0.04 Hz. At higher frequencies (0.04 to 0.09 Hz) the overall power decreased, but was significantly lower in areas exhibiting a lag in BOLD signal (see Figure 2 in Siegel et al., 2016). This finding provides evidence for a low pass filter effect of NVC whose efficiency increases in the presence of perfusion delays. However, it has to be noted that Siegel et al. investigated the dependence of BOLD-FC on systemic BOLD signal time lags instead of timing aspects of local NVC as in our current study. However, systemic perfusion delays are well known to occur in vascular diseases, as is the case in our cohort of asymptomatic ICAS patients (Kaczmarz et al., 2021). Thus, further studies are clearly needed to disentangle the effects of local and systemic perfusion delays.

2.3.3 Linking empirical and simulation results of local NVC impact on BOLD-FC

2.3.3.1 CTH and CBF responses

As outlined in methods section '2.1.2 Theoretical considerations regarding the link between CTH and CBF response', we suggest that increased CTH could serve as a marker for broadened and delayed CBF responses. Based on this kind of 0th-order approximation, the simulation model might help us to understand how timing aspects of the CBF response influence BOLD-FC. In accordance with previous work, we assumed a normal CMRO2 response with τ_m = 2 sec (Archila-Meléndez et al., 2020). An equally fast and narrow CBF response with τ_f = 2 sec causes a positive BOLD signal change when the delivery of oxygen surpasses its consumption. In our simulations, this condition is well met by assuming CBF and CMRO2 response amplitudes of 50% and 25%, respectively. When the CBF response is now delayed and broadened – while keeping the absolute amount of delivered blood constant – the delivery of oxygenated blood is stretched across a longer period of time, resulting in a diminished short-term delivery of oxygen and in turn, a diminished positive BOLD response. With increasing τ_f, the peak CBF response is increasingly delayed and the maximum amplitude diminished so that at a certain point, the oxygen consumption, i.e., the simulated normal CMRO2 response, surpasses the oxygen delivery, eventually resulting in an increase of deoxyhemoglobin and thus a negative BOLD response and consequently also a negative BOLD-FC. The point in parameter space where exactly this happens depends on the frequency of the neuronal input (see **Fig. 8c**) but also on the assumptions with regard to the reference seed.

In general, my empirical finding of decreasing BOLD-FC with increasing |ΔCTH| between VOI pairs, fits very well with our simulation result of decreasing BOLD-FC with increasing τ_f, particularly if one accepts a link between CTH and CBF response timing. As discussed above, in our sample of asymptomatic ICAS patients, an increase in |ΔCTH| corresponds to CTH increases ipsilateral to the stenosis. As the reference seed BOLD-TC was chosen to represent a 'healthy' NVC response, BOLD-FC values with increasing τ_f correspond to situations with increasingly delayed and broadened CBF responses in an impaired target region. This corresponds to the situation in our asymptomatic ICAS patients, where CTH is increased in VOIs ipsilateral to the stenosis compared to the contralateral (healthy) VOIs. As we can see in **Figure 8** across the range of simulated frequencies, BOLD-FC decreases with increasing τ_f across the entire range of simulated frequencies, which perfectly fits our empirical results, where we found that unilateral CTH increases cause decreases in pairwise homotopic BOLD-FC. Thus, it appears plausible to consider CTH as an indicator for the CBF response's characteristic time constant τ_f, where |ΔCTH| roughly relates to differences in characteristic time constants τ_f, which causes phase shifts and amplitude modulations between BOLD-TCs in paired homotopic VOIs. BOLD-FC between pairwise VOIs is in turn diminished even though neural activity is most likely largely comparable across homotopic VOI pairs as discussed above.

As indicated by my empirical analysis, BOLD-FC is also influenced by baseline values of CBF. However, baseline CBF is not explicitly considered in our simulation approach. All changes are simulated relative to a normalized baseline. What actually matters are the changes relative to this baseline, and in this respect, it would be important to know if and how baseline CBF influences the CBF response amplitude. Since increased rCBV as well as reduced CVR have been detected in our cohort of asymptomatic ICAS patients (Kaczmarz et al., 2021), it is likely that reduced baseline CBF is often accompanied by a reduced CBF response amplitude, which according to our previous simulations also predicts reduced BOLD-FC (Archila-Meléndez et al., 2020). However, one should be aware that this is not necessarily the case (Amemiya et al., 2012; Powers et al., 1988; Siero et al., 2015).

With respect to rCBV, my empirical analyses did not show a significant influence. This again fits with our simulations because the assumed slow CBV response acts to dampen the influence of CBV in the presence of fast oscillatory neuronal activity as can be seen in **Figure 2b** and has been discussed in detail previously (Archila-Meléndez et al., 2020).

3.3.3.2 Pathophysiology of local NVC in ICAS and its impact on BOLD-FC

The ICAS patients included in my study showed mild to moderate capillary dysfunction, which, beyond increases in CTH, manifested in reduced baseline CBF and CVR as well as elevated rCBV (Kaczmarz et al., 2021) with ipsilateral CMRO2 comparable to healthy controls (Göttler, Kaczmarz, et al., 2019). Mean grey matter CTH was found to be about 2.8 sec in healthy elderly (Kaczmarz et al., 2021) and mean CTH differences between VOI pairs are about 0.9 sec and 0.7 sec for ICAS patients and healthy controls, respectively (with a small fraction of VOIs showing lager |ΔCTH| values up to ≈ 3s sec). These values indicate that in the majority of voxels pathological CBF responses in ICAS patients do not differ too much from the reference seed assumed in our simulation approach. This means that the simulated τ_f range exceeds the pathophysiological range in ICAS patients by far.

The reduction in baseline CBF certainly also plays a role, especially in combination with the observed ipsilateral rCBV increase, indicating potentially chronic compensatory vasodilation and simultaneously reduced CVR, which has indeed been demonstrated on group level (Kaczmarz et al., 2021). According to our previous simulation study (Archila-Meléndez et al., 2020) and results from other groups (D'Esposito et al., 2003; Göttler, Kaczmarz, et al., 2019; Lewis et al., 2020; Mark et al., 2015; van Niftrik et al., 2019, intact CVR is an important prerequisite of BOLD fMRI studies not only in the resting state.

Finally, as CTH is expected to depend on baseline CBF (Jespersen & Østergaard, 2012), ICAS patients might also be affected from an inability to reduce CTH in response to neuronal activity that has been observed in animal studies (Jespersen & Østergaard, 2012; Kleinfeld et al., 1998; Schulte et al., 2003; Stefanovic et al., 2008).

2.3.4 Limitations

There are several shortcomings for this Project, which have to be acknowledged. In the following, I list these limitations together with a brief discussion point-by-point.

Multi-parametric hemodynamic MRI: With respect to ASL, there are a number of known issues with regard to regional differences in arterial transit times, which potentially impede baseline CBF quantification with single-PLD ASL, especially in elderly subjects and patients with vascular diseases (Göttler, Preibisch, et al., 2019; Kaczmarz et al., 2021). We tried to minimize respective bias by using a PLD of 2000 ms as recommended (Alsop et al., 2015) and carefully checked data for

arterial transit time artefacts (Kaczmarz et al., 2021). In addition, reduced labeling efficiency due to increased flow velocities in the stenosed vessel (Chen et al., 2017) as well as reduced compliance in patients could impact on CBF data quality. Furthermore, I included pCASL data with 2D EPI readouts in 15 subjects because pCASL with 3D GRASE readout was either not available (6 subjects) or rated of inferior quality. While these deviant data were distributed evenly between groups and a rating-based group comparison of CBF data quality (data not shown) does not indicate significant group differences, I cannot exclude that measurement accuracy and SNR could potentially influence the results of my analyses. Similarly, there are a number of known issues with DSC MRI, starting from the valid definition of an arterial input function to potential influences of contrast agent leakage effects (Hedderich et al., 2019; Kluge et al., 2016). Likewise, CTH calculation relies on a number of assumptions that might not necessarily be fulfilled (Kaczmarz et al., 2021; Mouridsen et al., 2014). In addition, contrast agent application in itself is potentially problematic due to contrast agent accumulations (Kanda et al., 2015).

Analysis of BOLD-FC predictors: Since BOLD signal is well known to be confounded by numerous influences, I included several control variables in my analysis. Importantly, I included age because detrimental effects of age on BOLD-FC have been repeatedly demonstrated (Farras-Permanyer et al., 2019; Varangis et al., 2019) and sex because it has been found to influence cerebral blood flow and metabolism (Aanerud et al., 2017; Alisch et al., 2021; Daniel et al., 1989; Duque et al., 2017). An analysis regarding sex differences in CTH did not reveal a significant effects in my subject cohort (data not shown). Other potentially confounding participant traits, e.g., hypertension or diabetes, were clearly associated with the grouping structure, i.e., more prevalent in ICAS patients (see **Table 1**), which prevented individual inclusion due to multicollinearity. Thus, I included the factor group as an overarching control variable, also to avoid fitting an overly complex model. While such variables could, therefore, have an individual impact on BOLD-FC or moderate the influence of NVC differences in BOLD-FC, the present study design is not suited to disentangle such individual effects. The larger impact of |ΔCTH| on BOLD-FC for ICAS patients could therefore also be related to additional factors associated with ICAS, beyond an impaired CTH. However, hypertension was found to be associated with both BOLD hyper-and hypo-connectivity only for few selected regions (Carnevale et al., 2020; Feng et al., 2020; Son et al., 2015). Blood pressure likewise has been found to only impair the BOLD signal under conditions of rapid change (Kalisch et al., 2001; Reimann et al., 2018). Even though CVR, besides CBF and CBV, is well known to influence the BOLD signal

(Archila-Meléndez et al., 2020), I decided not to include CVR for mainly two reasons: (1) sufficient quality breath-hold CVR data are only available from about two thirds of my study participants, (2) missing endtidal CO2 data restrict analysis to purely qualitative statistical maps. However, the additional influence of CVR is an important factor that needs to be addressed in future studies.

My model explains 23% of the BOLD-FC variance, clearly indicating that further factors impact BOLD-FC. Among these, cardiac and respiratory pulsations are best known (Beall & Lowe, 2007; Yoshikawa et al., 2020) but more recently, influence of systemic perfusion delays has also been demonstrated, e.g., in Moyamoya disease, stroke, stenosis patients and even healthy controls (Christen et al., 2015, p. 20; Y. Lv et al., 2013; Siegel et al., 2016; Tong et al., 2017; Tong, Yao, et al., 2019). Beyond that, intrinsic local fluctuations in arteriole diameter, partially independent from resting-state neural activity, may drive blood flow oscillations and impact on BOLD-FC (Mateo et al., 2017; Winder et al., 2017). Likewise, the global brain signal, which I decided not to regress out certainly has an impact on BOLD-FC (Liu et al., 2017). Further factors include motion not detected by common motion regression procedures (Beall & Lowe, 2014). Lastly simply spontaneous differences in the underlying neuronal activity would lead to reduced BOLD-FC as well.

BOLD-FC modelling and the link between CTH and CBF response timing: A major strength of our simulation approach is that it allows detailed simulations regarding the impact of NVC impairments on BOLD-FC. The most important general issues about the validity of our approach have already been discussed (Archila-Meléndez et al., 2020).

As outlined above, our simulations demonstrate that delayed and broadened CBF responses can explain reductions of BOLD-FC independent of reductions in neuronal activity. With regard to experimental evidence, we proposed a link between CTH increases and broadened and delayed CBF responses. This appears plausible on a qualitative level, however, for future studies, our simulation model clearly needs to be developed further. To establish a firm link between BOLD-FC and measurable physiological parameters in humans, an improved model needs to consider the interplay of MTT, CTH, CBV and CBF (Østergaard et al., 1996, 1999) as well as the complexities introduced by the effects of CTH on brain oxygenation (Jespersen & Østergaard, 2012) and in particular BOLD responses (Angleys et al., 2018; Rasmussen et al., 2015). Moreover, the influence of the baseline physiology has been neglected in this study because OEF was unimpaired in our sample of ICAS patients (Kaczmarz et al., 2021) and statistical analysis did not indicate influence of CBV (**Fig. 7c**). However, future studies need to consider that BOLD signal changes also depend on

baseline physiology, in particular OEF and venous blood volume (Archila-Meléndez et al., 2020; Obata et al., 2004).

In addition, ICAS patients feature additional hemodynamic impairments, most importantly reductions in CVR and CBF, which could explain BOLD-FC reductions equally well. While my statistical analysis supports the view that the influence of CTH is stronger than the influence of baseline CBF, I cannot completely rule out that CVR might play an important role as well. This point certainly also needs further investigation based on high quality multi-parametric MRI data and more specific and detailed modelling.

2.3.5 Conclusions

My empirical results demonstrate that increasing CTH differences between homotopic brain areas lead to BOLD-FC reductions, which can be well explained by our simulation results when considering increased CTH as an indicator of delayed and broadened CBF responses. Given these complex and non-linear influences as well as variable sources of vascular delays, i.e., macrovascular systemic as well as local microvascular contributions, I suggest that calibration approaches like linear regression of BOLD-TCs with vascular noise predictors (Christen et al., 2015; Erdoğan et al., 2016; Liu et al., 2017; Siegel et al., 2016) are not sufficient to fully recover information on underlying neuronal activity. I suggest to overcome the limitations of conventional rs-fMRI-based BOLD-FC analyses by combining our recent BOLD-FC simulation approach (Archila-Meléndez et al., 2020) with comprehensive hemodynamic-oxygenation MRI, i.e., CVR, CBF, CBV and OEF, to aid the interpretation of BOLD-FC alterations in patient populations.

3. Project 2: Comparison of influence on BOLD-FC by local and systemic hemodynamic-vascular parameters

Results of this Project have previously been published as an original research article in NeuroImage, 281, in 2023 (Schneider et al., 2023) with chapters 3.1 to 3.3 of this thesis adapted from this publication:

Schneider, S. C., Kaczmarz, S., Göttler, J., Kufer, J., Zott, B., Priller, J., Kallmayer, M., Zimmer, C., Sorg, C., & Preibisch, C. (2023). Stronger influence of systemic than local hemodynamic-vascular factors on resting-state BOLD functional connectivity. *NeuroImage*, *281*, 120380. https://doi.org/10.1016/j.neuroimage.2023.120380

3.1. Methods of Project 2

My investigations are based on data from the same quantitative multimodal MRI study in asymptomatic unilateral ICAS patients and healthy controls (HC) as Project 1 (Schneider et al., 2022). For this project, I analyzed rs-fMRI for estimation of BOLD-FC and BOLD time lags, dynamic susceptibility contrast (DSC) MRI for estimation of TTP, relative CBV (rCBV) and CTH, and pseudo-continuous ASL (pCASL) for estimation of CBF.

3.1.1 Participants

From a previously analyzed sample of 29 ICAS patients and 30 healthy controls (Göttler et al., 2020; Göttler, Kaczmarz, et al., 2019; Kaczmarz et al., 2021; Schneider et al., 2022), I analyzed a subsample of 51 participants, 26 ICAS patients (10 females) and 25 controls (14 females), from whom all necessary data existed in sufficient quality. Overall 4 participants from Project 1 (Schneider et al., 2022) had to be excluded due to either bad or missing data. Healthy elderly controls were age-matched to ICAS patients. Median age across ICAS patients and HC in the present study sample was 72 years (range: 52 to 84 years). All participants underwent neuro-radiological, neurological, psychiatric, cognitive and kidney function testing to ensure inclusion criteria. The study was approved by the medical ethical board of the Klinikum rechts der Isar of the Technical University of Munich; all participants provided written informed consent to all conducted examinations. For a detailed description of the overall sample characteristics see **Table 5**.

Table 5. Summary of participant characteristics for Project 2 and 3.

Parameter	**Control (N=25)**	**ICAS (N=26)**	***p***
Age [years]: mean (SD)	70.4 (4.9)	70.3 (7.3)	0.94
Sex – female: N (%)	14 (56.0%)	10 (38.5%)	0.21
Side of stenosis – left: N (%)	-	11 (39.3)	
Stenotic degree (% NASCET): mean (SD)	-	81% (10%)	
BMI: mean (SD)	27.2 (4.2)	25.9 (4.8)	0.31
Smoking [packs per year]: mean (SD)	7.1 (12.5)	13.3 (18.7)	0.18
Fazekas: mean (SD)	0.9 (0.9)	1.5 (0.8)	**0.01**
PAOD: N (%)	3 (12.0%)	8 (30.8%)	0.1
CHD: N (%)	2 (8.0%)	8 (32.0%)	**0.03**
Hypertension: N (%)	15 (60.0%)	20 (76.9%)	0.19
BP [mmHG]			
- systolic: mean (SD)	142 (19.3)	153.6 (25.3)	0.08
- diastolic: mean (SD)	85.1 (7.1)	85.5 (10.3)	0.86
Diabetes: N (%)	2 (8.0%)	5 (20.0%)	0.22
Statins: N (%)	5 (20.0%)	18 (69.2%)	**< 0.001**
Antiplatelets: N (%)	5 (20.0%)	23 (88.5%)	**< 0.001**
Antihypertensives: N (%)	11 (44.0%)	17 (65.4%)	0.13
Antidiabetics: N (%)	2 (8.0%)	2 (7.7%)	0.97
MMSE: mean (SD)	28.6(1.4)	28.3 (2.4)	0.61
TMT-A: mean (SD)	42.7 (13.2)	49.9 (24.3)	0.2
TMT-B: mean (SD)	104 (40.8)	139.2 (66.4)	**0.03**
LBT [abs. % deviation from center]: mean (SD)	3.1 (1.8)	2.3 (2.2)	0.18
BDI: mean (SD)	8.3 (5.3)	8.4 (8.2)	0.96
STAI: mean (SD)	35 (10.5)	37.9 (10.4)	0.34

Note: Variables are represented by either mean and standard deviation (SD) or absolute number N and fraction in percent. Two-sample t-tests were used for group comparisons in age, mean pack-years, BP, BMI, MMSE, TMT-A/B, BDI, STAI, and LBT; Chi-squared test for remaining group comparisons. Bold print indicates significant group differences $p < 0.05$. Abbreviations: BMI, body mass index; PAOD, peripheral artery occlusive disease; CHD, coronary heart disease; BP, blood pressure; MMSE, mini mental state exam; TMT-A/B, trail making test-A/B; LBT, line bisection test; BDI, Beck's depression inventory; STAI, state trait anxiety inventory.

3.1.2 MRI data acquisition

As for Project 1 (Schneider et al., 2022), MR imaging was performed on a 3T Philips Ingenia MR-Scanner (Philips Healthcare, Best, The Netherlands). Anatomical imaging comprised a T1-weighted magnetization prepared rapid gradient echo (MPRAGE; TE = 4 ms, TR = 9 ms, α = 8°, TI = 1000 ms, shot interval = 2300 ms, SENSE AP/RL 1.5/2.0, 170 slices, matrix size = 240x238, voxel size = 1x1x1 mm^3) and a T2-weighted fluid attenuated inversion recovery (FLAIR; TE = 289 ms, TR = 4800 ms, inversion delay = 1650 ms, TSE factor = 167, 163 slices, matrix size = 224x224, voxel size = 1.12 mm^3 isotropic). BOLD-FC and BOLD temporal lags were derived from T2*-weighted multiband echo planar imaging (EPI) time series (TE = 30 ms, TR = 1.2 s, α = 70°, multiband factor 2, SENSE factor 2, 38 slices, matrix size = 192x192, voxel size = 3x3x3 mm^3, 500 dynamic scans, scan duration 10 min). TTP, rCBV and CTH were derived from DSC MRI (80 single-shot EPI volumes, TE = 30 ms, TR = 1513 ms, α = 60°, 26 slices, voxel size = 2.0x2.0x3.5 mm^3, bolus injection of Gd-Dota with a concentration of 0.5 mmol/ml, a dose of 0.1 mmol/kg and at least 7.5 mmol per subject). Pseudo-continuous arterial spin labeling (pCASL) acquisitions (post label delay (PLD) = 2000 ms, label duration = 1800 ms, 16 slices) were evaluated for baseline CBF. From the pCASL data that were acquired for sequence comparisons (Kaczmarz et al., 2016), I included for each subject the highest quality CBF data. For 36 subjects, a 3D gradient spin echo (GRASE) readout with 4 background suppression (BGS) pulses, TE/TR/α = 7.4 ms/ 4377 ms/90°, turbo spin echo factor 19, EPI factor 7, voxel size = 2.75x2.75x6 mm^3 was employed. For the remaining subjects, a 2D EPI readout with similar acquisition parameters was used, with either 4 BGS pulses (6 subjects), 2 BGS pulses (7 subjects), or no BGS (1 subject).

3.1.3 BOLD signal preprocessing

The BOLD fMRI data was minimally preprocessed with the Data Processing Assistant for Resting-State fMRI advanced edition (DPARSFA) toolbox V5.0_200401 (Yan, C.G. & Zang, Y.F., 2010) and SPM12 (v7771; Wellcome Trust Centre for Neuroimaging, UCL, London, UK) using MATLAB (R2019b; MathWorks, Natick, MA, USA). Preprocessing included removal of the first ten volumes to reach steady-state magnetization, spatial realignment of acquired EPI volumes, slice time correction, reorientation to the anterior-posterior commissure (AC-PC), a nuisance covariate regression including six motion parameter and a linear trend, 6mm full width at half maximum (FWHM) smoothing and lastly temporal bandpass filtering from 0.01 to 0.1 Hz.

The anatomical images were initially neck cropped and then co-registered with the functional images, which was followed by segmentation using Diffeomorphic Anatomical Registration Through Exponentiated Lie Algebra (DARTEL; Ashburner, 2007).

3.1.4 Calculation of hemodynamic-vascular parameter maps

Parameter maps were calculated and spatially coregistered with custom MATLAB programs (R2016b; MathWorks, Natick, MA, USA) and SPM12 (Wellcome Trust Centre for Neuroimaging, UCL, London, UK) as previously described in detail (Kaczmarz et al., 2021; Schneider et al., 2022). In short, TTP, rCBV and CTH were derived from DSC data. Relative CBV was calculated by integrating the leakage corrected concentration time curve that was derived from DSC data (Hedderich et al., 2019; Kluge et al., 2016). Resulting rCBV maps were re-referenced to normal appearing white matter (NAWM) with CBV=2.5% (Leenders, 1994). CTH parameter maps were created based on parametric modeling (Jespersen & Østergaard, 2012; Mouridsen et al., 2014) assuming a gamma variate function as probability density distribution of the capillary transit times. CTH represents the standard deviation of the capillary transit times in seconds, with larger values indicating a larger heterogeneity. Quantitative baseline CBF maps were derived from the pCASL data following recommendations outlined in the ISMRM perfusion study group consensus paper (Alsop et al., 2015). In short, the label and control images were motion corrected, averaged and subtracted, with M0 being used for normalization.

BOLD lag maps were derived from preprocessed BOLD fMRI data via cross-correlation of the individual participants' superior sagittal sinus (SSS) time course signal with signals from all voxels within the brain. Lag mapping was conducted with rapidtide, a Python based toolbox providing automated time delay analysis for fMRI data (Frederick et al., 2022; Tong et al., 2011; Tong, Hocke, et al., 2019; Tong & Frederick, 2014). For the analysis, a predefined set of options refining the analysis was chosen, which included temporal up-sampling of the input fMRI data by a factor of 3, repeated measures control and recursive selection of a reference time course for each lag to improve the mapping. The initial SSS reference time course was extracted from a SSS mask, which was individually created for each participant using multi-echo gradient-spin echo data, where the SSS could be segmented based on the vascular voxels' accelerated signal decay with TE (see **Fig. 9**). The cross-correlation between the SSS reference and each voxel BOLD-TC was conducted within the range of -20 to +20 TRs. The temporal shift at which the maximum correlation is achieved constitutes the voxel specific BOLD lag. Negative lag values indicate that the SSS time course lags

behind the tissue VOIs BOLD-TC, i.e., BOLD time course features appear earlier in tissue than SSS blood. Positive BOLD lag values on the other hand indicate a lead of the SSS BOLD signal.

For generation of group averages, all parameter maps were transformed to MNI space and then separately averaged for healthy controls and ICAS patients. To ensure consistent averaging of unilateral ICAS-related hemodynamic impairments, all hemodynamic-vascular data from left-sided ICAS patients were flipped to the right side along the x-axis after MNI normalization.

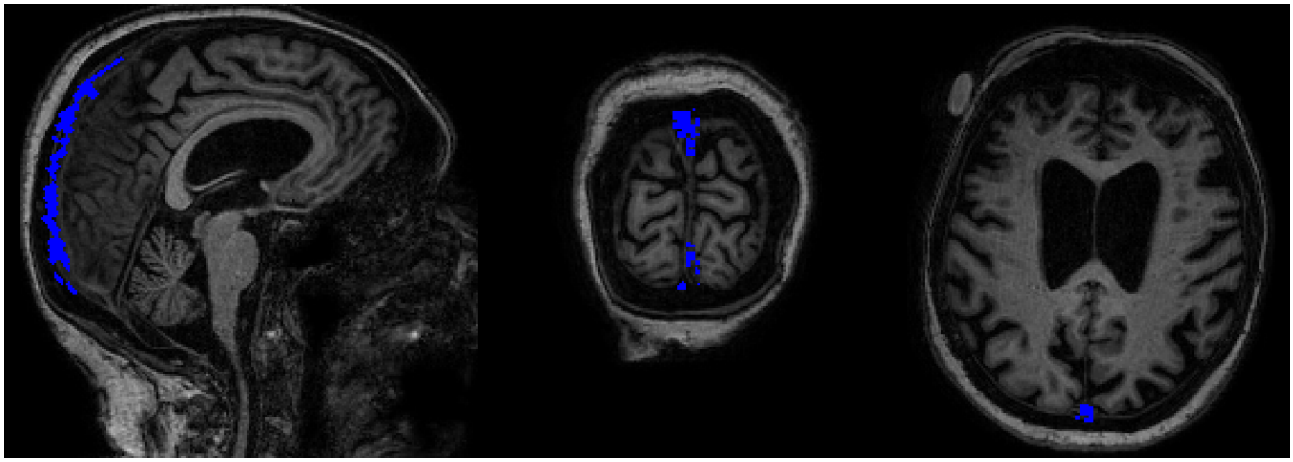

Figure 9. Superior Sagittal Sinus (SSS) mask.

Exemplary mask of a participant's segmented SSS that was used for the creation of BOLD lag maps. The segmented voxels (blue) are overlaid on sagittal (left) coronal (middle), and axial (right) slices of the participant's T1-weighted MPRAGE.

3.1.5 Homotopic VOI analyses of BOLD-FC and hemodynamic-vascular parameters

Homotopic VOIs. Analysis between homotopic VOIs ensured that BOLD-FC measures were mostly unaffected by confounding factors such as differing vascular geometry and anatomically based blood arrival times, vasomotion and neural activity. Homotopic VOI pairs were taken from the Atlas of Intrinsic Connectivity of Homotopic Areas , derived from a sample of 281 healthy participants. The AICHA parcellation is explicitly weighted towards homotopic organization and functional separation, containing 192 cross-hemispheric VOI pairs across cortical and subcortical grey matter.

BOLD-FC analysis. All analyses were carried out in the participants' native space, to which the AICHA was transformed via the reverse flow field, initially obtained by MNI normalization of the participants' anatomical MPRAGE data. The atlas was subsequently resliced to fMRI resolution and, to reduce contributions from non-GM areas, masked by an individual gray matter (GM) mask

(pGM>0.3), derived from the participants' segmented anatomical data. From the 384 GM-masked VOIs, average BOLD-TCs were then extracted, correlated (Pearson's) between respective left and right homotopic areas, and then Fisher-r-to-Z transformed to obtain BOLD-FC values (see **Fig. 10**).

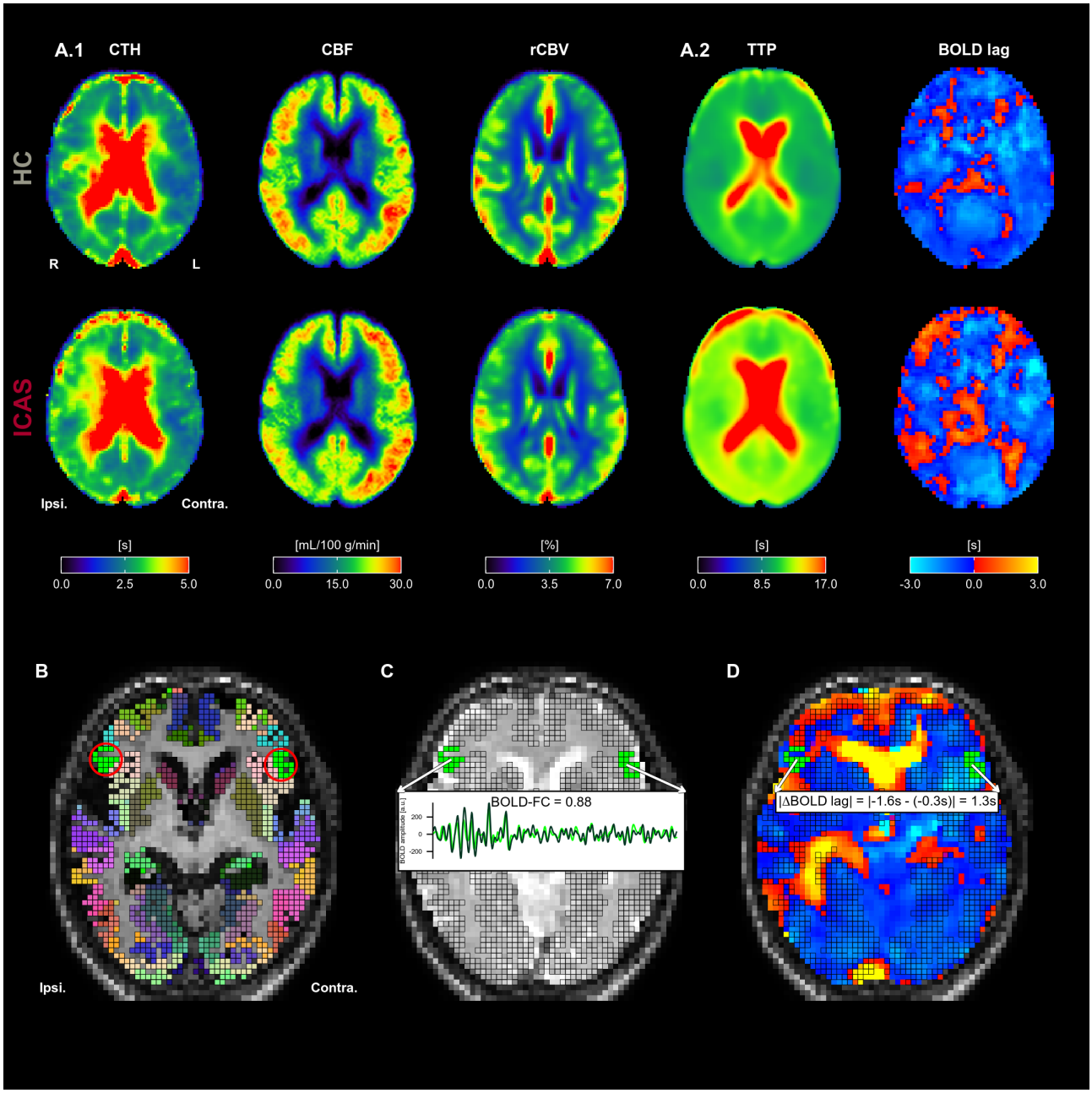

Figure 10. Subject-average hemodynamic-vascular parameter maps, homotopic VOI atlas and illustration of homotopic VOI pair value extraction procedure.

(A) For healthy controls (top) and ICAS patients (bottom), subject average local hemodynamic-vascular parameter maps (MNI space) are depicted in panel A.1 and systemic parameter maps in panel A.2. Units and color scheme for the respective parameter maps are indicated below each column. An axial slice of a right sided ICAS patient in native space is depicted in Panels B to D, hemispheres are indicated at the bottom of B. (B) Atlas of homotopic regions, AICHA (Joliot et al., 2015), resampled to fMRI resolution in subject space and masked by a grey matter mask (p>0.3) on top of

the resampled T1w MPRAGE. Identically colored voxels on the ipsi- and contralateral hemispheres indicate homotopic VOI pairs. Voxels belonging to any VOI are marked by black outlines in all panels. The VOI pair indicated by the red circles was used to demonstrate matching VOIs for BOLD-FC (panel C) and |ΔBOLD lag| (panel D). (C) Overlay of BOLD-fMRI data on top of accordingly resampled T1w MPRAGE data. The inset depicts left (light green) and right (dark green) hemispheric BOLD signal time courses averaged across all voxels from the respective VOIs highlighted in green. BOLD-FC between this homotopic VOI pair is indicated in the same panel. (D) BOLD lag map on top of the same anatomical slice. The inset illustrates the calculation of |ΔBOLD lag|, based on lag values extracted from the green VOI pair. Abbreviations: CTH, capillary transit time heterogeneity; CBF, cerebral blood flow; rCBV, relative cerebral blood volume; TTP, time-to-peak; BOLD lag, blood oxygenation level dependent lag; HC, healthy controls; ICAS, Internal carotid artery stenosis; R, right; L, left; Ipsi., Ipsilateral to the stenosis; Contra., Contralateral to the stenosis; VOI, volume of interest; BOLD-FC, BOLD functional connectivity.

Hemodynamic-vascular parameter analysis. Similarly, hemispheric differences in local (CTH, baseline CBF and rCBV) and systemic (TTP and BOLD lag) hemodynamic-vascular parameter values were extracted from these homotopic VOI pairs. The AICHA atlas, already in subject-space, was resliced to the respective parameter maps and subsequently masked by an accordingly resliced GM mask. For each metric, VOI-average values were then extracted, and the differences between pairwise homotopic VOIs calculated by subtracting the right from the left sided VOI values, e.g., for CTH: ΔCTH [sec] = $CTH_{VOI\text{-}Left}$ - $CTH_{VOI\text{-}Right}$ (see **Fig. 10 B - D**). While a difference of 0 indicates an equilibrium between the respective hemodynamic-vascular parameters, values unequal to 0 indicate a homotopic cortical imbalance. Positive values relate to larger left-sided values and vice versa for negative values. For BOLD lag values, however, this order is reversed, with negative values indicating earlier blood arrival times for the left-sided region and positive values indicating earlier arrival times for the right-sided region. This is due to the lag range spanning both negative and positive values.

Outlier exclusion: Prior to the statistical analysis, the extracted VOI data were cleaned considering VOI size and possible outlier values to achieve sufficient data quality. As brain coverage varied for different sequences, parameter maps did cover GM to different extents. VOIs were therefore excluded if, after GM masking, more than 25% of voxels within the respective VOI were missing or constituted NaN values. Second, a minimal VOI size was determined for VOIs across the hemodynamic-vascular maps, by excluding the 10% smallest VOIs. Minimal VOI volumes (in mm^3) depended on spatial resolution along with the modality specific outlier exclusion procedure and resulted in $V_{BOLD\text{-}FC/BOLD\ lag}$ = 297 mm^3, $V_{CTH/rCBV}$ = 252 mm^3, V_{CBF} = 275 mm^3, V_{TTP} = 282 mm^3. Further, to

exclude physiologically implausible values resulting from artifacts or partial volume effects, VOI-average values were z-standardized (to 0 instead of the distribution mean, for z-scores of 0 to be in-line with a difference of 0) and values below and above 3 standard deviations were excluded. VOIs with a missing homotopic partner VOI after this procedure were excluded as well.

3.1.6 Statistical analysis.

Hemodynamic-vascular VOI-average parameters: Potential baseline differences between healthy controls and ICAS patients among the collected VOI data were examined via a Wilcoxon rank sum test. Group comparisons were conducted for both subject-averaged VOI parameter values and homotopic VOI difference values.

Between-hemisphere comparisons: To assess unilateral hemodynamic-vascular impairments of the ICAS patients, I compared VOI-average values ipsilateral and contralateral to the stenosis for ICAS patients using the Wilcoxon signed-rank test; for the healthy controls, the left and right hemispheric VOI values were likewise compared.

Parameter relationships: To assess relationships between the different local and systemic hemodynamic-vascular parameters and their differences, I conducted a repeated measures correlation (Bakdash & Marusich, 2017; AICHA; Joliot et al., 2015), which assesses the average within-participant correlation strength across multiple participants. Repeated measures correlation relies on an ANCOVA approach, which in comparison to other common correlation approaches, does neither rely on the assumption of independence nor does it require an aggregation or averaging of single subject data, which increases power. As an output, this analysis provided the average correlation coefficient across subjects between each hemodynamic-vascular parameter and their differences. Resulting p-values were corrected for false-discovery rate (FDR) due to the multiple comparison.

Regression analysis: With respect to the main aim of my study, I analyzed distinct influences of systemic and local hemodynamic-vascular parameters on BOLD-FC, by means of a linear mixed model (LMM), incorporating BOLD-FC as the dependent variable of interest and the homotopic VOI differences $|\Delta X|$ of each systemic and local hemodynamic-vascular parameter X as regression predictors. Further control variables were the participants' group affiliation, ICAS or healthy

controls, and age. Using a LMM allowed for assessing the full complexity of a potential association by capturing the between-subject variance with regard to the individual influence of the hemodynamic-vascular predictors and baseline BOLD-FC.

To achieve comparable effect sizes, z-standardized hemodynamic-vascular regressors were used for the regression model. This yielded an identical scale for all included parameters, i.e., |ΔX| of 1 always indicates a change of 1 standard deviation (σ), even though the standard deviations of different parameter values differed in unit and size, e.g., σ_{CTH} = 1.1 sec and σ_{CBF} = 4.9 ml/100g/1 min. The regression coefficient β then indicates a standardized change in BOLD-FC, ΔBOLD-FC, for a hemodynamic-vascular parameter difference of one standard deviation, i.e. $\beta\,[\frac{\Delta BOLD-FC}{\sigma_{|\Delta|}}]$.

For the LMM, the participants' pairwise homotopic BOLD-FC values were the dependent variable and the differences in local and systemic hemodynamic-vascular parameters, i.e. |ΔCTH|, |ΔCBF| and |ΔrCBV|, |ΔTTP| and |ΔBOLD lag|, were setup as the regression predictors |ΔX|. To control for the effects of group (healthy control or ICAS) and age, group affiliation and participants' age (centered on the sample median age, i.e., 72 years) were further included as both stand-alone and interaction terms in the model. Importantly, the model (random-coefficient) allowed for both intercepts and regression coefficients of participants to deviate from the estimated group-wise intercepts and coefficients (random slopes for |ΔrCBV| had to be eventually excluded for the *local* model and along with and |ΔCTH| also for the *local and systemic* model, see below, as variation between subjects was too little, leading to a *singular fit*). The regression model itself was calculated using the lme4 package (Bates et al., 2015) for R (R Core Team, 2020) within Rstudio (RStudio Team, 2019). Degrees of freedom and p-values for regressors and interactions were estimated using Satterthwaite's method with the Tests in Linear Mixed Effects Models (*lmerTest*) package (Kuznetsova et al., 2017).

Model comparison: I further compared the predictive value, i.e., the overall explained variance of pairwise BOLD-FC across all participants, between three nested regression models with increasing complexity. Explained variance (including both fixed and random effects) was determined using the method proposed by Nakagawa, Johnson and Schielzeth (Nakagawa et al., 2017) via the performance package (Lüdecke et al., 2021). As baseline, only the participants' intercepts, group affiliation and age were chosen (*Intercept* model). The intercepts, in this case, represent the participants' overall average BOLD-FC. For the second model, the local hemodynamic-vascular VOI

differences, |ΔCTH|, |ΔCBF| and |ΔrCBV| were added (*intercept + local* model). By the inclusion of these VOI differences, the intercepts now represent the participants' average pairwise BOLD-FC in the absence of any pairwise local hemodynamic-vascular parameter differences. Finally, the local model was supplemented with the two systemic hemodynamic-vascular VOI differences |ΔTTP| and |ΔBOLD lag| to achieve a *local and systemic* model, where all measured hemodynamic-vascular VOI differences along with the participants' group affiliation and age were accounted for. For this local and systemic model (*full* model), the intercepts indicate the participants' average pairwise BOLD-FC in the absence of any pairwise local and systemic hemodynamic-vascular differences. Models were subsequently estimated and incrementally compared by means of a X^2 – test (chi-squared).

3.2 Results of Project 2

The focus of my study is on a comparison of influences from local and systemic hemodynamic-vascular factors (see **Fig. 10 A** for average parameter maps) on homotopic BOLD-FC (see **Fig. 10 B – D** for workflow demonstration) in healthy controls and a group of patients with ICAS, representing a lesion-model. Since the interpretation of my main results depends on both these *factors' distributions* and their *inherent pairwise correlation*s, I present an overview of pairwise homotopic differences for the five local and systemic hemodynamic-vascular factors (**Fig. 11 A** for distributions and **B** for group differences), as well as their inherent correlations (in **Fig. 11 C**). I additionally present – as background information – distributions, inherent correlations and between-hemisphere differences of regional values of hemodynamic-vascular factors in **Figure 13** and **Figure 14**.

Pairwise homotopic hemodynamic-vascular parameter differences and their correlations: When comparing average homotopic VOI differences (averaged across all VOI pairs within participants), i.e., average |ΔX|, I found significantly larger homotopic differences in |ΔCBF| and |ΔBOLD lag| for ICAS patients, while other parameter homotopic differences were not significantly different across groups (see **Fig. 11 B.1** and **B.2**). Concerning relationships among these variables, |ΔCTH| was moderately correlated with |ΔrCBV| for both groups (ICAS: r = 0.26; healthy controls: r = 0.3). |ΔCTH| was furthermore significantly correlated with |ΔTTP| in ICAS patients (r = 0.24) but to a lesser degree in healthy controls (r = 0.11). In addition, |ΔTTP| was moderately correlated with |

ΔCBF| in ICAS patients (r = 0.17) but again much less in controls (r = 0.08). The remaining differences showed again either weak (-0.1 <= r <= 0.1) or no correlations (see **Fig. 11 C**).

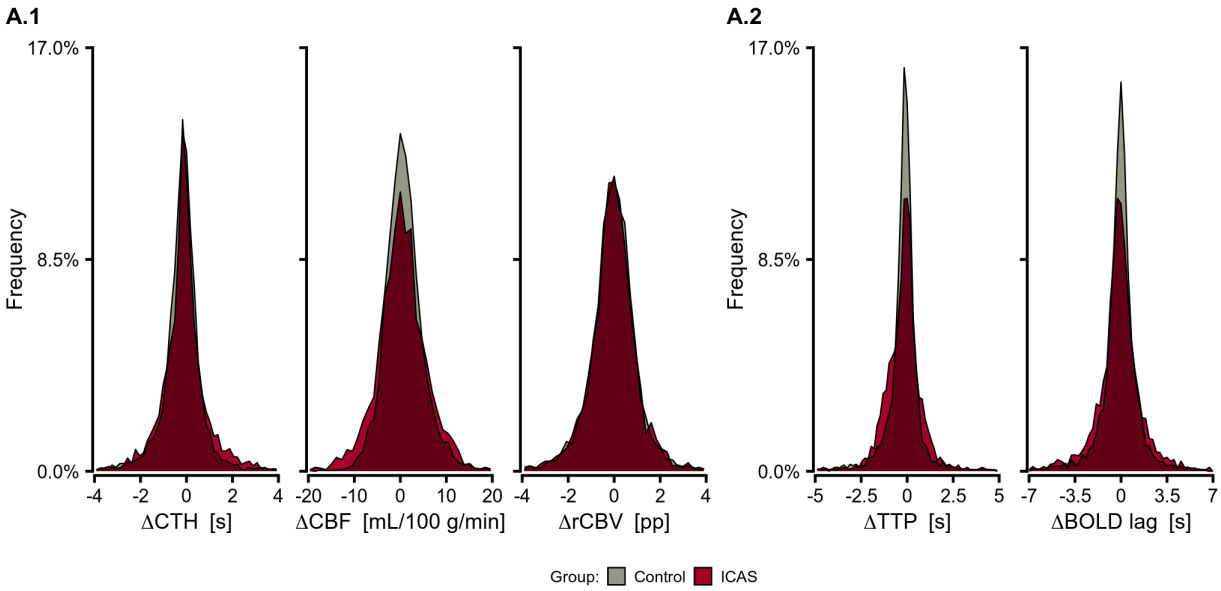
A.1
A.2
17.0%
8.5%
0.0%
Frequency
ΔCTH [s]
ΔCBF [mL/100 g/min]
ΔrCBV [pp]
ΔTTP [s]
ΔBOLD lag [s]
Group: Control ICAS

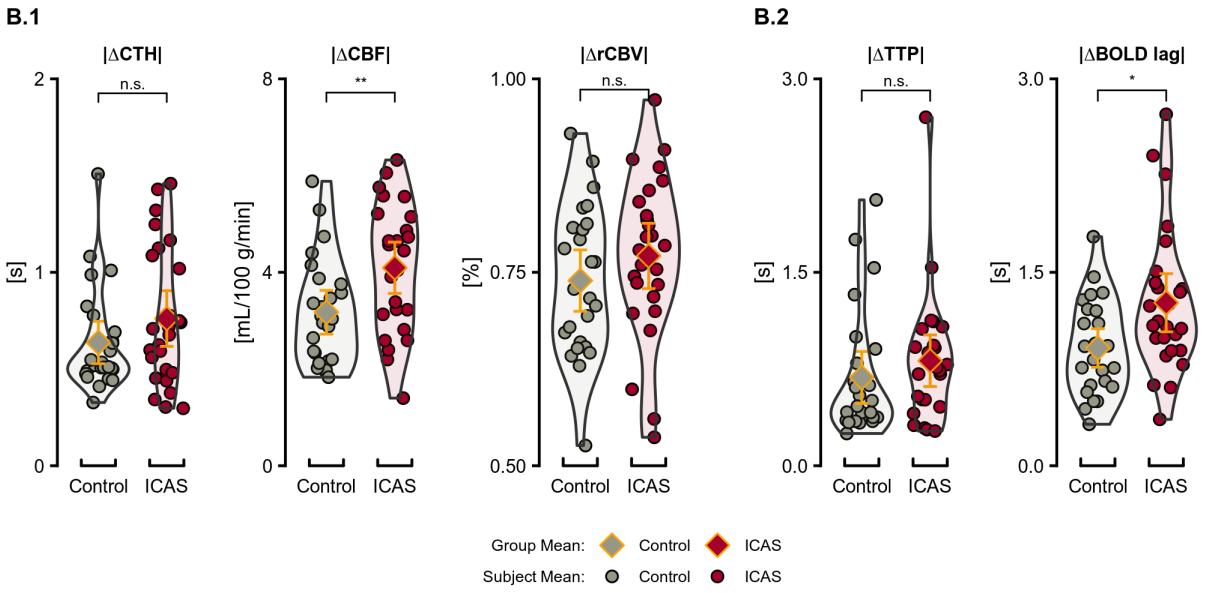
B.1
B.2
|ΔCTH|
|ΔCBF|
|ΔrCBV|
|ΔTTP|
|ΔBOLD lag|
n.s.
**
*
[s]
[mL/100 g/min]
[%]
Control
ICAS
Group Mean: Control ICAS
Subject Mean: Control ICAS

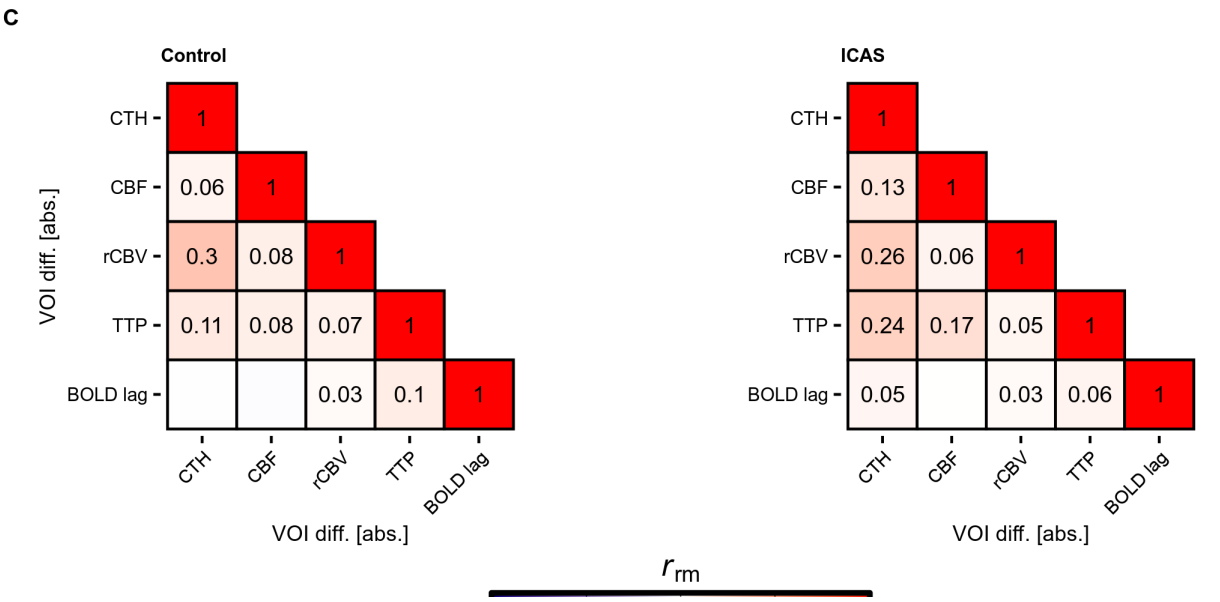
C
Control
ICAS
CTH
CBF
rCBV
TTP
BOLD lag
VOI diff. [abs.]
r rm

Figure 11. Frequency distribution, group differences and inter-correlation of hemodynamic-vascular homotopic VOI-parameter differences between hemispheres.

The first row depicts the frequency distributions of homotopic differences for each of the local (A.1), i.e., ΔCTH, ΔCBF and ΔrCBV, as well as systemic (A.2), i.e., ΔTTP and ΔBOLD lag, hemodynamic-vascular parameters across all participants and separately for the two participant groups. Negative values imply larger values for the right-sided VOI of a pair and vice versa for positive values, except BOLD lag where the direction is reversed. Darkened areas indicate an overlap between the two groups. For these two panels the x-axis were truncated to encompass values within -4σ to +4σ, i.e. 99.9% of included values. The second row depicts participants' average local (B.1) and systemic (B.2) homotopic VOI differences as dots. Diamonds with orange outlines indicate group means. Group means were compared between HC and ICAS with a Wilcoxon test, revealing significantly larger CBF and BOLD lag homotopic VOI differences on average for ICAS patients, indicated by the brackets on top (n.s. = not significant, *: p<=0.05, **: p<= 0.01, ***: p< 0.001, ****: p<=0.0001). Panel C in the bottom row depicts the average correlation between the different homotopic hemodynamic-vascular VOI differences across participants (repeated measures correlation). Numbers within tiles indicate the participants' average correlation coefficients between the respective parameter differences. Correlations between differences were calculated separately for participant groups. Correlations were considered significant after group-wise FDR correction ($p < 0.05$), empty tiles indicate insignificant correlations. Abbreviations: CTH, capillary transit time heterogeneity; CBF, cerebral blood flow; rCBV, relative cerebral blood volume; TTP, time-to-peak; BOLD lag, blood oxygenation level dependent lag; VOI, volume of interest; ICAS, internal carotid artery stenosis.

Group differences in average homotopic connectivity: Comparing intercepts across my models did not reveal significant group differences for average homotopic BOLD-FC (see **Fig. 12**). However, there was a strong trend towards significance between healthy controls (1.19) and ICAS (1.09) for the intercept model ($p = 0.06$; **see Table 6**). ICAS patients exhibited a lower average homotopic BOLD-FC, as the interaction of intercept and group factor for this model represents the estimated average group-wise homotopic BOLD-FC (for participants of median sample age). For the both the local as well as the local and systemic model this trend vanished ($p = 0.46$ and $p = 0.68$, see **Table 8** and **7** respectively) and intercepts were on comparable levels (local: healthy controls 1.23 and ICAS 1.19, systemic and local: healthy controls 1.35 and ICAS 1.33). Note that for these models intercepts do no longer represent generally estimated average homotopic BOLD-FC, but average homotopic BOLD-FC in absence of the respective included local and systemic hemodynamic-vascular predictors. Thus, the inclusion of hemodynamic-vascular differences between homotopic VOIs led to an alignment of estimated homotopic BOLD-FC between groups. The respective estimated average BOLD-FC, as indicated by the intercepts, furthermore increased with model complexity and was lowest when hemodynamic-vascular predictors were not considered.

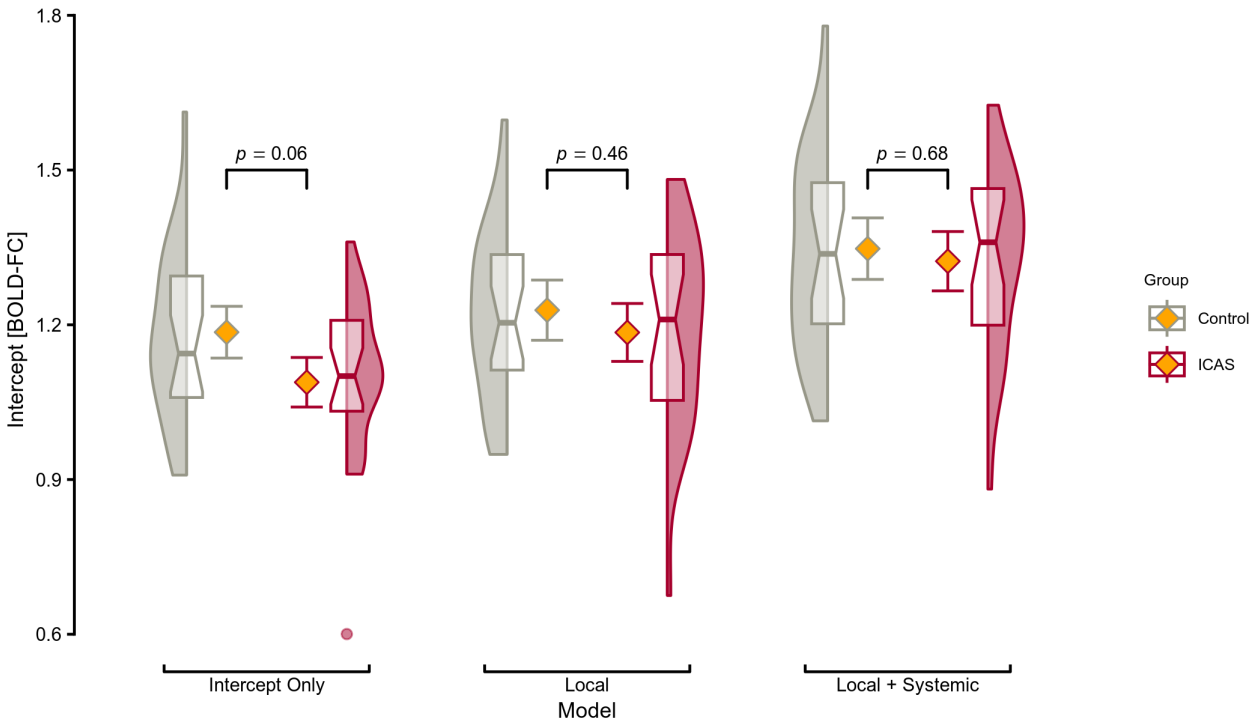

Figure 12. Group-wise intercepts and participant distributions across all regression models.

The y-axis depicts estimated intercepts, i.e., BOLD-FC, for the three regression models depicted on the x-axis. Diamonds represent the respective group-wise average. For the boxplots, notches indicate median estimated intercept values across participants, upper and lower borders of the boxes the interquartile range (IQR), or the 75th and 25th percentile of estimated intercept values, respectively. Lines extending beyond the boxes and meeting with the density estimates indicate the largest and smallest values lying within 1.5 times the IQR above or below the 75th and 25th percentile, respectively. Dots indicate outliers beyond that range. The shaded areas indicate distribution density estimates of participants' intercepts. Brackets on top indicate p-values of the estimated between-group intercept differences, as indicated in the models. Note that the interpretation of intercepts changes across models, as described in Methods section 'Group differences in average homotopic connectivity'. Abbreviations: BOLD-FC, blood oxygenation level dependent functional connectivity; ICAS, internal carotid artery stenosis.

Table 6. Summary of *Intercept* regression model.

Predictors	**Estimates**	**CI**	**Statistic**	***p***
(Intercept)	1,14	1.09 – 1.19	45,99	**<0.001**
Group	0,05	0 – 0.1	1,96	0.06
Age	0,00	-0.01 – 0.01	0,08	0.93
Group:Age	0,00	0 – 0.01	0,98	0.33

Note: Under predictors the variables incorporated in the model are listed. Categorical variables were deviation coded (Group: ICAS = 1, Controls = 1). Age was centered on the median age in the sample (participants with a median age equal 0 in the coding). The intercept estimate describes average BOLD-FC when all other predictor variables are 0, i.e.

for all included participants of median age. Estimates for other variables indicate the estimated change in BOLD-FC should the predictor value increase by 1 (Group: to health controls, age to one year above median of 72 years of age). Interactions between participant group and predictors are indicated by a colon. Confidence intervals for the estimates are indicated by CI. If no CI is indicated this means that the effect was always smaller than 0.001. The test statistic is derived from a one-sample t-test, against the null-hypothesis that the estimate does not differ significantly from 0. Effects for the ICAS patients are identical to those of the healthy control group, except being reversed in polarity (Group coding for ICAS patients = -1).

Influence of local and systemic hemodynamic-vascular factors on BOLD-FC: To study both local and systemic hemodynamic-vascular influences on BOLD-FC, I applied a linear mixed model approach with homotopic BOLD-FC as the dependent variable and the homotopic VOI differences |ΔX| of each systemic and local hemodynamic-vascular parameter X as independent variables or regression predictors. According to this, BOLD-FC is most strongly influenced by systemic BOLD lags (|ΔBOLD lag|; β = -0.19; 95% confidence interval, CI: -0.21 to -0.16; σ = 1.6 s), followed by systemic |ΔTTP| (β = -0.07; 95% CI: -0.09 to -0.04; σ = 1.4 s), local |ΔCBF| (β = -0.04; 95% CI: -0.06 to -0.02; σ = 4.9 [mL/100 g/min]) and finally local |ΔCTH| (β = -0.03; 95% CI: -0.05 to -0.02; σ = 1.1 s). Differences in rCBV had no significant influence on BOLD-FC (see **Fig. 13 A** and **B**). These estimates were not significantly influenced by age or group, i.e., healthy controls and ICAS patients (**Table 7** for full result presentation).

Table 7. Summary of *Intercept + Local + Systemic hemodynamic-vascular parameter* regression model.

Predictors	**Estimates**	**CI**	**Statistic**	***p***
Intercept	1,34	1.28 – 1.39	45,29	**<0.001**
Group	0,01	-0.05 – 0.07	0,41	0.68
Age	0,00	-0.01 – 0.01	0,37	0.71
|ΔCTH|	-0,03	-0.05 – -0.02	-6,20	**<0.001**
|ΔCBF|	-0,04	-0.06 – -0.02	-3,28	**<0.001**
|ΔrCBV|	0,00	-0.01 – 0.01	0,35	0.72
|ΔTTP|	-0,07	-0.09 – -0.04	-4,76	**<0.001**
|ΔBOLD lag|	-0,19	-0.21 – -0.16	-16,06	**<0.001**
Group:Age	0,00	-0.01 – 0.01	0,81	0.42
Group:|ΔCTH|	0,01	-0.01 – 0.02	1,07	0.28
Age: |ΔCTH|	0,00	0 – 0	1,46	0.14
Group:|ΔCBF|	0,01	-0.02 – 0.03	0,61	0.54

Age:|ΔCBF|	0,00	-0.01 – 0	-1,38	0.18
Group:|ΔrCBV|	0,00	-0.01 – 0.01	-0,01	0.99
Age:|ΔrCBV|	0,00	0 – 0	0,11	0.91
Group:|ΔTTP|	0,00	-0.03 – 0.03	0,08	0.93
Age:|ΔTTP|	0,00	-0.01 – 0	-0,24	0.82
Group:|ΔBOLD lag|	-0,01	-0.03 – 0.02	-0,53	0.6
Age:|ΔBOLD lag|	0,00	0 – 0	0,47	0.64
Group:Age:|ΔCTH|	0,00	0 – 0	1,96	0.05
Group:Age:|ΔCBF|	0,00	-0.01 – 0	-1,56	0.13
Group:Age:|ΔrCBV|	0,00	0 – 0	0,95	0.34
Group:Age:|ΔTTP|	0,00	-0.01 – 0	-0,84	0.41
Group:Age:|ΔBOLD lag|	0,00	0 – 0.01	0,68	0.5

Note: Under predictors the variables incorporated in the model are listed. Categorical variables were deviation coded (Group: ICAS = -1, Controls = 1). Age was centered on the median age in the sample (participants with a median age equal 0 in the coding). The intercept estimate describes average BOLD-FC when all other predictor variables are 0, i.e. for all included participants of median age and without the presence of any local and systemic hemodynamic-vascular parameter differences. Estimates for other variables indicate the estimated change in BOLD-FC should the predictor value increase by 1 (Group: to health controls, age: to one year above median age of 72 and |ΔX| by one respective standard deviation). Interactions between participant group and predictors are indicated by a colon. Confidence intervals for the estimates are indicated by CI. If no CI is indicated this means that the effect was always smaller than 0.001. The test statistic is derived from a one-sample t-test, against the null-hypothesis that the estimate does not differ significantly from 0. Effects for the ICAS patients are identical to those of the healthy control group, except being reversed in polarity (Group coding for ICAS patients = -1).

Hemodynamic-vascular factors explain about 20% of BOLD-FC variability: In my comparison of three nested regression models (see **Fig. 13 C**), the baseline model encompassing only the participants' intercepts, age and group affiliation explained 20.5% of overall pairwise BOLD-FC across all participants in the sample (see **Table 6** for full results). Adding differences in local hemodynamic-vascular parameters significantly increased the explained variance, reaching 27.7% overall (see **Table 8** for full results). The additional inclusion of differences in systemic hemodynamic-vascular parameters further significantly increased the explained BOLD-FC variance, reaching 40.7% (**Fig. 13 C**). Thus, local and systemic hemodynamic-vascular VOI differences alone can explain about 20% of variance in pairwise BOLD-FC. Note that the inclusion of systemic parameters led to a larger increase in explained variance (+13 percent points; pp.), as compared to the local parameters (+7.2 pp.).

Table 8. Summary of *Intercept + Local hemodynamic-vascular parameter* regression model.

Predictors	**Estimates**	**CI**	**Statistic**	***p***
(Intercept)	1,21	1.15 – 1.26	41,88	**<0.001**
Group	0,02	-0.03 – 0.08	0,75	0.46
Age	0,00	-0.01 – 0.01	0,39	0.7
|ΔCTH|	-0,05	-0.07 – -0.04	-5,88	**<0.001**
|ΔCBF|	-0,04	-0.07 – -0.01	-2,92	**0.01**
|ΔrCBV|	0,00	-0.02 – 0.01	-0,55	0.58
Group:Age	0,00	0 – 0.01	0,97	0.33
Group:|ΔCTH|	0,02	0 – 0.03	1,86	0.07
Age:|ΔCTH|	0,00	0 – 0.01	1,71	0.09
Group:|ΔCBF|	0,01	-0.02 – 0.04	0,85	0.4
Age:|ΔCBF|	0,00	-0.01 – 0	-1,19	0.24
Group:|ΔrCBV|	0,00	-0.02 – 0.01	-0,50	0.61
Age:|ΔrCBV|	0,00	0 – 0	-0,71	0.48
Group:Age:|ΔCTH|	0,00	0 – 0	0,74	0.47
Group:Age:|ΔCBF|	0,00	-0.01 – 0	-0,92	0.36
Group:Age:|ΔrCBV|	0,00	0 – 0	0,20	0.84

Note: Under predictors the variables incorporated in the model are listed. Categorical variables were deviation coded (Group: ICAS = -1, Controls = 1). Age was centered on the median age in the sample (participants with a median age equal 0 in the coding). The intercept estimate describes average BOLD-FC when all other predictor variables are 0, i.e. for all included participants of median age and without the presence of any local hemodynamic-vascular parameter differences. Estimates for other variables indicate the estimated change in BOLD-FC should the predictor value increase by 1 (Group: to health controls, age: to one year above median age of 72 and |ΔX| by one respective standard deviation). Interactions between participant group and predictors are indicated by a colon. Confidence intervals for the estimates are indicated by CI. If no CI is indicated this means that the effect was always smaller than 0.001. The test statistic is derived from a one-sample t-test, against the null-hypothesis that the estimate does not differ significantly from 0. Effects for the ICAS patients are identical to those of the healthy control group, except being reversed in polarity (Group coding for ICAS patients = -1).

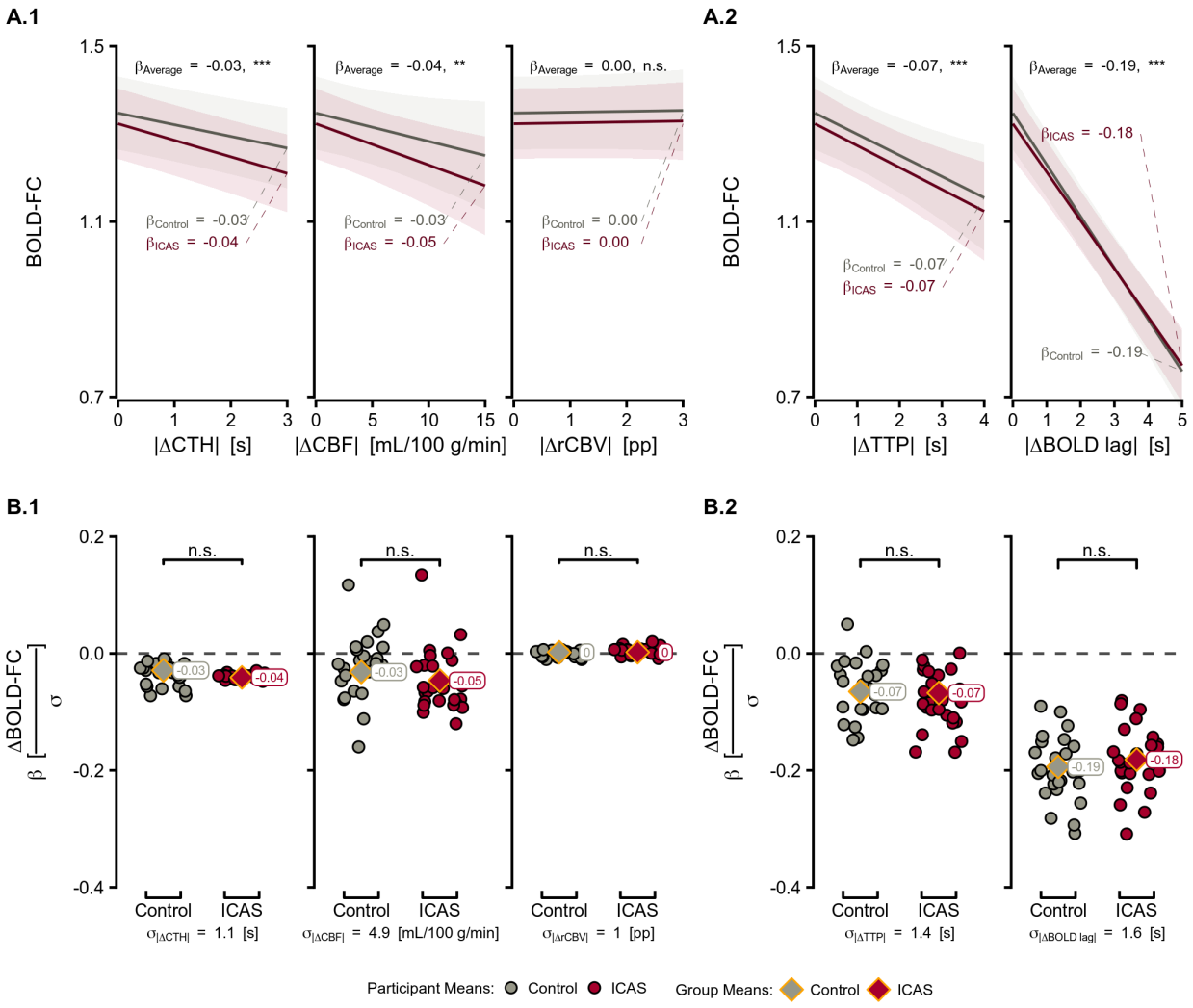

C

	Models	Variance explained [%]	Improvement
1	Intercept only	20.5	-
2	+ Local Hemodyn.-Vasc.	27.7	***
3	+ Systemic Hemodyn.-Vasc.	40.7	***

Figure 13. Group and subject effects of BOLD-FC variance explained by hemodynamic-vascular parameter differences.

Group regression lines for local (A.1), |ΔCTH|, |ΔCBF|, |ΔrCBV| and systemic (A.2), |ΔTTP| and |ΔBOLD lag|, hemodynamic-vascular parameter differences are depicted in the first row. Group-wise regression coefficients (β) are indicated below the respective lines, the estimated average regression coefficient and significance is indicated above the lines (n.s. = not significant, *: p <=0.05, **: p <= 0.01, ***: p <= 0.001; not adjusted for age, depicted for participants with the median age of 72). Slopes indicate the decrease in pairwise BOLD-FC with increasing |ΔX| between pairwise VOIs. |ΔX| on the x-axis were limited to a range of 3σ. Shaded areas around the lines indicate the 95% confidence intervals. Subject specific regression coefficients, including random effects and interactions with age

and group affiliation, are depicted in panels (B.1) for local and (B.2) systemic hemodynamic-vascular parameter differences. Dots indicate individual participant values, diamonds the respective group-wise average. Brackets on top indicate significant group differences in β values (α = 5%, n.s. = not significant). Regression coefficients β indicate a change in pairwise BOLD-FC (ΔBOLD-FC) for hemodynamic-vascular parameter differences, |ΔX|, of one standard deviation (σ). Standard deviations for the respective hemodynamic-vascular parameter differences are indicated at the bottom of panels B.1 and B.2. Panel C shows a tabular comparison of regression models. The first column, Models, indicates which hemodynamic-vascular variables were included in the respective model. The last column indicates whether the listed model constitutes a significant improvement in variance explained over the previous one, as indicated by a χ^2-test (***: p <= 0.001). Abbreviations: BOLD-FC, blood oxygenation level dependent functional connectivity; CTH, capillary transit time heterogeneity; CBF, cerebral blood flow; rCBV, relative cerebral blood volume; TTP, time-to-peak; BOLD lag, blood oxygenation level dependent lag; ICAS, internal carotid artery stenosis.

Hemodynamic-vascular parameter values for the whole-brain, the hemispheres and their correlation: The whole-brain VOI-average parameter values (averaged across all VOIs within participants in native space) did not significantly differ between healthy controls and ICAS patients (see **Fig. 14 B.1** and **B.2**). The comparison of hemisphere-averaged VOI values within groups revealed that all hemodynamic-vascular parameters differed significantly between hemispheres for ICAS patients (see **Fig. 15**). While CTH, rCBV and TTP were significantly increased ipsilateral to the stenosis, CBF was significantly reduced. BOLD lags were significantly less negative on the ipsilateral hemisphere. Healthy controls also exhibited significant between-hemispheric differences for CTH, with on average slightly larger CTH values the right hemisphere. There were no significant between-hemispheric differences for the remaining hemodynamic-vascular parameters in the control group.

The repeated measures correlation analysis revealed several correlations and anti-correlations between hemodynamic-vascular parameters (see **Fig. 14 C**). In ICAS patients as well as healthy controls, CTH was moderately correlated with both rCBV (ICAS: r = 0.37-ipsilateral/0.37-contralateral; healthy controls: r = 0.44-left/0.43-right) and TTP (ICAS: r = 0.39/0.38; healthy controls: r = 0.34/0.35). In addition, CTH showed a weak negative correlation with CBF (ICAS: r = -0.24/-0.22; healthy controls: r = -0.18/-0.26) and TTP was weakly negatively correlated with CBF (ICAS: r = -0.15/-0.13; healthy controls: r = -0.1/-0.12). The remaining parameters showed either weak (-0.1 <= r <= 0.1) or insignificant correlations.

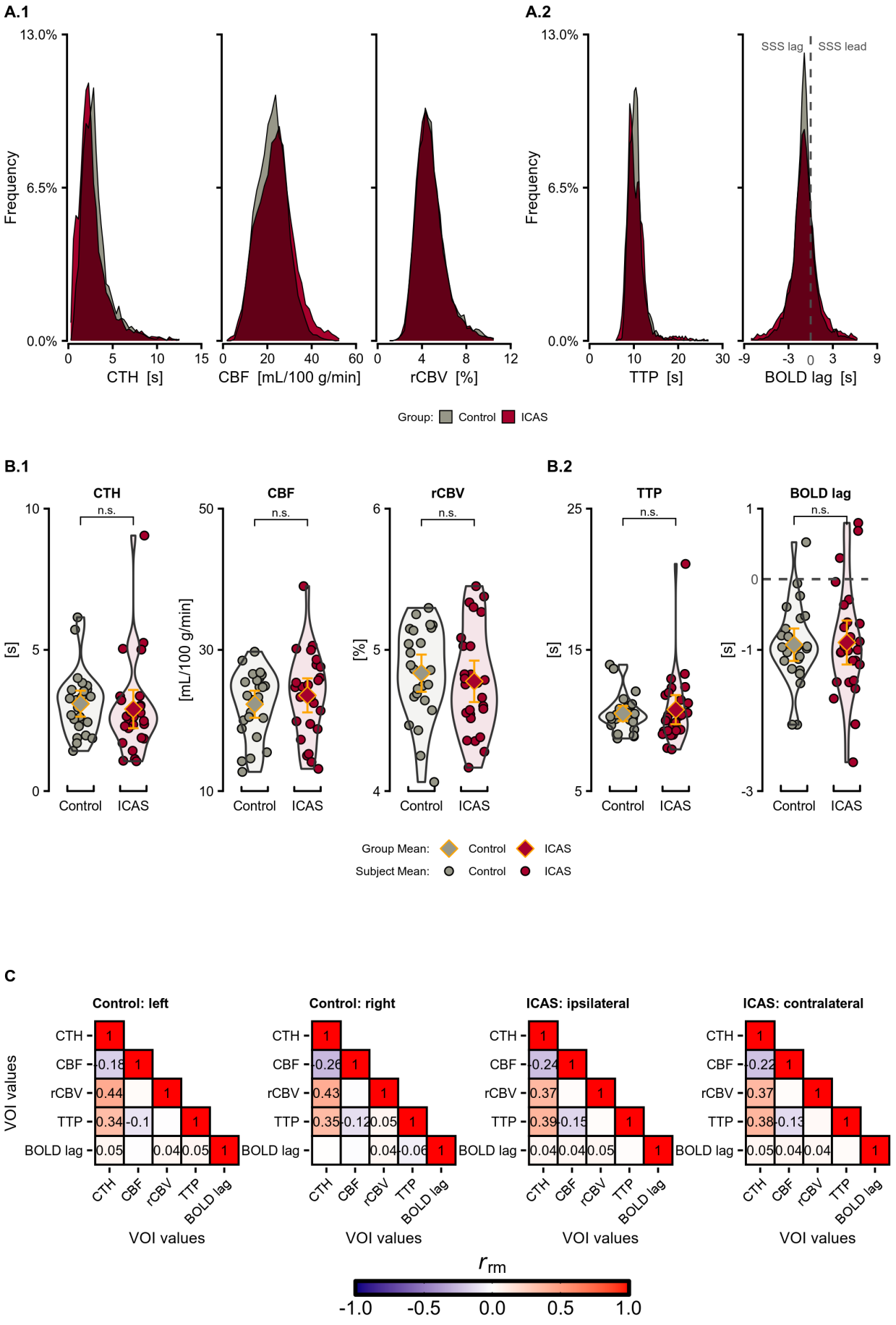
A.1
A.2
13.0%
6.5%
0.0%
Frequency
CTH [s]
CBF [mL/100 g/min]
rCBV [%]
TTP [s]
BOLD lag [s]
SSS lag
SSS lead
Group: Control ICAS
B.1
B.2
CTH
CBF
rCBV
TTP
BOLD lag
n.s.
[s]
[mL/100 g/min]
[%]
Control
ICAS
Group Mean: Control ICAS
Subject Mean: Control ICAS
C
Control: left
Control: right
ICAS: ipsilateral
ICAS: contralateral
VOI values
r_{rm}
-1.0 -0.5 0.0 0.5 1.0

Figure 14. Frequency distribution, group differences and inter-correlation of brain averaged hemodynamic-vascular VOI parameter values.

The first row depicts the frequency distributions of VOI-average hemodynamic-vascular parameter values for the local (A.1) parameters CTH, CBF and rCBV as well as systemic (A.2) parameters, i.e., TTP and BOLD lag, across all participants and separately for the two participant groups. Darkened areas indicate an overlap between the two groups. The second row depicts participants' local (B.1) and systemic (B.2) parameter averages across VOIs as dots. Diamonds with orange outlines indicate group means, with the 95% confidence interval presented in orange as well. In the right panels A.2 and B.2, the dashed line marks a BOLD lag of zero; negative lags correspond to SSS time courses lagging behind tissue VOIs and vice versa for positive lags. For these two panels the x-axis were truncated to encompass values within -4σ to +4σ, i.e. 99.9% of included values. Means for healthy controls and ICAS patients were compared with a Wilcoxon tests, revealing no significant group differences as indicated by the brackets on top (n.s. = not significant). Panel C in the bottom row depicts the average correlation between the different hemodynamic-vascular VOI-average parameter values across participants (repeated measures correlation). Numbers within tiles indicate the average correlation coefficients between the respective parameters across participants. Correlations between parameter values were calculated separately for hemispheres and participant groups. Correlations were considered significant after group- and hemisphere-wise FDR correction at $p < 0.05$, empty tiles indicate insignificant correlations. Abbreviations: CTH, capillary transit time heterogeneity; CBF, cerebral blood flow; rCBV, relative cerebral blood volume; TTP, time-to-peak; BOLD lag, blood oxygen level dependent lag; VOI, volume of interest; ICAS, internal carotid artery stenosis; SSS, superior sagittal sinus.

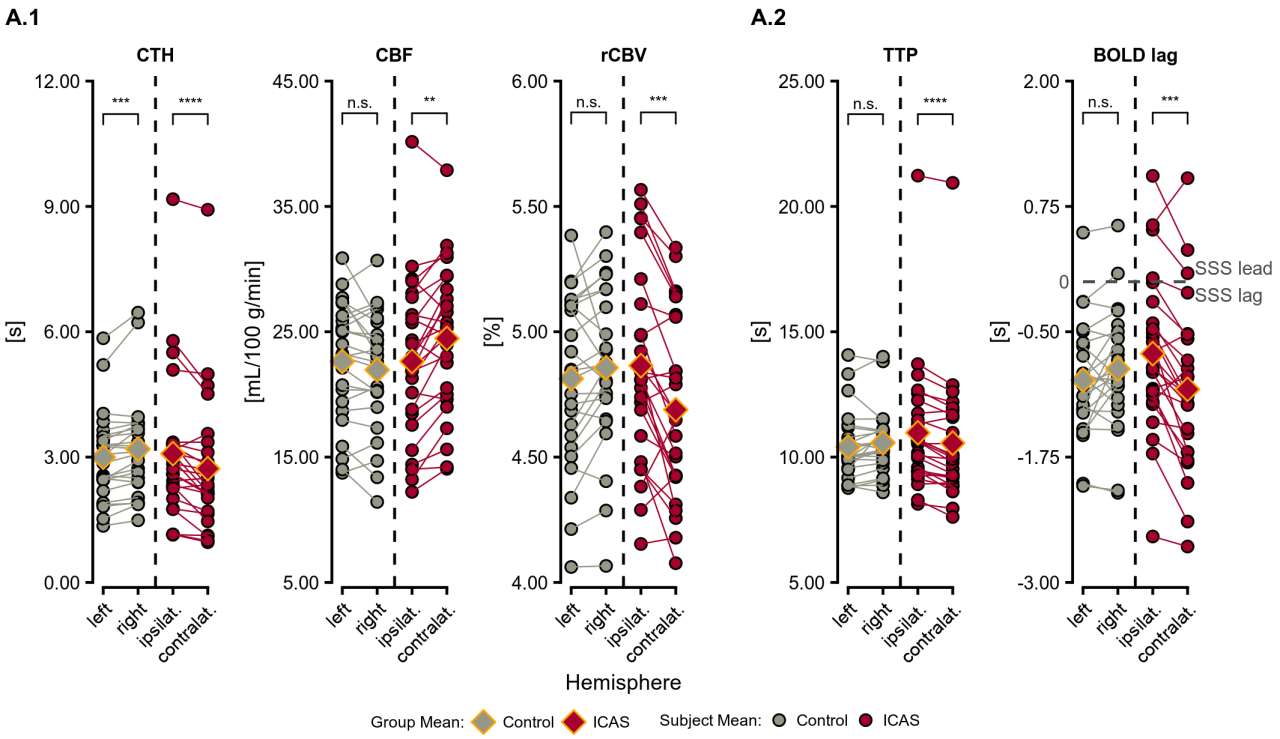

Figure 15. Between-hemisphere comparison of VOI-average hemodynamic-vascular parameters.

Dots indicate individual participants' local (A.1), CTH, CBF and rCBV, as well as systemic (A.2), TTP and BOLD lag, VOI-averaged hemodynamic-vascular parameters across all included VOIs for the respective hemispheres. For ICAS patients, values were compared between the hemispheres ipsi- and contralateral to the stenosis; for healthy controls, between the left and right hemispheres. Diamonds with orange outlines indicate group means. Brackets on top indicate significance of pairwise hemisphere value comparisons with Wilcoxon's signed rank test (n.s. = not significant, *: p<=0.05, **: p<= 0.01, ***: p< 0.001, ****: p<=0.0001). In the right panel of A.2 the horizontal dashed line marks a lag of zero, negative lags correspond to the SSS time courses lagging behind tissue VOIs and vice versa for positive lags. Abbreviations: CTH, capillary transit time heterogeneity; CBF, cerebral blood flow; rCBV, relative cerebral blood volume; TTP, time-to-peak; BOLD lag, blood oxygen level dependent lag; VOI, volume of interest; SSS, superior sagittal sinus.

3.3 Interim-Discussion of Project 2

To compare the impact of systemic and local hemodynamic-vascular factors on BOLD-FC in humans, I conducted an analysis of multiple hemodynamic-vascular MRI parameters and their impact on homotopic BOLD-FC. Equally for both healthy controls and patients with ICAS, I found that local (CTH, CBV, and CBF) and systemic (TTP and BOLD lag) hemodynamic factors together accounted for about 20% of homotopic BOLD-FC variance. Systemic hemodynamic-vascular parameters exerted about twice the influence on BOLD-FC as compared to local hemodynamic-vascular parameters. Considering inter-subject differences in baseline BOLD-FC (i.e., estimated

average BOLD-FC in absence of any hemodynamic-vascular difference), my model explains 40.7% of BOLD-FC variance. My results provide – to the best of my knowledge – the first comprehensive and direct comparisons of systemic and local hemodynamic-vascular influences on BOLD-FC in humans. Results demonstrate that about one-fifth of homotopic BOLD-FC variance is explained by hemodynamic-vascular factors in humans, with a larger impact of systemic versus local factors. Data suggest that BOLD-FC in patient populations with potential local and/or systemic hemodynamic-vascular impairments need to be interpreted with care.

3.3.1 Systemic and local hemodynamic-vascular influences on BOLD-FC

By means of a linear mixed model approach, I found that most of the investigated hemodynamic-vascular parameters explained some BOLD-FC variance in both groups (**Fig. 13 A** and **B**). Specifically, VOI differences in the local parameters CTH and CBF and the systemic parameters TTP and BOLD lag lead to a reduced BOLD-FC.

3.3.1.1 Comparing local and systemic hemodynamic-vascular influences on BOLD-FC.

I compared the relative influence of hemodynamic-vascular factors – in categories of systemic and local – on BOLD-FC by the use of nested multiple regression models. The baseline model, which only included the participants' intercepts (average BOLD-FC across all homotopic VOIs) and interactions with age and Group as predictors, explained 20.5% of overall BOLD-FC variance in the sample, with no significant interaction. This indicates that there is clear inter-subject variability of average homotopic BOLD-FC in the sample, which is not associated with the participants' age or group affiliation. Such variability between participants has previously been found to be region specific and linked to differences in cortical surface area and folding patterns (Mueller et al., 2013). Further factors such as the participants' arousal status might have varied as well due to the prolonged scanning sessions, which has also been shown to increase BOLD-FC variability (Gu et al., 2019), along with other variables such as individual hemoglobin level (Ward et al., 2020).

Adding local hemodynamic-vascular parameters, namely CTH, CBF and rCBV, to the model led to a significantly better fit of the model and increased explained variance by 7.2 percent points to 27.7% overall. In line with previously reported results (Schneider et al., 2022) both homotopic VOI differences in CTH and CBF led to decreased BOLD-FC, with significantly higher decreases due to CTH differences for ICAS patients. Using an approach combining simulations and empirical analyses, BOLD-FC decreases due to CTH differences were previously related to the timing of blood

flow responses to neuronal activity (Schneider et al., 2022). The influence of baseline CBF has repeatedly been reported and tentatively related to differing systemic physiological noise levels between VOIs exhibiting different baseline CBF (Champagne et al., 2020; Chu et al., 2018; Göttler, Preibisch, et al., 2019; Jann et al., 2015; Schneider et al., 2022).

Finally, I included two systemic hemodynamic-vascular parameters, namely TTP and BOLD lag, into the full model. This further increased explained BOLD-FC variance by 13 percent points to overall 40.7%. The addition of these systemic parameters therefore led to a substantially larger gain in variance explained, i.e., 13 percent points compared to 7.2 percent points for the local hemodynamic-vascular parameters alone. This is in line with previous findings, for example, systemic BOLD lags have been demonstrated to explain BOLD-FC variability within brain networks (Erdoğan et al., 2016) to create spurious BOLD-FC (Tong et al., 2015) and cause a recoverable reduction in BOLD-FC (Christen et al., 2015). Together, local and systemic hemodynamic-vascular parameters explained about 20% of overall BOLD-FC variance in my sample, with a two times stronger contribution of systemic parameters.

3.3.1.2 Individual hemodynamic-vascular influences on BOLD-FC:

Next, I discuss the individual influence of single hemodynamic-vascular factors on BOLD-FC and how they link with other factors and their influences, respectively.

BOLD lag: In the full model, encompassing all available local and systemic hemodynamic-vascular parameters, the strongest influence on BOLD-FC was exerted by homotopic VOI differences in BOLD lag. This is line with previous results showing a strong influence of BOLD lags on BOLD-FC in simulations (Christen et al., 2015; Tong et al., 2015), healthy controls (Erdoğan et al., 2016; Tong et al., 2015) and populations with systemic hemodynamic-vascular impairments, for example in patients with Moyamoya-disease (Amemiya et al., 2014; Christen et al., 2015; Jahanian et al., 2018; Y. Lv et al., 2013; Siegel et al., 2016; T. Wang et al., 2017). The origin of lags in the BOLD signal has previously been strongly linked to systemic cerebral blood transit times and intrinsic hemodynamic properties of the traveling blood (Amemiya et al., 2020; Aso et al., 2019; Donahue et al., 2016; Khalil et al., 2020; Tong et al., 2017; Tong, Yao, et al., 2019; Tong & Frederick, 2014; Yao et al., 2019). Temporal differences in blood delivery between brain regions are supposed to result in temporally mismatched BOLD signal components, which finally – and without relation to neuronal activity – lead to reduced BOLD-FC (Erdoğan et al., 2016; Jahanian et al., 2018; Tong et

al., 2015). Interestingly, in my sample, BOLD lag and in particular lag differences between hemispheres (ΔBOLD lag) were only very weakly correlated to the other parameters and parameter differences, indicating that BOLD lag represents a hemodynamic-vascular parameter rather independent from the selected others. Actually, I expected a higher correlation with TTP because of previous studies that compared TTP with BOLD lag maps albeit with different approaches as in the present study. However, BOLD lag maps and DSC-derived TTP depend on a voxels' vascular composition, i.e., the relative percentage of arteries, capillaries and veins, which matters because the BOLD signal is less sensitive to arterial signals (Amemiya et al., 2014; Tong et al., 2017). Such effects may well contribute to the observed difference between TTP and BOLD lags in my VOI-based analyses.

TTP: VOI differences in contrast agent-based TTP exerted the second strongest influence on BOLD-FC, which, to the best of my knowledge, has not yet been investigated. While – as discussed above – TTP actually resembles some aspects of BOLD lags and is an established indicator for systemic cerebral perfusion delay, it also represents a summary signal that partially incorporates aspects of tissue transit times and arterial dispersion (Wouters et al., 2017), which can vary between regions as well. In line with previous physiological findings showing an association between TTP and CBF (Hara et al., 2017), TTP was moderately correlated to both CTH and CBF across all participants, with differences in TTP consequently being likewise correlated to differences in CTH and CBF for both groups, albeit much stronger in ICAS patients. This also indicates a small degree of multicollinearity between TTP, CTH and CBF, implying also some shared BOLD-FC variance, i.e., variance not unambiguously explained by TTP, CTH or CBF differences.

CTH and CBF: Finally, and in agreement with our previous study (Schneider et al., 2022), CTH and CBF differences were likewise found to significantly influence homotopic BOLD-FC. Interestingly, as compared to the hierarchically lower model, incorporating only participant intercepts and local hemodynamic-vascular parameters, the estimated influence of CTH differences on BOLD-FC was weaker in the full model and the group-effect likewise vanished. This is most likely due to the additional inclusion of TTP and BOLD lag, which may explain some of the variance that was previously solely attributed to CTH, as their simultaneous influence was previously not controlled for. Across participants, VOI-average CTH values, along with their pairwise differences, were additionally correlated with CBF and rCBV and their corresponding differences. This is in line with

previous work considering the interplay of CBF and CTH (Jespersen & Østergaard, 2012; Østergaard, 2020; Schneider et al., 2022). As already stated above, this indicates some degree of multicollinearity, resulting in some shared, not unambiguously explained BOLD-FC variance. This could also explain why no significant overall effect of rCBV on BOLD-FC was found. However, our previous simulation results also indicate that the influence of CBV should to be rather negligible in the realm of intrinsic low frequency BOLD signal oscillations (Archila-Meléndez et al., 2020).

Overall, both local and systemic hemodynamic-vascular parameters appear to be fundamental in shaping regionally specific BOLD signal fluctuations which are not necessarily related to neuronal activity. Differences in the timing of blood oxygenation changes, both on a local (CTH) but primarily on a systemic level (TTP and BOLD lag), seem to be the primary cause for mismatches in BOLD signal time courses and therefore decreased correlation, i.e., BOLD-FC.

3.3.2 Implications for BOLD-FC studies in populations with hemodynamic-vascular impairments

In general, my results support a BOLD model, where observed BOLD signal fluctuations are shaped by both local neurally-evoked and non-neural oxygenation fluctuations (Das et al., 2021; Drew, 2019), with hemodynamic-vascular factors being a substantial part of non-neuronal factors shaping BOLD signal fluctuations. This has considerable implications for rs-fMRI studies in populations with distinct hemodynamic-vascular disorders. In my sample including ICAS patients, I did not find differences between healthy controls and ICAS patients regarding the impact of hemodynamic-vascular differences between homotopic VOIs on BOLD-FC, i.e., there was no evidence for principally stronger effects in this patient population. However, there was a strong trend for an overall lower homotopic BOLD-FC among the ICAS patients, as compared to healthy controls, as indicated by the lower intercept ($p = 0.06$) in the intercept model. This intercept difference vanished once local hemodynamic-vascular differences were included and even more so after inclusion of systemic parameter differences in the full model. This shows that ICAS patients exhibit lower baseline homotopic BOLD-FC, if hemodynamic-vascular differences between VOI pairs are not considered. In other words, while the estimated absolute impact of hemodynamic-vascular differences on BOLD-FC is equally strong between healthy controls and ICAS patients, the larger between VOI differences among patients led to overall larger BOLD-FC impairments. These results, even though not significant, are well in line with previous reports of BOLD-FC aberrations in

samples of ICAS patients. These previous studies reported a significantly lower homotopic BOLD-FC for ICAS patients as compared to healthy controls, specifically in the bilateral putamen, lateral parietal lobes, premotor, somatosensory, planum temporale, and opercular cortices (Gao et al., 2019) as well as a generally reduced network symmetry and reduced BOLD-FC between bilateral dorsolateral prefrontal cortices and bilateral (intra) parietal lobules (Avirame et al., 2015; Cheng et al., 2012). In our previous work, I likewise found localized homotopic BOLD-FC differences between regions of the parahippocampal, superior orbitofrontal, lateral as well as medial occipital gyruses and orbital sulcus (see Figure S1 in Schneider et al., 2022). Overall these results corroborate the strong trend towards generally and significantly lower homotopic BOLD-FC in ICAS patients I found in this study. The fact that this trend vanishes with the inclusion of hemodynamic-vascular parameters, substantiates the conclusion that differences in BOLD-FC for ICAS patients are caused by and could be accounted for by hemodynamic-vascular differences between brain regions. A similar approach has also been shown to be successful for BOLD-FC estimates between healthy younger and older adults as well as healthy controls and mild-traumatic brain injury patients (Champagne et al., 2020, 2022).

Larger and less homogenously distributed hemodynamic-vascular differences between homotopic VOIs might occur in other disorders, which can explain larger BOLD-FC alterations as seen for example in patients with Moyamoya, stroke or Alzheimer's disease (Christen et al., 2015; Göttler, Preibisch, et al., 2019; Jahanian et al., 2018). Furthermore, my findings suggest a paradoxical effect of local and systemic hemodynamic-vascular disorders on BOLD-FC: I expect that *focal* impacts on the hemodynamic-vascular *system*, e.g., a stenosis of a feeding artery such as ICAS, lead to stronger BOLD-FC aberrations than broad and widespread disorders of local hemodynamic-vascular parameters, such as neurovascular coupling, NVC. Such NVC impairments are, for example, present across different neuropsychiatric disorder like schizophrenia or depression (Hoirisch-Clapauch et al., 2014; Katsel et al., 2017; Najjar et al., 2017; Shalev et al., 2009), stroke, dementia or multiple sclerosis (Merlini et al., 2012; Soto-Rojas et al., 2021; VanGilder et al., 2011; Yu et al., 2020; Zlokovic, 2011). NVC disorders may be expected to primarily cause alterations of local hemodynamic-vascular parameters such as CTH or CBF and less alterations of systemic parameters such as TTP or BOLD lag. However, as I have shown above, local NVC parameter aberrations exhibit less impact on BOLD-FC than aberrations of systemic parameters, which result from isolated and focal lesions, such as carotid artery stenosis or occlusion, Moyamoya or stroke (Amemiya et al., 2012, 2014; Christen et al., 2015; Ciacciarelli et al., 2020; Kaczmarz et al., 2021;

Siegel et al., 2016; Viticchi et al., 2021; L. Wang et al., 2021; Zou et al., 2022). The latter diseases lead to both sweeping systemic perfusion delays *and* alterations of local NVC, and thus, exert an influence on BOLD-FC by both impairments of local and systemic hemodynamic-vascular parameters. Largest BOLD-FC impairments would therefore be expected in populations with aberrations of systemic parameters, which are caused by focal disorders. The interpretation of BOLD-FC in patient populations should, therefore, consider which aspects of the cerebral hemodynamic-vascular system is affected, i.e., more local or systemic hemodynamic-vascular parameters.

3.3.3 Strength & Limitations

In this study, I implemented a procedure that allows a standardized comparison of multiple different hemodynamic-vascular parameters' influences on BOLD-FC via regression coefficients, offering an intuitive interpretation of these coefficients, namely standardized change in BOLD-FC, ΔBOLD-FC, for a hemodynamic-vascular parameter difference of one standard deviation, |ΔX|. This approach can be easily extended to include further parameters, is scalable to larger sample sizes, and can be used for different participant and patient groups. I thus argue that the current study design is suitable to implement a standardized comparison of hemodynamic-vascular parameter influences on BOLD-FC across different populations. Furthermore, the incorporation of hemodynamic-vascular parameters from different acquisitions, i.e., DSC, pCASL and functional BOLD MRI also strengthen my approach. Instead of being restricted to one modality and thus suffering from less generalizable results and less robust estimates, I could show a significant impact of various hemodynamic-vascular parameters on BOLD-FC, irrespective of acquisition modality. This also suggests that hemodynamic-vascular parameters from further acquisition methods can easily be incorporated in future studies.

However, *quantitative* measurement of physiological MRI parameters also suffers from a number of limitations that have been discussed in detail before, e.g., potential measurement bias due to prolonged arterial transit times in single PLD pCASL (Kaczmarz et al., 2021; Schneider et al., 2022). With respect to my statistical analysis, some of the parameters and parameter differences were *interrelated*, irrespective of acquisition method. While this is inevitable and even expected due to the nature of their interplay in orchestrating and indicating cerebral blood and oxygen supply, it raises the issue of multicollinearity in regression analysis. However, the average correlation strengths were sufficiently low and restricted to only very few parameters allowing them to be

included. Furthermore, I could not account for all potential hemodynamic-vascular influences on BOLD-FC in the model and had to restrict my analysis to a selected set of accessible parameters. The included parameters were, however, derived from both previous studies and theoretical implications covering a wide range of potential influences on both a local and systemic level. Nevertheless, future studies could benefit from *adding additional* parameters such as cerebrovascular reactivity or oxygen metabolism. In line with that, I also could not account for neuronal factors that could for example be covered by EEG-based regional brain activity. Lastly, I also did not account for interactions between hemodynamic-vascular parameters, i.e., the effect on BOLD-FC if differences among two or more of the parameters are concurrently present for a homotopic VOI pair. While this would likely constitute a model with better ecological validity and increase variance explained, the model complexity would also increase by a large margin. This would not only be computationally intense, but more importantly also significantly hinder interpretations because of a less stable and generalizable model. To keep the analysis robust, generalizable, and interpretable, I therefore restricted my approach to only include interactions with group affiliation and age.

3.3.4 Conclusion

In healthy elderly and patients with asymptomatic ICAS, about one-fifth of BOLD-FC variance is explained by hemodynamic-vascular factors, with systemic factors having plainly more impact than local ones. This implies that largest BOLD-FC impairments would be expected in patient populations with focal brain disorders that primarily exhibit aberrations of systemic hemodynamic-vascular parameters. In any case, acquisition of additional hemodynamic-vascular MRI aids interpretation of BOLD-FC in particular in patients.

4. Project 3: Comparison of hemodynamic-vascular influences on BOLD-FC between FC-types

Results of this Project have not been previously presented publicly or submitted to a journal.

4.1 Methods of Project 3

This project used a largely identical study sample, data and procedures as compared to Project 2 (Schneider et al., 2023). Therefore, identical aspects will not be described again in detail in the following methodological descriptions but I will refer to previous descriptions instead. New methods will be detailed in sections 4.1.5. and 4.1.6.

4.1.1 Participants

The same sample of 51 participants, 26 ICAS patients (10 females) and 25 controls (14 females) used for Project 2, from the previously described ICAS sample (Göttler, Kaczmarz, et al., 2019; Kaczmarz et al., 2021; Schneider et al., 2022, 2023) (see also Projects 1 and 2), were re-analyzed for Project 3. Mean age was 72 years (range: 52 to 84 years), see 3.1.1 and **Table 5** for a detailed description.

4.1.2 MRI data acquisition

As for Projects 1 and 2 (Schneider et al., 2022, 2023), MR imaging was performed on a 3T Philips Ingenia MR-Scanner (Philips Healthcare, Best, The Netherlands). Used images were derived from T1-weighted MPRAGE, T2*-weighted multiband EPI time series, Gd-Dota based DSC MRI and pCASL (see 3.1.2 for a detailed description).

4.1.3 BOLD signal preprocessing

The minimally preprocessed BOLD fMRI data from Project 2 (Schneider et al., 2023), was used again for Project 3 (see 3.1.3 for more details).

4.1.4 Calculation of hemodynamic-vascular parameter maps

Akin to the previous sections, calculation of hemodynamic-vascular parameters was identical to Project 2 and comprised calculation of CTH, rCBV and TTP from DSC data, quantitative baseline CBF from pCASL and BOLD lag maps from BOLD rs-fMRI (see 3.1.4 for a detailed description).

4.1.5 Calculation of BOLD-FC and hemodynamic-vascular differences for different FC-types

BOLD-FC calculation: Whereas previously only *homotopic* BOLD-FC was considered, the analysis for Project 3 required calculation of *heterotopic* as well as *intrahemispheric* BOLD-FC. To this end, I largely followed the same procedure as described in Projects 1 and 2 (Schneider et al., 2022, 2023). All analysis were carried out in the participants' native fMRI space, to which the *Atlas of Intrinsic Connectivity of Homotopic Areas* (AICHA; Joliot et al., 2015), comprising 384 VOIs, was resliced and masked by an individual GM mask (see 3.1.5 *BOLD-FC analysis* for more details). Then pairwise BOLD-FC was calculated between all 384 VOIs for each participant and classified into three FC-types: *Homotopic*-BOLD-FC, i.e., FC between interhemispheric left and right homotopic areas, *heterotopic* BOLD-FC, i.e., FC between interhemispheric, but non-homotopic, areas and *intrahemispheric* BOLD-FC, i.e., BOLD-FC between areas on the same hemisphere, left and right (see **Fig. 16** for a demonstration of FC-types). BOLD-FC was generally derived by calculating Pearson's correlation between the respective VOIs' BOLD-time courses and subsequently performing Fisher-r-to-Z transformation on the correlation values to obtain BOLD-FC values.

Hemodynamic-vascular parameter analysis: Pairwise differences in the respective hemodynamic-vascular parameters, local (CTH, baseline CBF and rCBV) and systemic (TTP and BOLD lag), were obtained similar to the above described BOLD-FC calculation (see 3.1.5 *Hemodynamic-vascular parameter analysis)*. From the same GM-masked AICHA atlas that was resliced to the individual parameter maps, VOI-average parameter values were extracted for all 384 VOIs for each participant. Pairwise absolute parameter differences between all VOIs were then calculated, e.g., for CTH, $|\Delta CTH|$ [sec] = $|CTH_{VOI\text{-}1} - CTH_{VOI\text{-}2}|$. Calculated differences were classified into different types, depending on the spatial relationship between the regions involved, i.e., *Homotopic difference* (if calculated between interhemispheric left and right homotopic areas), *heterotopic difference* (if calculated between interhemispheric, but non-homotopic, areas) and *intrahemispheric difference* (if calculated between areas on the same hemisphere, left and right). Differences of 0, therefore, indicate equal regional parameter values while differences unequal to 0 indicate a mismatch in the respective parameter between the involved regions.

Outlier exclusion: Following the procedure established for Project 2 (Schneider et al., 2023), some VOIs were excluded prior to the statistical analysis. This followed the same rational as described in

3.1.5 Outlier exclusion. VOIs previously excluded by that procedure were likewise excluded for Project 3. Further, to exclude physiologically implausible values resulting from artifacts or partial volume effects, VOI-average values were z-standardized and values below and above 3 standard deviations were excluded. VOIs with a missing homotopic partner VOI after this procedure were excluded as well. This lead to an overall number of 1.6 Million BOLD-FC estimates to be included in the analysis across all FC-types and participants.

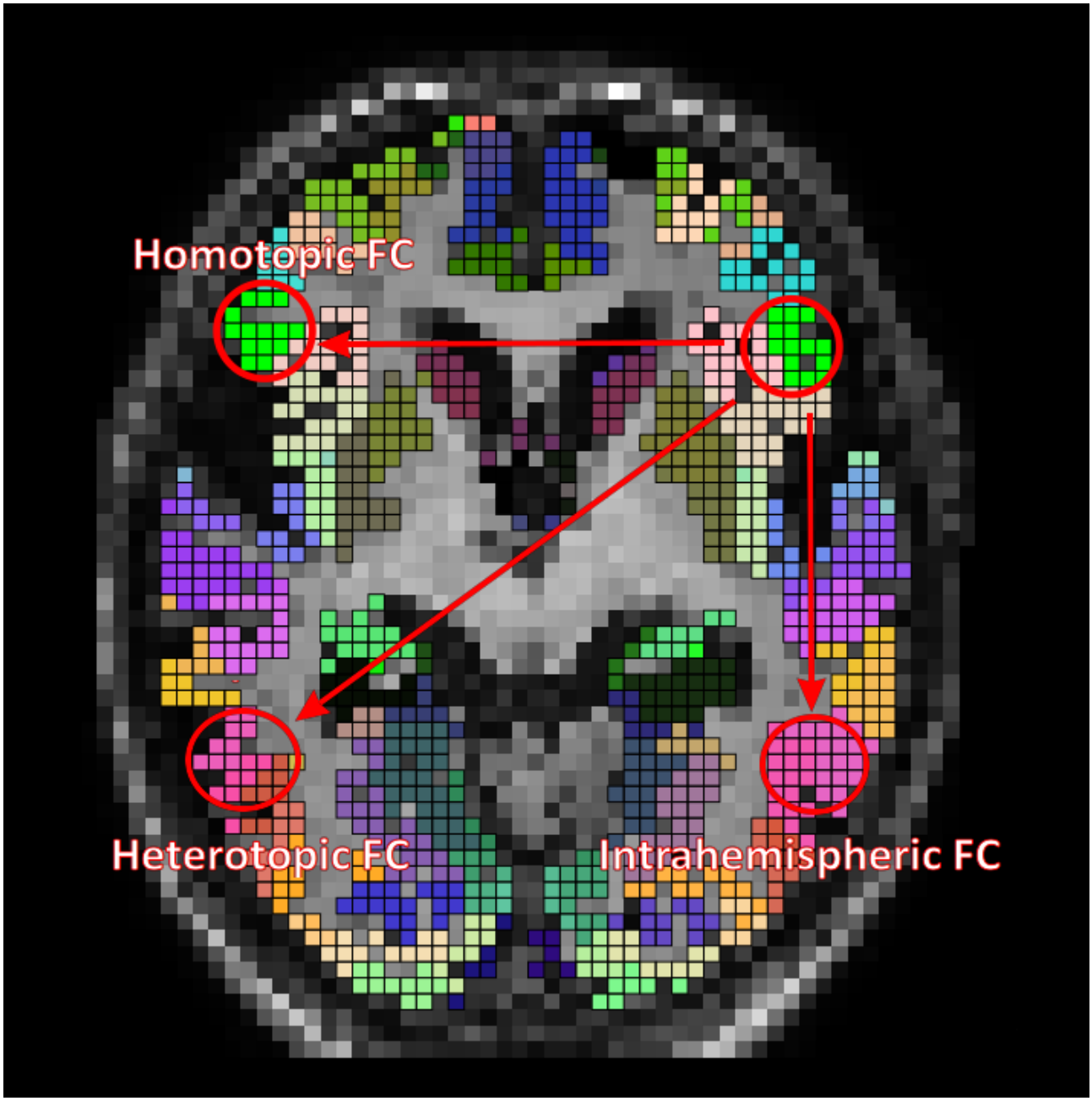

Figure 16. Overview of FC-types used for Project 3.

The different types of BOLD-FC are indicated with respect to the seed region in the upper right corner indicated with a red circle. Homotopic BOLD-FC is defined as the FC between the seed region and its homotopic partner region on the

contralateral hemisphere. Heterotopic BOLD-FC is the FC between the seed region and any other, non-homotopic, region on the contralateral hemisphere. Intrahemispheric BOLD-FC is the FC between the seed region and any other region on the ipsilateral hemisphere. Abbreviations: FC, functional connectivity, i.e. blood-oxygenation-level-dependent functional connectivity (BOLD-FC).

4.1.6 Statistical Analysis

Baseline differences in hemodynamic-vascular differences for FC-types: To assess potential baseline differences in hemodynamic-vascular VOI differences, I compared group average absolute VOI differences for each parameter and FC-type via a Wilcoxon rank sum test. In addition, I examined if VOI differences differed significantly between the FC-types within groups.

Baseline BOLD-FC differences between FC-types: Before comparing the influence of hemodynamic-vascular parameters between FC-types, I first wanted to examine potential baseline differences in connectivity strength between both the FC-types and the participant groups. For that, I used a regression model containing participants' BOLD-FC as dependent variable and FC-type as well as the factor group, ICAS or healthy controls, as sole predictor variables. This allowed both generally comparing average FC-strength between types of BOLD-FC, i.e., homotopic, heterotopic and intrahemispheric, as well as between group differences for each type of FC separately.

Regression analysis for hemodynamic-vascular differences: The approach for analyzing potential differences between FC-types with regard to the influence of hemodynamic-vascular parameters followed the same regression logic as in Projects 1 and 2 (Schneider et al., 2022, 2023): The distinct influence of systemic and local hemodynamic-vascular parameters on BOLD-FC across different FC-types was analyzed via a linear-mixed model (LMM). The model contained BOLD-FC as the dependent variable and the VOI differences $|\Delta X|$ of each systemic and local hemodynamic-vascular parameter as regression predictors, as well as the group variable, ICAS or healthy controls, and participant age (centered on the median of 72 years), akin to Projects 1 and 2 (Schneider et al., 2022, 2023). As a new feature, the variable FC-type was introduced, which allowed to discern the influence of hemodynamic-vascular parameters by type of BOLD-FC.
In order to achieve comparable effect sizes between hemodynamic-vascular regressors, differences were z-standardized as described in detail for Projects 1 and 2 (Schneider et al., 2022, 2023 and see 3.1.6). However, to specifically obtain effect sizes comparable to Project 2 (Schneider et al.,

2023), the hemodynamic-vascular differences for Project 3 were z-standardized using the standard deviation for homotopic differences only and not overall standard-deviation.
The regression analysis was carried out using lme4 package (Bates et al., 2015) for R (R Core Team, 2020) within Rstudio (RStudio Team, 2019). The p-values for prediction terms and respective degrees of freedom were estimated using Satterthwaite's method using the Tests in Linear Mixed Effects Models (lmerTest) package (Kuznetsova et al., 2017), as for Project 1 and 2 (Schneider et al., 2022, 2023).

Post-hoc analysis of FC-type differences: With the introduction of the factor FC-types in the regression model, not all pairwise comparisons could be directly assessed with the baseline regression models, because the FC-type factor features 3 levels. The baseline modesl itself only allow for a within-group comparison of a *change* in intercept or slopes between the reference level, i.e., homotopic BOLD-FC, and the two other levels, i.e., heterotopic as well as intrahemispheric BOLD-FC, respectively. However, a within-group comparison of *absolute* intercepts and slopes between all three FC-types cannot be directly assessed. Neither can the models directly provide between-group comparisons of *absolute* intercepts and slopes for all three FC-types, but solely group differences with regard to the respective *change* compared to the reference FC-type, i.e., homotopic BOLD-FC.
I therefore conducted additional Tukey post-hoc tests to assess pairwise differences between *absolute* intercepts and slopes across FC-types within groups and also differences of *absolute* intercepts and slopes between groups for each FC-type. For the intercept model, *mean* BOLD-FC (not change in BOLD-FC) was thus first compared between groups for each of the FC-types, i.e., difference in average BOLD-FC between healthy controls and ICAS for each homotopic, heterotopic and intrahemispheric BOLD-FC. Within-group differences of mean BOLD-FC were then compared pairwise across the three FC-types, i.e., first difference between homotopic and heterotopic BOLD-FC, second between homotopic and intrahemispheric BOLD-FC and lastly between heterotopic and intrahemispheric BOLD-FC. For the full-model containing hemodynamic-vascular differences, this procedure was then likewise conducted for the slopes of all five hemodynamic-vascular predictors. P-values were corrected for multiple comparison within each "set" of comparisons, i.e., for each slope and intercept separately.

4.2 Results of Project 3

Aim of Project 3 was to investigate whether the influence of hemodynamic-vascular parameters differs between different types of BOLD-FC, i.e., homotopic, heterotopic and intrahemispheric. I additionally examined if the average BOLD-FC strength of ICAS patients differs from healthy controls for the three connectivity types, respectively.

Pairwise homotopic hemodynamic-vascular parameter differences and their correlations: When comparing average VOI differences (averaged across all VOI pairs within participants), i.e., average |ΔX|, I found significantly larger homotopic differences in |ΔCBF| and |ΔBOLD lag| for ICAS patients, while other parameters homotopic differences were not significantly different across groups (see **Fig. 17** and **18**). For heterotopic VOI pairs, ICAS patients exhibited significantly larger BOLD lag differences (see **Fig. 18**). There were no significant group differences for intrahemispheric VOI pairs.

For within group differences a consistent pattern emerged for both groups and across all parameters. Homotopic VOI differences were always significantly smaller as compared to either heterotopic or intrahemispheric VOI differences (see **Fig. 19**). Likewise, intrahemispheric VOI differences were always slightly, but significantly smaller as compared to differences between heterotopic VOIs for all parameters (see **Fig. 19**)

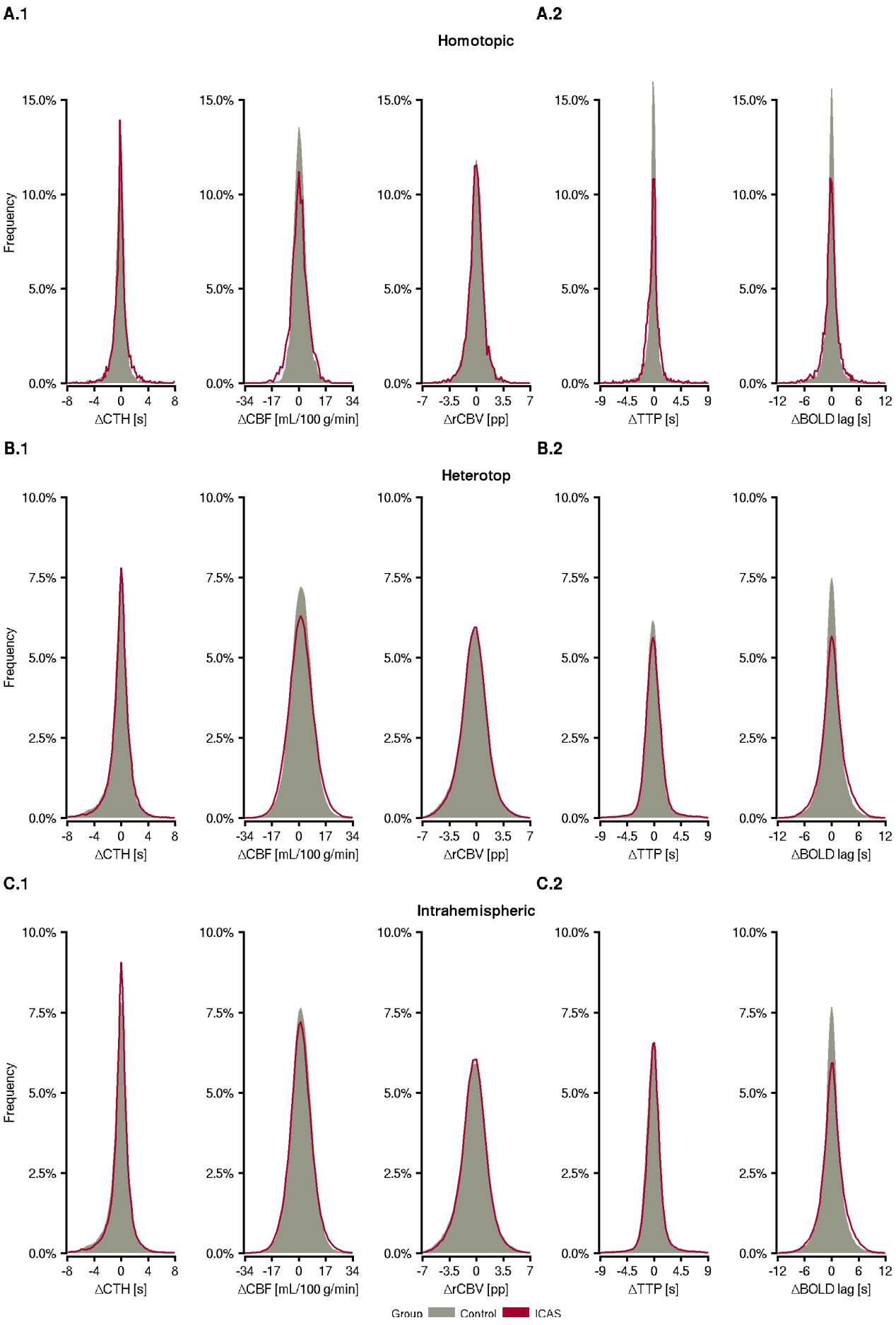
A.1
A.2
Homotopic
B.1
B.2
Heterotop
C.1
C.2
Intrahemispheric
Frequency
ΔCTH [s]
ΔCBF [mL/100 g/min]
ΔrCBV [pp]
ΔTTP [s]
ΔBOLD lag [s]
Group
Control
ICAS

Figure 17. Frequency distribution of hemodynamic-vascular VOI-average parameter differences for different FC-types.

The first row depicts the frequency distributions of homotopic VOI differences for each of the local (A.1), i.e., ΔCTH, ΔCBF and ΔrCBV, as well as systemic (A.2), i.e., ΔTTP and ΔBOLD lag, hemodynamic-vascular parameters across all participants and separately for the two participant groups. Rows 2 and 3 indicate these distributions for heterotopic (B.1 and B.2) and intrahemispheric (C.1 and C.2) VOI pairs, respectively. Negative values imply larger values for the right-sided VOI of a pair and vice versa for positive values, except BOLD lag where the directionality is reversed. For these two panels the x-axis were truncated to encompass values within -4σ to +4σ, i.e. 99.9% of included values. Abbreviations: CTH, capillary transit time heterogeneity; CBF, cerebral blood flow; rCBV, relative cerebral blood volume; TTP, time-to-peak; BOLD lag, blood oxygen level dependent lag; ICAS, internal carotid artery stenosis.

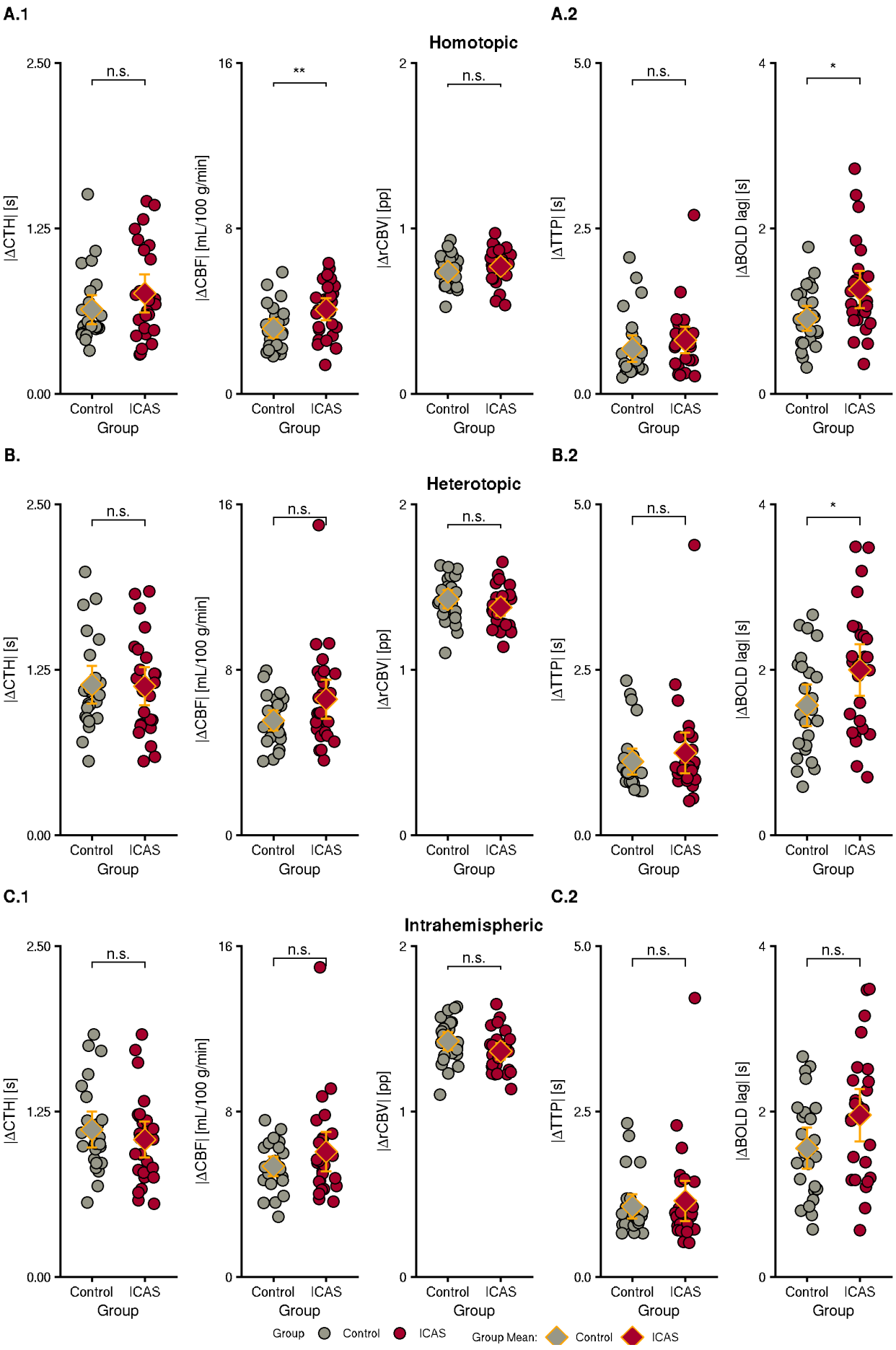
A.1
A.2
Homotopic
B.
B.2
Heterotopic
C.1
C.2
Intrahemispheric
|ΔCTH| [s]
|ΔCBF| [mL/100 g/min]
|ΔrCBV| [pp]
|ΔTTP| [s]
|ΔBOLD lag| [s]
n.s.
**
*
Control
ICAS
Group
Group Mean:

Figure 18. Between-group differences of hemodynamic-vascular VOI-parameter differences for different FC-types.

The first row depicts participants' average local (A.1) and systemic (A.2) homotopic VOI differences for homotopic VOI pairs as dots. Diamonds with orange outlines indicate group means. Rows 2 to 3 indicate the same for heterotopic (B.1 and B.2) and intrahemispheric (C.1 and C.2) VOI pairs respectively. Group means were compared between HC and ICAS with a Wilcoxon test. Significance is indicated by the brackets on top (n.s. = not significant, *: p<=0.05, **: p<= 0.01, ***: p< 0.001, ****: p<=0.0001). Abbreviations: CTH, capillary transit time heterogeneity; CBF, cerebral blood flow; rCBV, relative cerebral blood volume; TTP, time-to-peak; BOLD lag, blood oxygenation level dependent lag; VOI, volume of interest; ICAS, internal carotid artery stenosis.

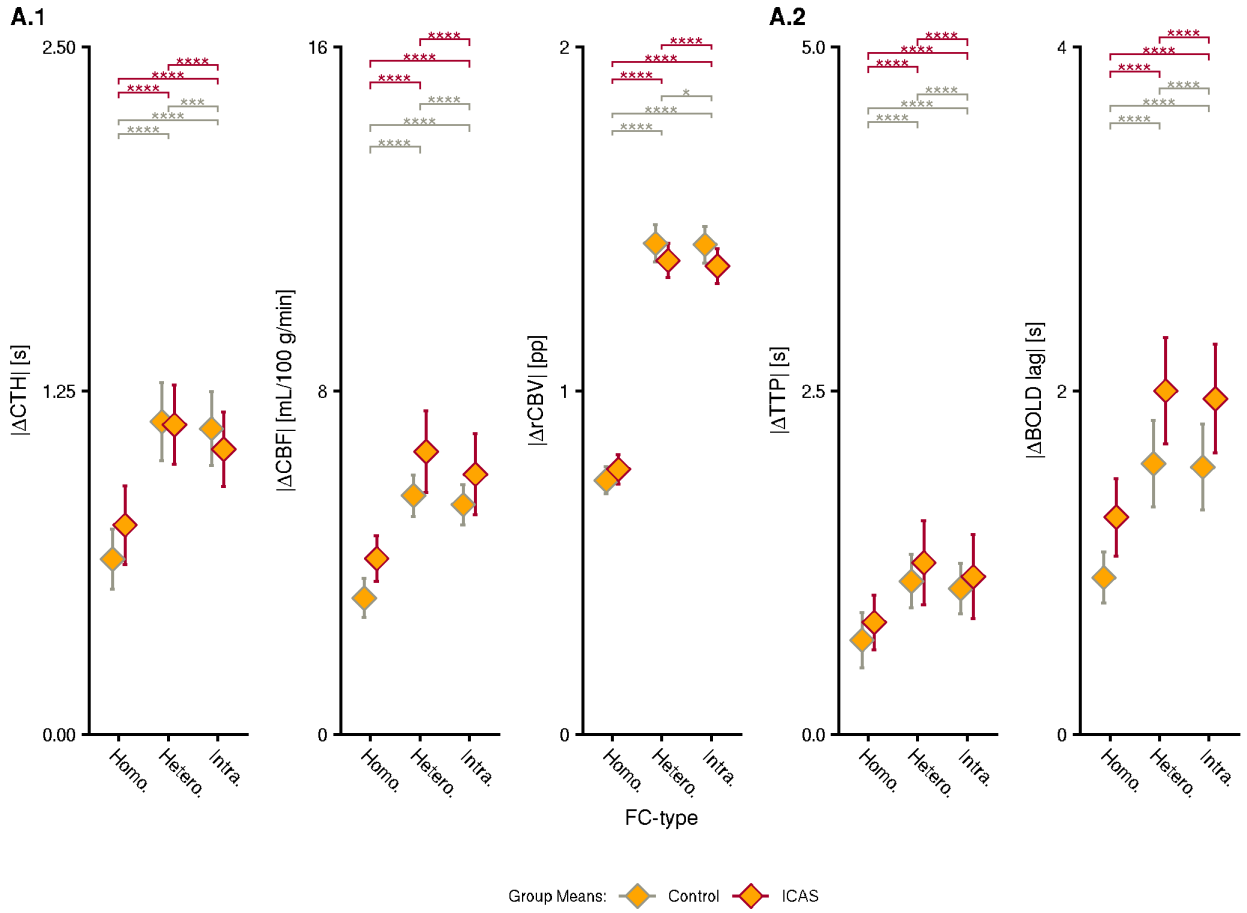

Figure 19. Within-group differences of hemodynamic-vascular VOI-parameter differences between FC-types.

Panels depicts group average local (A.1) and systemic (A.2) VOI differences for homotopic, heterotopic and intrahemispheric VOI pairs as diamonds. Larger values on the y-axis indicate larger VOI differences. Within group differences between the FC-types were compared with a paired Wilcoxon-test. Significance is indicated by the brackets on top (n.s. = not significant, *: p<=0.05, **: p<= 0.01, ***: p< 0.001, ****: p<=0.0001), with color depicting the respective groups. Abbreviations: CTH, capillary transit time heterogeneity; CBF, cerebral blood flow; rCBV, relative cerebral blood volume; TTP, time-to-peak; BOLD lag, blood oxygenation level dependent lag; VOI, volume of interest; ICAS, internal carotid artery stenosis.

Average BOLD-FC strength for FC-types and groups: Comparing group-wise average BOLD-FC strength across FC-types via the intercept regression model revealed clearly and significantly ($p < 0.001$) lower average BOLD-FC strength for heterotopic (-0.68) and intrahemispheric (-0.652) BOLD-FC as compared to homotopic BOLD-FC (1.135, see **Table 9**) across both groups (see **Fig. 20**). This decrease in FC strength was slightly but significantly stronger for healthy controls as compared to ICAS patients ($p < 0.001$, see interaction of FC types with group factor in **Table 9**). The regression analysis furthermore indicated a strong trend towards overall significantly lower homotopic connectivity strength for ICAS patients as compared to the healthy controls, as likewise detected in Project 2 ($p = 0.06$, see also interaction of intercept and group factor in **Table 9**).

To obtain absolute group-wise estimates (not only differences) of mean BOLD-FC and all pairwise comparisons, I furthermore conducted a post-hoc analysis of the intercept regression model. For between-group comparisons the post-hoc analysis revealed largely similar average BOLD-FC between healthy controls and ICAS patients for both heterotopic ($p = 0.4$) and intrahemispheric BOLD-FC ($p = 0.5$), but highlighted again the different homotopic BOLD-FC ($p=0.06$) (see **Table 10** and **Fig. 20**).

For within-group comparisons, this additionally revealed slightly, but significantly higher intrahemispheric BOLD-FC as compared to heterotopic BOLD-FC for both groups (see **Table 11** and **Fig. 20**) and corroborated the significant differences between homotopic FC and the other types, as found in the regression model (see **Table 9** and **11**). For full results, including absolute estimates of average BOLD-FC and within-as between-group differences see **Tables 10** and **11**.

Table 9. Summary of *FC-type Intercept* regression model.

Predictors	**Estimates**	**CI**	**Statistic**	***p***
(Intercept)	1.14	1.085 – 1.186	44.05	**<0.001**
Group	0.05	-0.002 – 0.099	1.9	0.06
Age	0	-0.008 – 0.009	0.1	0.93
Group:Age	0	-0.004 – 0.013	1.02	0.31
FC-type[Hetero.]	-0.68	-0.687 – -0.674	-203.74	**<0.001**
FC-type[Hetero.]:Group	-0.03	-0.034 – -0.021	-8.26	**<0.001**
FC-type[Hetero.]:Age	0	-0.001 – 0.001	-0.2	0.84
FC-type[Hetero.]:Group:Age	0	-0.003 – -0.001	-3.98	**<0.001**

FC-type[Intra.]	-0.65	-0.659 – -0.645	-195.19	**<0.001**
FC-type[Intra.]:Group	-0.03	-0.039 – -0.026	-9.85	**<0.001**
FC-type[Intra.]:Age	0	-0.001 – 0.001	-0.35	0.73
FC-type[Intra.]:Group:Age	0	-0.004 – -0.001	-4.27	**<0.001**

Note: Under predictors the variables incorporated in the model are listed. Group variable was deviation coded (Group: ICAS = -1, Controls = 1). The FC-type variable consisted of three levels, homotopic BOLD-FC as the reference level (coded as 0), and heterotopic as intrahemishpheric BOLD-FC as the two further levels. and Age was centered on the median age in the sample (participants with a median age equal 0 in the coding). The intercept estimate describes average BOLD-FC when all other predictor variables are 0, i.e. for all included participants of median age and for homotopic BOLD-FC. Estimates for other variables indicate the estimated change in BOLD-FC should the predictor value increase by 1 (Group: to health controls, age: to one year above median age of 72 and FC-type to heterotopic or intrahemispheric BOLD-FC respectively). Interactions between participant group and predictors are indicated by a colon. Confidence intervals for the estimates are indicated by CI. If no CI is indicated this means that the effect was always smaller than 0.001. The test statistic is derived from a one-sample t-test, against the null-hypothesis that the estimate does not differ significantly from 0. Effects for the ICAS patients are identical to those of the healthy control group, except being reversed in polarity (Group coding for ICAS patients = -1).

Table 10. Summary of *post-hoc analysis* for *between* group-differences of the *FC-type Intercept* regression model.

FC-type	**Control: mean**	**ICAS: mean**	**Difference**	***p***
Homotopic	1.18	1.09	0.1	0.06
Heterotopic	0.48	0.43	0.04	0.41
Intrahemispheric	0.5	0.47	0.03	0.54

Note: Columns 2 and 3 indicate group-wise mean BOLD-FC for the respective FC-type. P-values were derived from Tukey's test of multiple comparison.

Table 11. Summary of *post-hoc analysis* for *within* group-differences of the *FC-type Intercept* regression model.

Contrast	**Control: mean**	**Control: difference**	**ICAS: mean**	**ICAS: difference**
Homo : Hetero	1.18 : 0.48	0.71, ***p* < 0.001** (60 %)	1.09 : 0.43	0.65, ***p* < 0.001** (60 %)
Homo : Intra	1.18 : 0.50	0.69, ***p* < 0.001** (58 %)	1.09 : 0.47	0.62, ***p* < 0.001** (57 %)
Hetero : Intra	0.48 : 0.50	-0.02, ***p* < 0.001** (-5 %)	0.43 : 0.47	-0.03, ***p* < 0.001** (-8 %)

Note: Columns 2 and 4 indicate group-wise mean BOLD-FC for the respective FC-types, as indicated by the Contrast column. P-values were derived from Tukey's test of multiple comparison and adjusted for multiple comparison.

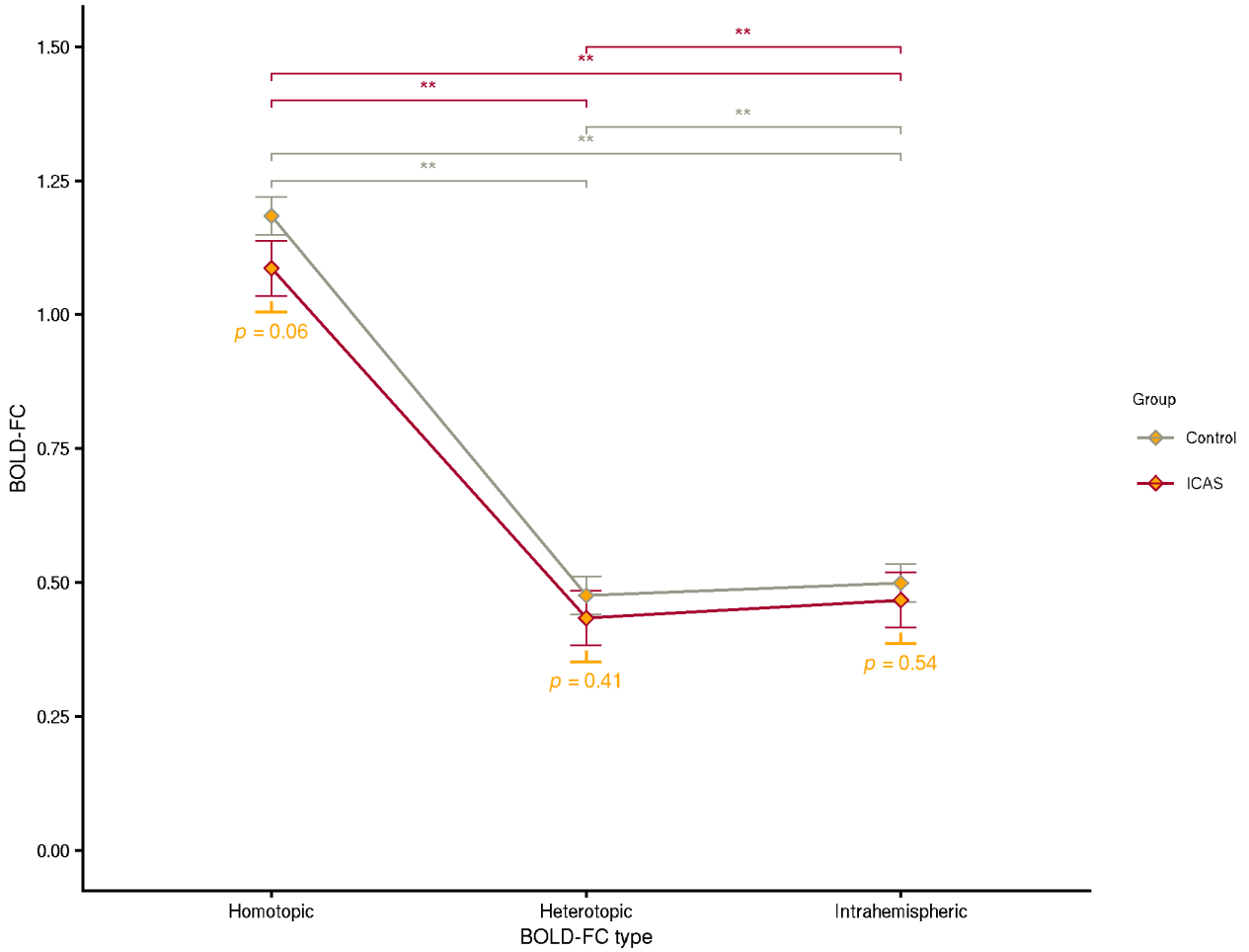

Figure 20. Comparison of average BOLD-FC between and within groups.

Estimated average BOLD-FC, i.e., intercept, (intercept model) for homotopic, heterotopic and intrahemispheric BOLD-FC is depicted for both groups, healthy controls and ICAS patients. The intercept estimate describes average BOLD-FC when all other predictor variables are 0, i.e., for all included participants of median age. Within and between groups differences across the FC-types were compared with Tukey's test. Within-group differences between the FC-types are depicted on top (n.s. = not significant, *: p<=0.05, **: p<= 0.001), with color depicting the respective groups. Between group differences are depicted below the respective estimates in orange. Abbreviations: CTH, capillary transit time heterogeneity; CBF, cerebral blood flow; rCBV, relative cerebral blood volume; TTP, time-to-peak; BOLD lag, blood oxygenation level dependent lag; VOI, volume of interest; ICAS, internal carotid artery stenosis.

Influence of hemodynamic-vascular parameters across FC-types: With this regression approach, I found overall, across *all* hemodynamic-vascular parameters and both groups, a significantly weaker influence on BOLD-FC for heterotopic and intrahemispheric connectivity as compared to the homotopic case (see **Fig . 21** and **22**, as also **Table 12**). One exception to this general finding was the difference between homotopic and heterotopic BOLD-FC for rCBV differences, which not significant (p = 0.07). Note that rCBV had in general (on average across groups) no significant

impact on BOLD-FC for homotopic BOLD-FC. While parameters differences between VOIs still caused reductions in BOLD-FC for heterotopic and intrahemispheric BOLD-FC, effects were strongly reduced as compared to reductions in homotopic BOLD-FC (see **Table 12** and **14**). While there were some significant differences between groups for some interactions, the majority only had a minuscule effect on the overall interpretation (see **Table 12**, e.g. a small difference of 0.003 regarding the influence of age on the influence of CTH differences). The only major group differences were found for the influence of TTP differences on BOLD-FC, which was significantly weaker (for the same absolute TTP difference) for healthy controls as compared to healthy controls for homotopic BOLD-FC ($p = 0.002$). Alongside that, the *change* in TTP slope between homotopic and heterotopic ($p < 0.001$) as well as intrahemispheric ($p < 0.001$) was less pronounced for healthy controls as compared to the ICAS patients, since the influence of TTP on homotopic BOLD-FC was already lower for healthy controls (see **Fig. 22** and **Table 12**).

To additionally examine all pairwise within-group and between-group comparisons of slope estimates, which are not indicated by the regression model, I conducted Tukey post-hoc analyses for each of the hemodynamic-vascular difference predictors. Between-group differences were only found for the impact of rCBV on intrahemispheric BOLD-FC, where the effect in healthy controls was minimally but significantly weaker(see **Table 13** and **Fig. 22**), and for the influence of TTP on homotopic BOLD-FC, where – for identical TTP differences – BOLD-FC decreases were significantly lower for healthy controls, as stated above (see **Table 12**). Otherwise, slope estimates were not significantly different between groups for all FC-types and parameter differences. For within group-differences between FC-types, this analysis revealed that rCBV did not show a significantly different influence between homotopic BOLD-FC and both heterotopic as well as intrahemispheric BOLD-FC for both groups (see **Table 14** and **Fig. 22**). It additionally revealed that CBF did not exert a significantly different impact between homotopic and intrahemispheric BOLD-FC for healthy controls only (see **Table 14** and **Fig.22**). All other within group-comparisons were significantly different with highest BOLD-FC reductions for homotopic BOLD-FC, but also slightly stronger reductions for intrahemispheric as compared to heterotopic BOLD-FC within both groups (see **Fig. 22** and **Table 14** for both absolute estimates and differences).

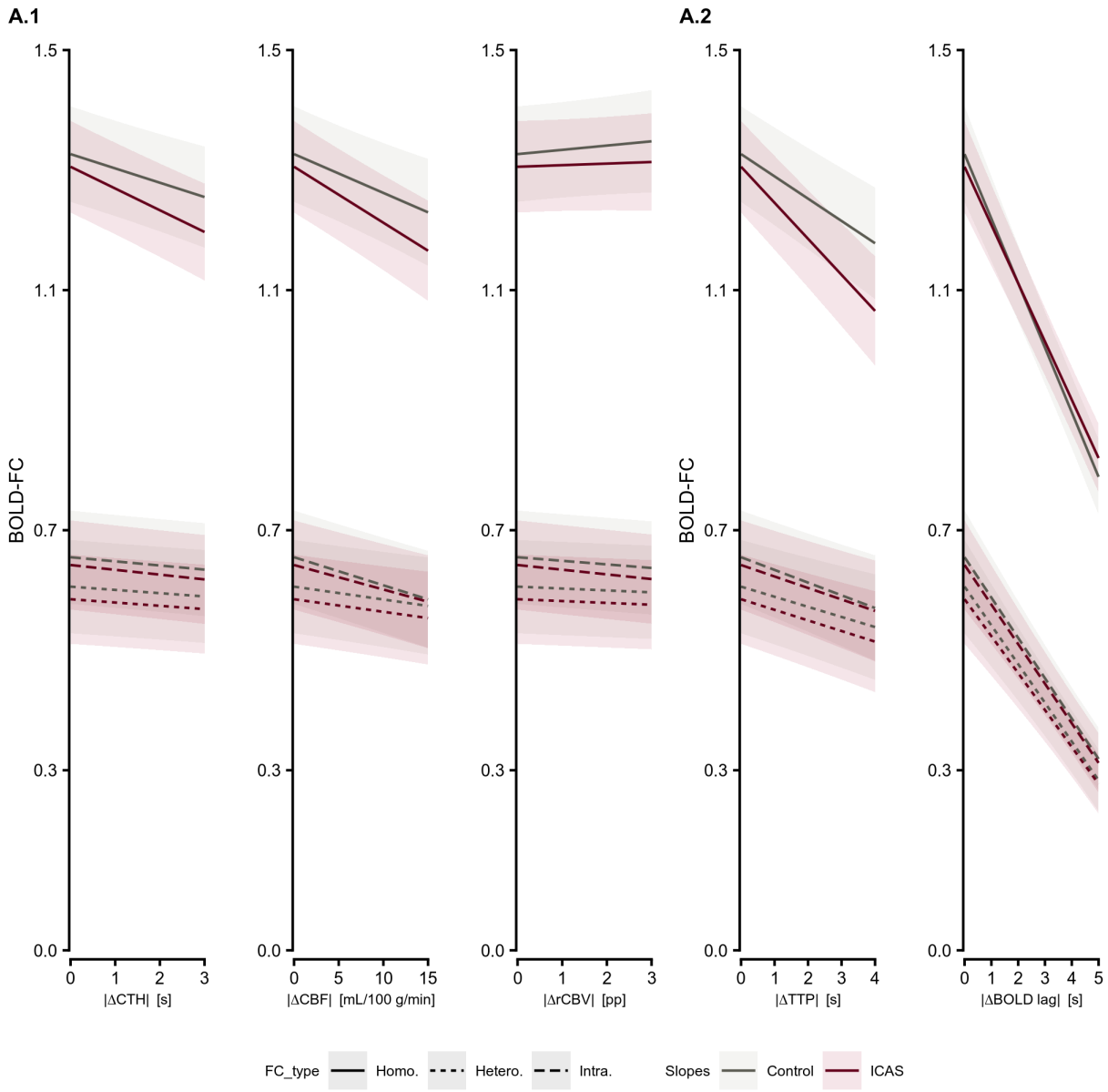

Figure 21. Effect of hemodynamic-vascular differences on BOLD-FC for each type of BOLD-FC.

Group regression lines for homotopic BOLD-FC and respective local (A.1), |ΔCTH|, |ΔCBF|, |ΔrCBV| as systemic (A.2), |ΔTTP| and |ΔBOLD lag|, hemodynamic-vascular parameter differences are depicted with solid lines. Regression lines for heterotopic and intrahemispheric BOLD-FC are depicted with dotted and dashed lines, respectively. Slopes indicate the decrease in pairwise BOLD-FC with increasing |ΔX| between pairwise VOIs. |ΔX| on the x-axis were limited to a range of 3σ. Shaded areas around the lines indicate the 95% confidence intervals. Abbreviations: BOLD-FC, blood oxygenation level dependent functional connectivity; CTH, capillary transit time heterogeneity; CBF, cerebral blood flow; rCBV, relative cerebral blood volume; TTP, time-to-peak; BOLD lag, blood oxygenation level dependent lag; ICAS, internal carotid artery stenosis.

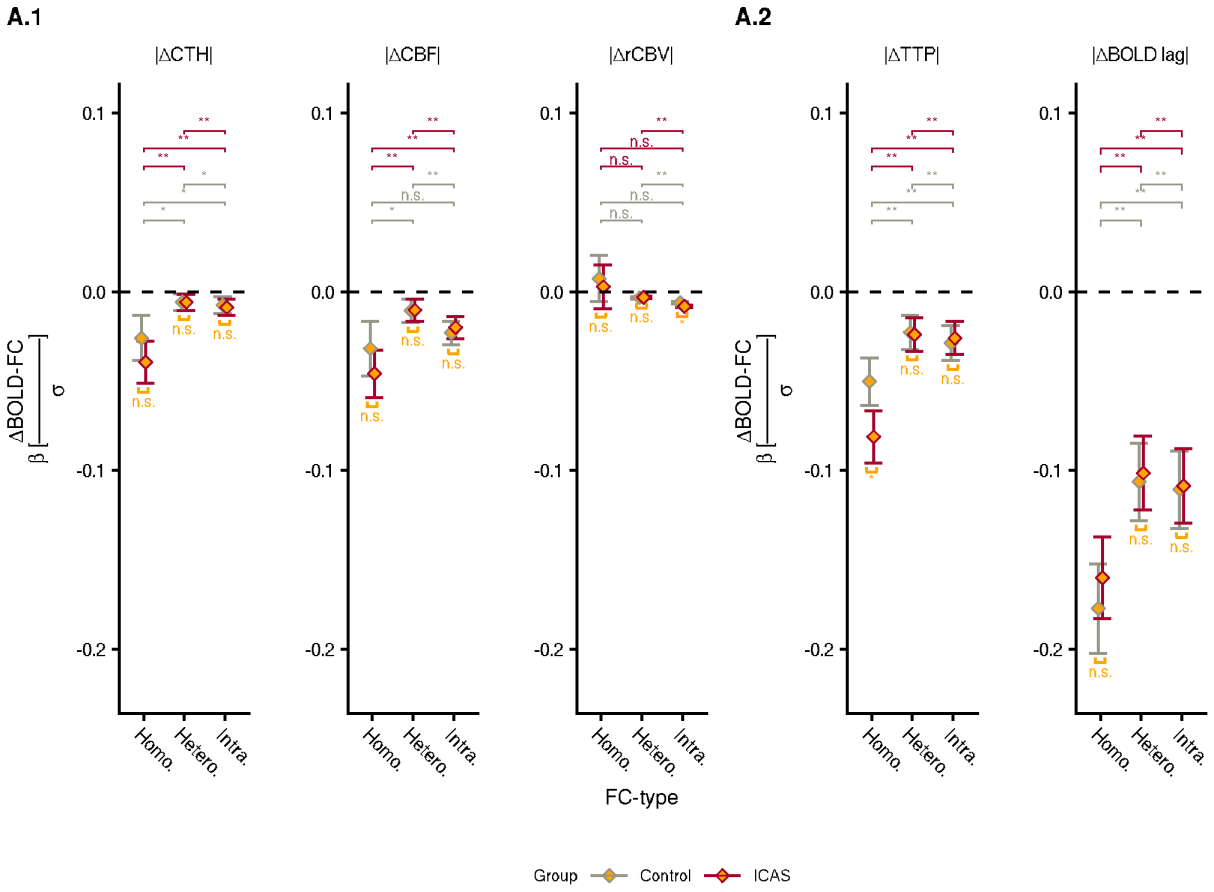

Figure 22. Within- and between-group comparison of regression coefficients for FC-types.

Diamonds represent slopes (β, i.e., decrease in BOLD-FC for one standard deviation of |ΔX|) for each hemodynamic-vascular differences, Group and FC-type. Error-bars indicate the 95% confidence intervals. Within and between group differences of slopes for the FC-types were compared with Tukey's test. Within-group differences between the FC-types are depicted on top (n.s. = not significant, *: p<=0.05, **: p<= 0.001), with color depicting the respective groups. Between group differences are depicted below the respective slope estimates in orange. Abbreviations: BOLD-FC, blood oxygenation level dependent functional connectivity; CTH, capillary transit time heterogeneity; CBF, cerebral blood flow; Homo., Homotopic BOLD-FC; Hetero., Heterotopic BOLD-FC; Intra., Intrahemispheric BOLD-FC; rCBV, relative cerebral blood volume; TTP, time-to-peak; BOLD lag, blood oxygenation level dependent lag; ICAS, internal carotid artery stenosis.

Table 12. Summary of *FC-type Intercept + local + systemic hemodynamic-vascular differences* regression model.

Predictors	**Estimates**	**CI**	**Statistic**	***p***
Intercept	1.32	1.261 – 1.371	46.84	**<0.001**
Group	0.01	-0.045 – 0.066	0.38	0.71
Age	0	-0.008 – 0.011	0.34	0.74

|ΔCTH|	-0.03	-0.041 – -0.024	-7.45	**<0.001**
|ΔCBF|	-0.04	-0.049 – -0.029	-7.5	**<0.001**
|ΔrCBV|	0.01	-0.004 – 0.014	1.12	0.26
|ΔTTP|	-0.07	-0.075 – -0.056	-13.13	**<0.001**
|ΔBOLD lag|	-0.17	-0.185 – -0.152	-19.75	**<0.001**
Group:Age	0.01	-0.004 – 0.015	1.22	0.23
Group:|ΔCTH|	0.01	-0.002 – 0.015	1.54	0.13
Group:|ΔCBF|	0.01	-0.003 – 0.017	1.36	0.18
Group:|ΔrCBV|	0	-0.007 – 0.011	0.51	0.61
Group:|ΔTTP|	0.02	0.006 – 0.025	3.09	0
Group:|ΔBOLD lag|	-0.01	-0.025 – 0.008	-1.01	0.32
Age:|ΔCTH|	0	-0.001 – 0.003	1.25	0.21
Age:|ΔCBF|	0	-0.004 – -0.001	-2.58	**0.01**
Age:|ΔrCBV|	0	-0.002 – 0.002	0.09	0.93
Age:|ΔTTP|	0	0.001 – 0.004	2.54	0.01
Age:|ΔBOLD lag|	0	-0.002 – 0.003	0.38	0.7
Group:Age:|ΔCTH|	0	0.002 – 0.005	3.67	**<0.001**
Group:Age:|ΔCBF|	-0.01	-0.007 – -0.003	-5.16	**<0.001**
Group:Age:|ΔrCBV|	0	-0.001 – 0.002	1.01	0.31
Group:Age:|ΔTTP|	0	-0.003 – 0.001	-1.01	0.31
Group:Age:|ΔBOLD lag|	0	-0.002 – 0.003	0.29	0.77
FC-type[Hetero.]	-0.72	-0.733 – -0.708	-115.16	**<0.001**
FC-type[Hetero.]:Group	0	-0.012 – 0.012	-0.01	0.99
FC-type[Hetero.]:Age	0	-0.005 – -0.001	-2.89	**0**
FC-type[Hetero.]:|ΔCTH|	0.03	0.019 – 0.035	6.54	**<0.001**
FC-type[Hetero.]:|ΔCBF|	0.03	0.019 – 0.038	6.07	**<0.001**
FC-type[Hetero.]:|ΔrCBV|	-0.01	-0.017 – 0.001	-1.84	0.07
FC-type[Hetero.]:|ΔTTP|	0.04	0.035 – 0.05	11.33	**<0.001**
FC-type[Hetero.]:|ΔBOLD lag|	0.07	0.057 – 0.073	15.54	**<0.001**
FC-type[Hetero.]:Group:Age	-0.01	-0.008 – -0.004	-5.22	**<0.001**
FC-type[Hetero.]:Group:|ΔCTH|:	-0.01	-0.015 – 0.001	-1.64	0.1
FC-type[Hetero.]:Group:|ΔCBF|	-0.01	-0.016 – 0.002	-1.52	0.13
FC-type[Hetero.]:Group:|ΔrCBV|	0	-0.011 – 0.007	-0.53	0.6
FC-type[Hetero.]:Group:|ΔTTP|	-0.02	-0.022 – -0.008	-3.99	**<0.001**

FC-type[Hetero.]:Group:|ΔBOLD lag|	0.01	-0.002 – 0.014	1.49	0.14
FC-type[Hetero.]:Age:|ΔCTH|	0	-0.002 – 0.001	-1	0.32
FC-type[Hetero.]:Age:|ΔCBF|	0	0.001 – 0.004	2.82	0.01
FC-type[Hetero.]:Age:|ΔrCBV|	0	-0.002 – 0.001	-0.45	0.65
FC-type[Hetero.]:Age:|ΔTTP|	0	-0.002 – 0.001	-0.98	0.33
FC-type[Hetero.]:Age:|ΔBOLD lag|	0	0 – 0.002	1.3	0.19
FC-type[Hetero.]:Group:Age:|ΔCTH|	0	-0.005 – -0.001	-3.53	**<0.001**
FC-type[Hetero.]:Group:Age:|ΔCBF|	0.01	0.003 – 0.006	5.2	**<0.001**
FC-type[Hetero.]:Group:Age:|ΔrCBV|	0	-0.002 – 0.001	-0.94	0.35
FC-type[Hetero.]:Group:Age:|ΔTTP|	0	0 – 0.003	2.66	**0.01**
FC-type[Hetero.]:Group:Age:|ΔBOLD lag|	0	0 – 0.003	1.5	0.13
FC-type[Intra.]	-0.67	-0.68 – -0.655	-106.72	**<0.001**
FC-type[Intra.]:Group	0	-0.016 – 0.008	-0.65	0.52
FC-type[Intra.]:Age	0	-0.005 – -0.001	-2.83	**0.01**
FC-type[Intra.]:|ΔCTH|	0.03	0.017 – 0.033	6.02	**<0.001**
FC-type[Intra.]:|ΔCBF|	0.02	0.008 – 0.026	3.69	**<0.001**
FC-type[Intra.]:|ΔrCBV|	-0.01	-0.021 – -0.003	-2.7	**0.01**
FC-type[Intra.]:|ΔTTP|	0.04	0.031 – 0.046	10.28	**<0.001**
FC-type[Intra.]:|ΔBOLD lag|	0.06	0.051 – 0.067	14.14	**<0.001**
FC-type[Intra.]:Group:Age	-0.01	-0.008 – -0.004	-5.34	**<0.001**
FC-type[Intra.]:Group:|ΔCTH|	-0.01	-0.014 – 0.002	-1.5	0.13
FC-type[Intra.]:Group:|ΔCBF|	-0.01	-0.018 – 0.001	-1.81	0.07
FC-type[Intra.]:Group:|ΔrCBV|	0	-0.01 – 0.008	-0.3	0.76
FC-type[Intra.]:Group:|ΔTTP|	-0.02	-0.024 – -0.01	-4.51	**<0.001**
FC-type[Intra.]:Group:|ΔBOLD lag|	0.01	-0.001 – 0.016	1.82	0.07
FC-type[Intra.]:Age:|ΔCTH|	0	-0.002 – 0.001	-0.89	0.37
FC-type[Intra.]:Age:|ΔCBF|	0	0 – 0.004	2.27	**0.02**
FC-type[Intra.]:Age:|ΔrCBV|	0	-0.002 – 0.001	-0.36	0.72
FC-type[Intra.]:Age:|ΔTTP|	0	-0.002 – 0.001	-0.82	0.41
FC-type[Intra.]:Age:|ΔBOLD lag|	0	0 – 0.003	1.59	0.11
FC-type[Intra.]:Group:Age:|ΔCTH|	0	-0.004 – -0.001	-3.23	**0**
FC-type[Intra.]:Group:Age:|ΔCBF|	0	0.003 – 0.006	5.08	**<0.001**
FC-type[Intra.]:Group:Age:|ΔrCBV|	0	-0.002 – 0.001	-0.78	0.43
FC-type[Intra.]:Group:Age:|ΔTTP|	0	0 – 0.003	2.17	**0.03**

FC-type[Intra.]:Group:Age:|ΔBOLD lag|	0	0 – 0.003	1.44	0.15

Note: Under predictors the variables incorporated in the model are listed. Group variable was deviation coded (Group: ICAS = -1, Controls = 1). The FC-type variable consisted of three levels, homotopic BOLD-FC as the reference level (coded as 0), and heterotopic as intrahemishpheric BOLD-FC as the two further levels. and Age was centered on the median age in the sample (participants with a median age equal 0 in the coding). The intercept estimate describes average BOLD-FC when all other predictor variables are 0, i.e. for all included participants of median age and for homotopic BOLD-FC and in the absence of any hemodynamic-vascular differences, |ΔX|. Estimates for other variables indicate the estimated change in BOLD-FC should the predictor value increase by 1 (Group: to health controls, age: to one year above median age of 72, |ΔX| by one respective standard deviation and FC-type to heterotopic or intrahemispheric BOLD-FC respectively). Interactions between participant group and predictors are indicated by a colon. Confidence intervals for the estimates are indicated by CI. If no CI is indicated this means that the effect was always smaller than 0.001. The test statistic is derived from a one-sample t-test, against the null-hypothesis that the estimate does not differ significantly from 0. Effects for the ICAS patients are identical to those of the healthy control group, except being reversed in polarity (Group coding for ICAS patients = -1).

Table 13. Summary of *post-hoc analysis* for *between* group-differences of the *FC-type Intercept + local + systemic hemodynamic-vascular differences* regression model.

Predictors	**FC-type**	**$\beta_{Control}$**	**β_{ICAS}**	**Difference**	***p***
|ΔCTH|	Homotopic	-0.03	-0.04	0.01	0.13
|ΔCTH|	Heterotopic	-0.01	-0.01	0	0.99
|ΔCTH|	Intrahemispheric	-0.01	-0.01	0	0.71
|ΔCBF|	Homotopic	-0.03	-0.05	0.01	0.18
|ΔCBF|	Heterotopic	-0.01	-0.01	0	0.96
|ΔCBF|	Intrahemispheric	-0.02	-0.02	0	0.52
|ΔrCBV|	Homotopic	0.01	0	0.01	0.61
|ΔrCBV|	Heterotopic	0	0	0	0.83
|ΔrCBV|	Intrahemispheric	-0.01	-0.01	0	**< 0.001**
|ΔTTP|	Homotopic	-0.05	-0.08	0.03	**< 0.001**
|ΔTTP|	Heterotopic	-0.02	-0.02	0	0.87
|ΔTTP|	Intrahemispheric	-0.03	-0.03	0	0.68
|ΔBOLD lag|	Homotopic	-0.18	-0.16	-0.02	0.32
|ΔBOLD lag|	Heterotopic	-0.11	-0.1	-0.01	0.74
|ΔBOLD lag|	Intrahemispheric	-0.11	-0.11	0	0.89

Note: Columns 2 and 3 indicate group-wise mean slopes (decrease in BOLD-FC for one standard deviation) for the respective predictor (column 1) and FC-type (column 2). P-values were derived from Tukey's test of multiple comparison.

Table 14. Summary of *post-hoc analysis* for *within* group-differences of the *FC-type Intercept + local + systemic hemodynamic-vascular differences* regression model.

Predictors	Contrast	Control: means	Control: diff.	ICAS: means	ICAS: diff.
|ΔCTH|	Homo:Hetero	-0.026:-0.006	-0.02, ***p* = 0.002** (77 %)	-0.039:-0.006	-0.033, ***p* < 0.001** (85 %)
|ΔCTH|	Homo:Intra	-0.026:-0.007	-0.018, ***p* = 0.006** (73 %)	-0.039:-0.009	-0.031, ***p* < 0.001** (77 %)
|ΔCTH|	Hetero:Intra	-0.006:-0.007	0.002, ***p* = 0.003** (-17 %)	-0.006:-0.009	0.003, ***p* < 0.001** (-50 %)
|ΔCBF|	Homo:Hetero	-0.032:-0.011	-0.021**, *p* = 0.009** (66 %)	-0.046:-0.01	-0.036, ***p* < 0.001** (78 %)
|ΔCBF|	Homo:Intra	-0.032:-0.023	-0.009, *p* = 0.438 (28 %)	-0.046:-0.02	-0.026, ***p* < 0.001** (57 %)
|ΔCBF|	Hetero:Intra	-0.011:-0.023	0.012, ***p* < 0.001** (-109 %)	-0.01:-0.02	0.01, ***p* < 0.001** (-100 %)
|ΔrCBV|	Homo:Hetero	0.007:-0.003	0.011, *p* = 0.241 (143 %)	0.003:-0.003	0.006, *p* = 0.601 (200 %)
|ΔrCBV|	Homo:Intra	0.007:-0.006	0.014, *p* = 0.101 (186 %)	0.003:-0.008	0.011, *p* = 0.183 (367 %)
|ΔrCBV|	Hetero:Intra	-0.003:-0.006	0.003, ***p* < 0.001** (-100 %)	-0.003:-0.008	0.005, ***p* < 0.001** (-167 %)
|ΔTTP|	Homo:Hetero	-0.05:-0.023	-0.027**, *p* < 0.001** (54 %)	-0.081:-0.024	-0.057, ***p* < 0.001** (70 %)
|ΔTTP|	Homo:Intra	-0.05:-0.029	-0.022, ***p* < 0.001** (42 %)	-0.081:-0.026	-0.055, ***p* < 0.001** (68 %)
|ΔTTP|	Hetero:Intra	-0.023:-0.029	0.006, ***p* < 0.001** (-26 %)	-0.024:-0.026	0.002, ***p* < 0.001** (-8 %)
|ΔBOLD lag|	Homo:Hetero	-0.177:-0.106	-0.071, ***p* < 0.001** (40 %)	-0.16:-0.101	-0.058, ***p* < 0.001** (37 %)
|ΔBOLD lag|	Homo:Intra	-0.177:-0.111	-0.066, ***p* < 0.001** (37 %)	-0.16:-0.109	-0.051, ***p* < 0.001** (32 %)
|ΔBOLD lag|	Hetero:Intra	-0.106:-0.111	0.004, ***p* < 0.001** (-5 %)	-0.101:-0.109	0.007, ***p* < 0.001** (-8 %)

Note: Columns 2 and 4 indicate group-wise mean slopes (decrease in BOLD-FC for one standard deviation) for the respective hemodynamic-vascular predictors (column 1) and contrasts (column 2). P-values were derived from Tukey's test of multiple comparison and adjusted for multiple comparison.

4.3 Interim-Discussion of Project 3

The goal of this study was to examine if the influence of hemodynamic-vascular parameters depends on the type of BOLD-FC, to be precise, if observed effects differ between homotopic, heterotopic and intrahemispheric FC. I found that hemodynamic-vascular differences exert a significantly stronger influence on homotopic BOLD-FC as compared to BOLD-FC between heterotopic and intrahemispheric VOIs. The influence of hemodynamic-vascular parameters on heterotopic and intrahemispheric BOLD-FC was largely comparable, but still slightly and significantly stronger for intrahemispheric BOLD-FC. This pattern was largely identical for both ICAS patients and healthy controls and applied to both local and systemic hemodynamic-vascular parameters. I furthermore found that ICAS patients compared to healthy controls only exhibited lower BOLD-FC between homotopic VOI pairs, but otherwise showed largely comparable average heterotopic and intrahemispheric BOLD-FC, which was overall lower for both groups as compared to homotopic BOLD-FC. To the best of my knowledge, this is the first study to systematically examine the impact of regional hemodynamic-vascular differences on BOLD-FC, demonstrating a stronger influence of hemodynamic-vascular parameters on homotopic BOLD-FC compared to heterotopic and intrahemispheric BOLD-FC. This implies a differing vulnerability for BOLD-FC aberrations across samples with hemodynamic-vascular impairments, depending on the type of BOLD-FC analyses.

4.3.1 Baseline differences between ICAS and healthy controls for different FC-types

I found that for both groups, average BOLD-FC estimates were lower between heterotopic and intrahemispheric VOIs as compared to homotopic VOIs. This is a pattern well in-line with previous studies, confirming the well-known dominant BOLD-FC strength for homotopic regions (Gee et al., 2011; Stark et al., 2008). Reasons for this have been discussed before in detail (Mancuso et al., 2019; Stark et al., 2008; Zuo et al., 2010), but the most important reasons are the particularly strong WM fiber connectivity (Johnston et al., 2008; Van Den Heuvel et al., 2009), the more synchronous neural and metabolic activity (Duffy et al., 1996; Lee et al., 2008; Nir et al., 2008) and also symmetrical hemodynamic-vascular properties (Mateo et al., 2017). Interestingly, marked differences in BOLD-FC between ICAS patients and healthy controls (even though not statistically significant at $p < 0.05$) were only found for homotopic, but not heterotopic and intrahemispheric BOLD-FC. As discussed for Project 2 (see 3.3.2), reductions in homotopic BOLD-FC among ICAS

patients have been reported before (Avirame et al., 2015; Cheng et al., 2012; Gao et al., 2019; Schneider et al., 2022, 2023) and vanished in my experiment, when controlling for hemodynamic-vascular differences. Similarly, for intrahemispheric VOIs, decreased BOLD-FC has been reported between dorsal lateral prefrontal cortices and the anterior inferior parietal lobules as well as between the PCC and hippocampus (Cheng et al., 2012), and further between PCC and supra- as medial prefrontal cortex (Avirame et al., 2015; Cheng et al., 2012; T. Wang et al., 2017). Graph-theory based analyses likewise indicated reduced connectivity on the ipsilateral hemisphere (T.-Y. Chang et al., 2016). However, results are mixed as also no significant differences in intrahemispheric BOLD-FC between ICAS patients and healthy controls on neither ipsi- nor contralateral hemispheres were previously reported (Fischer et al., 2022). For heterotopic BOLD-FC, reductions have been reported between contralateral primary motor cortex and ipsilateral premotor cortex, superior occipital gyrus and precuneus, along with BOLD-FC reductions between contralateral insula and ipsilateral right premotor area, inferior orbitofrontal - , supramarginal -, middle temporal – and cingular gyri (K.-L. Huang et al., 2018). Reductions in BOLD-FC between heterotopic areas of different RSN have likewise been reported before (C.-J. Lin et al., 2014). However, some findings of impaired heterotopic and intrahemispheric BOLD-FC have previously been noted (Fischer et al., 2022) to be potentially associated with the severity of stenosis in the underlying sample, i.e., to appear in samples with a high percentage of full occlusions (Avirame et al., 2015) or even previous strokes (T.-Y. Chang et al., 2016). This paints a picture of predominately impaired homotopic BOLD-FC, and fairly robust heterotopic- and intrahemispheric BOLD-FC, only exhibiting highly specific, small and localized changes, if any at all, which in addition have been linked to much stronger perfusion impairments as observed in the current sample (Fischer et al., 2022). As previous findings of non-homotopic BOLD-FC aberrations were highly regional, my approach of merely comparing mean connectivity values for FC-types between groups, likely averaged out potential more specific BOLD-FC differences. Overall, my finding of generally reduced homotopic BOLD-FC for ICAS patients, but comparable heterotopic and intrahemispheric BOLD-FC, therefore, fits with previous results. I furthermore found that the differences between homotopic and heterotopic as well as intrahemispheric BOLD-FC were slightly but significantly stronger for healthy controls as compared to ICAS patients. However, this is most likely due to the initially higher homotopic BOLD-FC for healthy controls, making the decrease in BOLD-FC for heterotopic and intrahemispheric BOLD-FC, where groups did not differ, more pronounced for healthy controls as compared to ICAS patients, who showed a lower homotopic BOLD-FC to begin with.

4.3.2 Stronger influence of hemodynamic-vascular impairments on homotopic BOLD-FC

Overall, I found a significantly weaker influence of hemodynamic-vascular differences on BOLD-FC between heterotopic and intrahemispheric VOIs, as compared to homotopic connections, with BOLD-FC decreases being as low as half the estimate for homotopic BOLD-FC. Following a model of both neural and non-neural BOLD components (Das et al., 2021; Drew, 2019), I suspect this is due to an inherent difference in *both* neural and non-neural components of non-homotopic brain regions.

Homotopic regions largely benefit from the often strongly symmetrical features of the brain, as discussed above (Duffy et al., 1996; Johnston et al., 2008; Lee et al., 2008; Mateo et al., 2017; Nir et al., 2008; Van Den Heuvel et al., 2009), leading to the robustly observed stronger BOLD-FC as compared to heterotopic and intrahemispheric connections – in healthy participants (Mancuso et al., 2019; Stark et al., 2008; Zuo et al., 2010). The strong homotopic BOLD-FC therefore relies on largely identical regional features – both neural and non-neural. Consequently an imbalance in one of the features, e.g., one or multiple hemodynamic-vascular parameters, leads to strong reductions in BOLD-FC, as I have shown.

For heterotopic and intrahemispheric BOLD-FC, this symmetry does not apply. Consequently, BOLD signal components between these regions differ not only in hemodynamic-vascular parameters, but also in other components, i.e., a potentially fundamentally different neural activity (Nir et al., 2008), metabolism or fiber connectivity (Garcés et al., 2016; Lee et al., 2008). BOLD-FC between such regions is therefore already reduced, even without differences in non-neural BOLD components such as the chosen hemodynamic-vascular parameters. Thus, it appears plausible that differences in these parameters play a less prominent role. It is important to note though, that I would assume the same impact of hemodynamic-vascular differences on BOLD-FC across different types of connectivities if region pairs either showed otherwise identical features or or all other potential differences would be controlled for in a hypothetical regression analysis. This interpretation is supported by findings of slightly increased BOLD-FC following revascularization for intrahemispheric BOLD-FC (Cheng et al., 2012; Fischer et al., 2022; C.-J. Lin et al., 2014), highlighting at least some relevance of hemodynamic-vascular differences for intrahemispheric BOLD-FC.

4.3.3 Interpretation of BOLD-FC in ICAS

In my analysis, I have shown that homotopic BOLD-FC is reduced in ICAS patients as compared to healthy controls, but largely identical for heterotopic and intrahemispheric BOLD-FC, in line with previous research. I additionally found that vascular-hemodynamic differences have a stronger influence on homotopic BOLD-FC as compared to heterotopic and intrahemispheric BOLD-FC, with at most minor differences between healthy controls and ICAS patients regarding the BOLD-FC decrease for given hemodynamic-vascular differences (with the exception for TTP, which will be discussed at the end of this chapter). Additionally I have shown (in Project 2, see **Figs. 11** and **15**), that ICAS patients exhibit overall larger homotopic hemodynamic-vascular parameter differences and hemispheric asymmetry due to the stenosis. While ICAS patients, therefore, do not principally demonstrate a stronger decrease in BOLD-FC for a given parameter difference, they show larger hemodynamic-vascular differences. It is then feasible to assume, that these lead to an overall decreased homotopic BOLD-FC, which is more prone to aberrations as compared to heterotopic and intrahemispheric BOLD-FC (as discussed above). Therefore, the repeatedly observed pattern of reduced homotopic BOLD-FC emerges because homotopic BOLD-FC is especially prone to the influence of stenosis related asymmetries, which exert less influence on the other FC-types.

One exception to this otherwise comparable influence of hemodynamic-vascular differences between groups was TTP for homotopic BOLD-FC of this analysis. For the same absolute TTP difference healthy controls exhibited a lesser decrease in BOLD-FC (-0.05) as compared to ICAS (-0.07). However, the mean effect estimated across both groups was -0.07, same as for the analysis of homotopic BOLD-FC in Project 2 (Schneider et al., 2023), where no significant group differences was found. It therefore seems that the introduction of different FC-types in this analysis curiously gave raise to group difference, not observed before for the same underlying data. Reasons for this could be changes in the model fitting procedure, due to the vastly increased sample size. Therefore I would hesitate to interpret this group difference as based on underlying features unique to either the ICAS or healthy control group, due to its instability across two analyses and especially as other parameters for homotopic BOLD-FC showed little to no change between Project 2 (Schneider et al., 2023) and 3, as expected.

4.3.4 Strength and Limitations

For this project, I extended my previous procedure to estimate the influence of hemodynamic-vascular differences on different types of BOLD-FC. I did so by including a further factorial term in

the regression analysis, FC-types, representing the three chosen variants, i.e., homotopic, heterotopic and intrahemispheric BOLD-FC. Other variables were kept identical as compared to Project 1 and 2 (Schneider et al., 2022, 2023). While I have chosen these types of connectivity based on my research question, this approach would also allow for incorporating other types of comparisons, e.g., a finer parcellation of connectivity types or a comparison between RSN, due to is simplicity. This project therefore extends the framework of Projects 1 and 2 (Schneider et al., 2022, 2023) to compare the influence of various differences, not limited to hemodynamic-vascular ones, on different kinds of BOLD-FC measurements in a standardized and straightforward way. By incorporating a large number of observations (1.6 million BOLD-FC estimates), I have furthermore shown that this approach can also be applied to samples of much larger size or with much more observations, opening the possibility to also examine pooled or public datasets, thus overcoming often observed limitation of small sample sizes in rs-fMRI studies.

Limitations of quantitative MRI parameter measurements used for this study as well as statistical limitations have been discussed before for projects 1 and 2 (see above and Kaczmarz et al., 2021; Schneider et al., 2022, 2023) and will not be repeated here. Uniquely, for this project, a new FC-type term with three levels has been introduced in the regression model. This lead to a steep increase of overall predictor terms in the model, from 36 in the already fairly complex full model for Project 2, to 72 terms in the regression model for this project. However, this increase in complexity went along with an even larger increase in the number of observations, thus, allowing for such a complex model, as available observations vastly outnumber the number of regression terms. Consequently, as larger sample sizes are generally more favorable for regression, the amount of observations in my model does not constitute an issue, but instead boosts statistical power.

4.3.5 Conclusion

In this project, I examined whether the influence of hemodynamic-vascular parameters, i.e., CTH, CBF, rCBV, TTP and BOLD lag, differs between types of BOLD-FC, i.e., homotopic, heterotopic and intrahemispheric. I found that hemodynamic-vascular differences had a much stronger influence on homotopic BOLD-FC as compared to heterotopic and intrahemispheric BOLD-FC. In contrast, heterotopic and intrahemispheric BOLD-FC did only differ slightly, which held for both groups, i.e., healthy controls and ICAS patients. Furthermore, I found that average heterotopic and intrahemispheric BOLD-FC were largely identical between ICAS patients as compared to healthy

controls, in contrast to homotopic BOLD-FC. Homotopic BOLD-FC, therefore, seems to be generally much more sensitive to hemodynamic-vascular impairments in ICAS patients, leading to the observed group differences.

5. General Conclusion

Within the scope of this work, I set out to examine how hemodynamic-vascular parameters can affect BOLD signal derived functional connectivity in the resting-state. To this end, I conducted several analyses on existing multi-parametric MRI data from ICAS patients and healthy elderly that examined different aspects of the hypothesized influence.

For Project 1, I combined experimental results from this multi-parametric human fMRI study with BOLD-FC simulations and probed causal mechanism of BOLD-FC aberrations due to local hemodynamic-vascular parameters, namely CTH, CBF and rCBV (Schneider et al., 2022). I found that for homotopic BOLD-FC, both differences in CTH and CBF between homotopic brain areas, lead to reduction in BOLD-FC – in line with the simulation results. In particular, we proposed that CTH constitutes an indicator for a delayed and broadened local CBF response, which exerts complex and non-linear influences on local BOLD signal time courses, thus affecting BOLD-FC. This has implications for possible correction strategies, often relying on linear approaches, which most likely do not capture all aspects, thus still leaving behind BOLD-FC affected by non-neural factors.

This analysis was then extended in Project 2, where I not only examined local hemodynamic-vascular parameters, but compared the influence of local, i.e., CTH, CBF and rCBV, and systemic, i.e., TTP and BOLD lag, hemodynamic vascular parameters on homotopic BOLD-FC (Schneider et al., 2023). For this, I set up a stepwise comparison of regression models, containing first only participants intercepts, i.e., average BOLD-FC, then local hemodynamic-vascular differences and lastly, both local and systemic hemodynamic-vascular differences. I found that overall, with the complete model, about 40% of homotopic BOLD-FC in my sample could be explained, with roughly 20% stemming from the hemodynamic-vascular VOI differences alone. Among these differences, the systemic parameters had a substantially larger impact on BOLD-FC as compared to the local ones. This implies that, paradoxically, participant samples with focal disorders, such as an ICAS, causing aberrations in systemic hemodynamic-vascular parameters, should have more pronounced BOLD-FC aberrations as compared to study samples with widespread local hemodynamic-vascular aberrations, which are affected less.

Lastly for Project 3, I extended my analyses to different types of BOLD-FC, which are commonly used in rs-fMRI analysis, i.e., not only homotopic, but also heterotopic and intrahemispheric BOLD-FC. For this, I largely extended the initial analyses of Projects 1 and 2 to extract all possible pairwise BOLD-FC and hemodynamic-vascular differences from the chosen VOI atlas, which were then categorized into the three FC-types. The factor FC-types, was then incorporated into the regression approach, once into an intercept-only model, to assess average BOLD-FC across the FC-types, and once into the full model of Project 2, containing both local and systemic hemodynamic-vascular differences. Based on this, I confirmed that ICAS patients exhibit lower average homotopic BOLD-FC as compared to healthy controls, but show largely similar heterotopic and intrahemispheric BOLD-FC. Secondly, I found that hemodynamic-vascular differences exert a significantly larger influence on homotopic, as compared to heterotopic and intrahemispheric BOLD-FC. This paints the picture that homotopic BOLD-FC is much more sensitive with regard to hemodynamic-vascular aberrations, which consequently manifests in reduced BOLD-FC in ICAS patients and most likely also other patient groups with hemodynamic-vascular aberrations.

With respect to my initial research question regarding the influences of hemodynamic-vascular parameters on BOLD-FC, I can therefore conclude: Hemodynamic-vascular parameters have both linear and complex non-linear influences on BOLD-FC, leading to reduced BOLD-FC, with systemic parameters exerting an overall stronger influence and homotopic BOLD-FC being particularly vulnerable to hemodynamic-vascular impairments. This indicates that the widely accepted nature of BOLD-FC as a proxy measure for synchronized neural activity between brain regions can be flawed, due to non-neural hemodynamic-vascular influences on BOLD-FC, distorting any underlying truly neuronal association.

These results have several consequences for the study of both healthy participants and patient samples with suspected hemodynamic-vascular aberrations. With regard to largely non-significant group differences concerning the influence of individual hemodynamic-vascular parameters, I conclude that some aspects of BOLD-FC in healthy samples are likewise affected by naturally occurring hemodynamic-vascular differences between brain regions, shrouding the underlying true neural coherence. In samples with suspected hemodynamic-vascular aberrations, this effect is amplified as hemodynamic-vascular differences are more pronounced, leading to stronger BOLD-FC impairments, depending on the underlying aberrations. Interpretation of BOLD-FC alterations as neural alterations in such samples need, therefore, be taken with care, especially in comparisons to

healthy control samples, if hemodynamic-vascular factors are not considered or controlled for. While some techniques for controlling for hemodynamic-vascular factors have been developed in recent years, these were either limited to singular factors or relying on simple linear procedures. In contrast, I have shown that multiple factors can affect BOLD-FC, with some potentially also exert complex non-linear influences. Therefore, in order to assure more informative rs-fMRI BOLD-FC results, I propose to combine rs-fMRI measurements with additional modalities. Ideally, these would consist of precise measurement of all influencing physiological parameters during resting-state recordings. Particularly relevant parameters, beyond heart rate, breathing and blinking, would be electrophysiological measurements and a comprehensive assessment of additional hemodynamic-vascular parameters via pCASL and DSC MRI. As a combination of all of these steps is most likely not possible for all study setups and samples or scanning environments, a thorough (literature based) investigation of potential hemodynamic-vascular aberrations among the relevant participant pool seems to be the minimally expected procedure. However, since BOLD lag can directly be derived from rs-fMRI data, this information should be evaluated in any case.

Therefore, while rs-fMRI based BOLD-FC overall has come a long way since its inception in 1995 and a lot of its initial obstacles have been overcome, there are still fundamental issues regarding its specific relationship to neural activity and connectivity, which have to be resolved in order to make it a trustworthy method for sampling ongoing neural activity in humans.

6. Acknowledgments

First I would like to deeply thank everyone involved in the collection of the ICAS and healthy controls multimodal hemodynamic MRI dataset for their incredible effort in collecting this data and even more so for allowing me to use it for my dissertation research. My deepest thanks also go to my supervisor PD Dr. Christian Sorg and to the members of my PhD committee, Prof. Dr. Christine Preibisch and Prof. Dr. Simon Jacob, for their invaluable advice, critique and guidance during the past years. I would then also like thank my current and former colleagues for their help in practical issues, but also for making my research time a much more memorable and joyful experience.

Lastly I would like to especially thank my friends and family but above all Saskia for their unwavering support during the past years without which none of this would have been possible.

7. References

Aanerud, J., Borghammer, P., Rodell, A., Jónsdottir, K. Y., & Gjedde, A. (2017). Sex differences of human cortical blood flow and energy metabolism. *Journal of Cerebral Blood Flow & Metabolism*, *37*(7), 2433–2440. https://doi.org/10.1177/0271678X16668536

Alisch, J. S. R., Khattar, N., Kim, R. W., Cortina, L. E., Rejimon, A. C., Qian, W., Ferrucci, L., Resnick, S. M., Spencer, R. G., & Bouhrara, M. (2021). Sex and age-related differences in cerebral blood flow investigated using pseudo-continuous arterial spin labeling magnetic resonance imaging. *Aging*, *13*(4), 4911–4925. https://doi.org/10.18632/aging.202673

Alsop, D. C., Detre, J. A., Golay, X., Günther, M., Hendrikse, J., Hernandez-Garcia, L., Lu, H., MacIntosh, B. J., Parkes, L. M., Smits, M., van Osch, M. J. P., Wang, D. J. J., Wong, E. C., & Zaharchuk, G. (2015). Recommended implementation of arterial spin-labeled perfusion MRI for clinical applications: A consensus of the ISMRM perfusion study group and the European consortium for ASL in dementia. *Magnetic Resonance in Medicine*, *73*(1), 102–116. https://doi.org/10.1002/mrm.25197

Amemiya, S., Kunimatsu, A., Saito, N., & Ohtomo, K. (2012). Impaired hemodynamic response in the ischemic brain assessed with BOLD fMRI. *NeuroImage*, *61*(3), 579–590. https://doi.org/10.1016/j.neuroimage.2012.04.001

Amemiya, S., Kunimatsu, A., Saito, N., & Ohtomo, K. (2014). Cerebral Hemodynamic Impairment: Assessment with Resting-State Functional MR Imaging. *Radiology*, *270*(2), 548–555. https://doi.org/10.1148/radiol.13130982

Amemiya, S., Takao, H., & Abe, O. (2020). Origin of the Time Lag Phenomenon and the Global Signal in Resting-State fMRI. *Frontiers in Neuroscience*, *14*, 596084. https://doi.org/10.3389/fnins.2020.596084

Amemiya, S., Takao, H., Watanabe, Y., Miyawaki, S., Koizumi, S., Saito, N., & Abe, O. (2022). Reliability and sensitivity to altered hemodynamics measured with resting-state fMRI metrics: Comparison with 123I-IMP SPECT. *NeuroImage*, *263*, 119654. https://doi.org/10.1016/j.neuroimage.2022.119654

Ances, B. M., Liang, C. L., Leontiev, O., Perthen, J. E., Fleisher, A. S., Lansing, A. E., & Buxton, R. B. (2009). Effects of aging on cerebral blood flow, oxygen metabolism, and blood oxygenation level dependent responses to visual stimulation. *Human Brain Mapping*, *30*(4), 1120–1132. https://doi.org/10.1002/hbm.20574

Angleys, H., Jespersen, S. N., & Østergaard, L. (2018). The effects of capillary transit time heterogeneity on the BOLD signal. *Human Brain Mapping*, *39*(6), 2329–2352. https://doi.org/10.1002/hbm.23991

Archila-Meléndez, M. E., Sorg, C., & Preibisch, C. (2020). Modeling the impact of neurovascular coupling impairments on BOLD-based functional connectivity at rest. *NeuroImage*, *218*, 116871. https://doi.org/10.1016/j.neuroimage.2020.116871

Arsava, E. M., Hansen, M. B., Kaplan, B., Peker, A., Gocmen, R., Arat, A., Oguz, K. K., Topcuoglu, M. A., Østergaard, L., & Dalkara, T. (2018). The effect of carotid artery stenting on capillary transit time heterogeneity in patients with carotid artery stenosis. *European Stroke Journal*, *3*(3), 263–271. https://doi.org/10.1177/2396987318772686

Ashburner, J. (2007). A fast diffeomorphic image registration algorithm. *NeuroImage*, *38*(1), 95–113. https://doi.org/10.1016/j.neuroimage.2007.07.007

Aso, T., Urayama, S., Fukuyama, H., & Murai, T. (2019). Axial variation of deoxyhemoglobin density as a source of the low-frequency time lag structure in blood oxygenation level-dependent signals. *PLOS ONE*, *14*(9), e0222787. https://doi.org/10.1371/journal.pone.0222787

Avirame, K., Lesemann, A., List, J., Witte, A. V., Schreiber, S. J., & Flöel, A. (2015). Cerebral Autoregulation and Brain Networks in Occlusive Processes of the Internal Carotid Artery. *Journal of Cerebral Blood Flow & Metabolism*, *35*(2), 240–247. https://doi.org/10.1038/jcbfm.2014.190

Bakdash, J. Z., & Marusich, L. R. (2017). Repeated Measures Correlation. *Frontiers in Psychology*, *8*, 456. https://doi.org/10.3389/fpsyg.2017.00456

Bandettini, P. A., Wong, E. C., Hinks, R. S., Tikofsky, R. S., & Hyde, J. S. (1992). Time course EPI of human brain function during task activation. *Magnetic Resonance in Medicine*, *25*(2), 390–397. https://doi.org/10.1002/mrm.1910250220

Bates, D., Mächler, M., Bolker, B., & Walker, S. (2015). Fitting Linear Mixed-Effects Models Using lme4. *Journal of Statistical Software*, *67*(1), 1–48. https://doi.org/10.18637/jss.v067.i01

Bazzari, A. H., & Bazzari, F. H. (2022). BDNF Therapeutic Mechanisms in Neuropsychiatric Disorders. *International Journal of Molecular Sciences*, *23*(15), 8417. https://doi.org/10.3390/ijms23158417

Beall, E. B., & Lowe, M. J. (2007). Isolating physiologic noise sources with independently determined spatial measures. *NeuroImage*, *37*(4), 1286–1300. https://doi.org/10.1016/j.neuroimage.2007.07.004

Beall, E. B., & Lowe, M. J. (2014). SimPACE: Generating simulated motion corrupted BOLD data with synthetic-navigated acquisition for the development and evaluation of SLOMOCO: A new, highly effective slicewise motion correction. *NeuroImage*, *101*, 21–34. https://doi.org/10.1016/j.neuroimage.2014.06.038

Beishon, L., Clough, R. H., Kadicheeni, M., Chithiramohan, T., Panerai, R. B., Haunton, V. J., Minhas, J. S., & Robinson, T. G. (2021). Vascular and haemodynamic issues of brain ageing. *Pflügers Archiv - European Journal of Physiology*, *473*(5), 735–751. https://doi.org/10.1007/s00424-020-02508-9

Birn, R. M., Smith, M. A., Jones, T. B., & Bandettini, P. A. (2008). The respiration response function: The temporal dynamics of fMRI signal fluctuations related to changes in respiration. *NeuroImage*, *40*(2), 644–654. https://doi.org/10.1016/j.neuroimage.2007.11.059

Biswal, B., Zerrin Yetkin, F., Haughton, V. M., & Hyde, J. S. (1995). Functional connectivity in the motor cortex of resting human brain using echo-planar mri. *Magnetic Resonance in Medicine*, *34*(4), 537–541. https://doi.org/10.1002/mrm.1910340409

Blockley, N. P., Francis, S. T., & Gowland, P. A. (2009). Perturbation of the BOLD response by a contrast agent and interpretation through a modified balloon model. *NeuroImage*, *48*(1), 84–93. https://doi.org/10.1016/j.neuroimage.2009.06.038

Boxerman, J. L., Quarles, C. C., Hu, L. S., Erickson, B. J., Gerstner, E. R., Smits, M., Kaufmann, T. J., Barboriak, D. P., Huang, R. H., Wick, W., Weller, M., Galanis, E., Kalpathy-Cramer, J., Shankar, L., Jacobs, P., Chung, C., Van Den Bent, M. J., Chang, S., Al Yung, W. K., … Haynes, C. (2020). Consensus recommendations for a dynamic susceptibility contrast MRI protocol for use in

high-grade gliomas. *Neuro-Oncology*, *22*(9), 1262–1275. https://doi.org/10.1093/neuonc/noaa141

Brandl, F., Avram, M., Weise, B., Shang, J., Simões, B., Bertram, T., Ayala, D. H., Penzel, N., Gürsel, D. A., Bäuml, J., Wohlschläger, A. M., Vukadinovic, Z., Koutsouleris, N., Leucht, S., & Sorg, C. (2019). Specific Substantial Dysconnectivity in Schizophrenia: A Transdiagnostic Multimodal Meta-analysis of Resting-State Functional and Structural Magnetic Resonance Imaging Studies. *Biological Psychiatry*, *85*(7), 573–583. https://doi.org/10.1016/j.biopsych.2018.12.003

Bright, M. G., Whittaker, J. R., Driver, I. D., & Murphy, K. (2020). Vascular physiology drives functional brain networks. *NeuroImage*, *217*, 116907. https://doi.org/10.1016/j.neuroimage.2020.116907

Burns, S. P., Xing, D., & Shapley, R. M. (2010). Comparisons of the Dynamics of Local Field Potential and Multiunit Activity Signals in Macaque Visual Cortex. *The Journal of Neuroscience*, *30*(41), 13739–13749. https://doi.org/10.1523/JNEUROSCI.0743-10.2010

Buxton, R. B. (2013). The physics of functional magnetic resonance imaging (fMRI). *Reports on Progress in Physics*, *76*(9), 096601. https://doi.org/10.1088/0034-4885/76/9/096601

Buxton, R. B., Uludağ, K., Dubowitz, D. J., & Liu, T. T. (2004). Modeling the hemodynamic response to brain activation. *NeuroImage*, *23*, S220–S233. https://doi.org/10.1016/j.neuroimage.2004.07.013

Buxton, R. B., Wong, E. C., & Frank, L. R. (1998). Dynamics of blood flow and oxygenation changes during brain activation: The balloon model. *Magnetic Resonance in Medicine*, *39*(6), 855–864. https://doi.org/10.1002/mrm.1910390602

Carnevale, L., Maffei, A., Landolfi, A., Grillea, G., Carnevale, D., & Lembo, G. (2020). Brain Functional Magnetic Resonance Imaging Highlights Altered Connections and Functional Networks in Patients With Hypertension. *Hypertension*, *76*(5), 1480–1490. https://doi.org/10.1161/HYPERTENSIONAHA.120.15296

Champagne, A. A., Coverdale, N. S., Allen, M. D., Tremblay, J. C., MacPherson, R. E. K., Pyke, K. E., Olver, T. D., & Cook, D. J. (2022). The physiological basis underlying functional connectivity

differences in older adults: A multi-modal analysis of resting-state fMRI. *Brain Imaging and Behavior*, *16*(4), 1575–1591. https://doi.org/10.1007/s11682-021-00570-0

Champagne, A. A., Coverdale, N. S., Ross, A., Chen, Y., Murray, C. I., Dubowitz, D., & Cook, D. J. (2020). Multi-modal normalization of resting-state using local physiology reduces changes in functional connectivity patterns observed in mTBI patients. *NeuroImage. Clinical*, *26*, 102204–102204. PubMed. https://doi.org/10.1016/j.nicl.2020.102204

Chang, C., Cunningham, J. P., & Glover, G. H. (2009). Influence of heart rate on the BOLD signal: The cardiac response function. *NeuroImage*, *44*(3), 857–869. https://doi.org/10.1016/j.neuroimage.2008.09.029

Chang, C., Leopold, D. A., Schölvinck, M. L., Mandelkow, H., Picchioni, D., Liu, X., Ye, F. Q., Turchi, J. N., & Duyn, J. H. (2016). Tracking brain arousal fluctuations with fMRI. *Proceedings of the National Academy of Sciences*, *113*(16), 4518–4523. https://doi.org/10.1073/pnas.1520613113

Chang, T.-Y., Huang, K.-L., Ho, M.-Y., Ho, P.-S., Chang, C.-H., Liu, C.-H., Chang, Y.-J., Wong, H.-F., Hsieh, I.-C., Lee, T.-H., & Liu, H.-L. (2016). Graph theoretical analysis of functional networks and its relationship to cognitive decline in patients with carotid stenosis. *Journal of Cerebral Blood Flow & Metabolism*, *36*(4), 808–818. https://doi.org/10.1177/0271678X15608390

Chen, Z., Zhang, X., Yuan, C., Zhao, X., & Van Osch, M. J. P. (2017). Measuring the labeling efficiency of pseudocontinuous arterial spin labeling. *Magnetic Resonance in Medicine*, *77*(5), 1841–1852. https://doi.org/10.1002/mrm.26266

Cheng, H.-L., Lin, C.-J., Soong, B.-W., Wang, P.-N., Chang, F.-C., Wu, Y.-T., Chou, K.-H., Lin, C.-P., Tu, P.-C., & Lee, I.-H. (2012). Impairments in Cognitive Function and Brain Connectivity in Severe Asymptomatic Carotid Stenosis. *Stroke*, *43*(10), 2567–2573. https://doi.org/10.1161/STROKEAHA.111.645614

Cheung, E. Y. W., Shea, Y. F., Chiu, P. K. C., Kwan, J. S. K., & Mak, H. K. F. (2021). Diagnostic Efficacy of Voxel-Mirrored Homotopic Connectivity in Vascular Dementia as Compared to Alzheimer's Related Neurodegenerative Diseases—A Resting State fMRI Study. *Life*, *11*(10), 1108. https://doi.org/10.3390/life11101108

Christen, T., Jahanian, H., Ni, W. W., Qiu, D., Moseley, M. E., & Zaharchuk, G. (2015). Noncontrast mapping of arterial delay and functional connectivity using resting-state functional MRI: A study in Moyamoya patients: Maps of Arterial Delay Using BOLD Signal. *Journal of Magnetic Resonance Imaging*, *41*(2), 424–430. https://doi.org/10.1002/jmri.24558

Chu, P. P. W., Golestani, A. M., Kwinta, J. B., Khatamian, Y. B., & Chen, J. J. (2018). Characterizing the modulation of resting-state fMRI metrics by baseline physiology. *NeuroImage*, *173*, 72–87. https://doi.org/10.1016/j.neuroimage.2018.02.004

Ciacciarelli, A., Sette, G., Giubilei, F., & Orzi, F. (2020). Chronic cerebral hypoperfusion: An undefined, relevant entity. *Journal of Clinical Neuroscience*, *73*, 8–12. https://doi.org/10.1016/j.jocn.2020.01.026

Claeys, E. H. I., Mantingh, T., Morrens, M., Yalin, N., & Stokes, P. R. A. (2022). Resting-state fMRI in depressive and (hypo)manic mood states in bipolar disorders: A systematic review. *Progress in Neuro-Psychopharmacology and Biological Psychiatry*, *113*, 110465. https://doi.org/10.1016/j.pnpbp.2021.110465

Cohen, E. R., Ugurbil, K., & Kim, S.-G. (2002). Effect of Basal Conditions on the Magnitude and Dynamics of the Blood Oxygenation Level-Dependent fMRI Response. *Journal of Cerebral Blood Flow & Metabolism*, *22*(9), 1042–1053. https://doi.org/10.1097/00004647-200209000-00002

Damaraju, E., Allen, E. A., Belger, A., Ford, J. M., McEwen, S., Mathalon, D. H., Mueller, B. A., Pearlson, G. D., Potkin, S. G., Preda, A., Turner, J. A., Vaidya, J. G., Van Erp, T. G., & Calhoun, V. D. (2014). Dynamic functional connectivity analysis reveals transient states of dysconnectivity in schizophrenia. *NeuroImage: Clinical*, *5*, 298–308. https://doi.org/10.1016/j.nicl.2014.07.003

Daniel, D. G., Mathew, R. J., & Wilson, W. H. (1989). Sex roles and regional cerebral blood flow. *Psychiatry Research*, *27*(1), 55–64. https://doi.org/10.1016/0165-1781(89)90009-7

Das, A., Murphy, K., & Drew, P. J. (2021). Rude mechanicals in brain haemodynamics: Non-neural actors that influence blood flow. *Philosophical Transactions of the Royal Society B: Biological Sciences*, *376*(1815), 20190635. https://doi.org/10.1098/rstb.2019.0635

De Vis, J. B., Hendrikse, J., Bhogal, A., Adams, A., Kappelle, L. J., & Petersen, E. T. (2015). Age-related changes in brain hemodynamics; A calibrated MRI study: Age-Related Changes in Brain Hemodynamics. *Human Brain Mapping*, *36*(10), 3973–3987. https://doi.org/10.1002/hbm.22891

D'Esposito, M., Deouell, L. Y., & Gazzaley, A. (2003). Alterations in the BOLD fMRI signal with ageing and disease: A challenge for neuroimaging. *Nature Reviews Neuroscience*, *4*(11), 863–872. https://doi.org/10.1038/nrn1246

Dirnagl, U. (2012). Pathobiology of injury after stroke: The neurovascular unit and beyond: Pathobiology of injury after stroke. *Annals of the New York Academy of Sciences*, *1268*(1), 21–25. https://doi.org/10.1111/j.1749-6632.2012.06691.x

Donahue, M. J., Strother, M. K., Lindsey, K. P., Hocke, L. M., Tong, Y., & Frederick, B. deB. (2016). Time delay processing of hypercapnic fMRI allows quantitative parameterization of cerebrovascular reactivity and blood flow delays. *Journal of Cerebral Blood Flow & Metabolism*, *36*(10), 1767–1779. https://doi.org/10.1177/0271678X15608643

Drew, P. J. (2019). Vascular and neural basis of the BOLD signal. *Current Opinion in Neurobiology*, *58*, 61–69. https://doi.org/10.1016/j.conb.2019.06.004

Drew, P. J. (2022). Neurovascular coupling: Motive unknown. *Trends in Neurosciences*, S0166223622001618. https://doi.org/10.1016/j.tins.2022.08.004

Drew, P. J., Mateo, C., Turner, K. L., Yu, X., & Kleinfeld, D. (2020). Ultra-slow Oscillations in fMRI and Resting-State Connectivity: Neuronal and Vascular Contributions and Technical Confounds. *Neuron*, *107*(5), 782–804. https://doi.org/10.1016/j.neuron.2020.07.020

Du, Y., Fu, Z., & Calhoun, V. D. (2018). Classification and Prediction of Brain Disorders Using Functional Connectivity: Promising but Challenging. *Frontiers in Neuroscience*, *12*, 525. https://doi.org/10.3389/fnins.2018.00525

Duffy, F. H., Mcanulty, G. B., & Albert, M. S. (1996). Effects of age upon interhemispheric EEG coherence in normal adults. *Neurobiology of Aging*, *17*(4), 587–599.

Duque, C., Feske, S., & Sorond, F. (2017). Cerebrovascular Hemodynamics in Women. *Seminars in Neurology*, *37*(06), 679–688. https://doi.org/10.1055/s-0037-1608881

Erdoğan, S. B., Tong, Y., Hocke, L. M., Lindsey, K. P., & deB Frederick, B. (2016). Correcting for Blood Arrival Time in Global Mean Regression Enhances Functional Connectivity Analysis of Resting State fMRI-BOLD Signals. *Frontiers in Human Neuroscience*, *10*. https://doi.org/10.3389/fnhum.2016.00311

Esteban, O., Markiewicz, C. J., Blair, R. W., Moodie, C. A., Isik, A. I., Erramuzpe, A., Kent, J. D., Goncalves, M., DuPre, E., Snyder, M., Oya, H., Ghosh, S. S., Wright, J., Durnez, J., Poldrack, R. A., & Gorgolewski, K. J. (2019). fMRIPrep: A robust preprocessing pipeline for functional MRI. *Nature Methods*, *16*(1), 111–116. https://doi.org/10.1038/s41592-018-0235-4

Farras-Permanyer, L., Mancho-Fora, N., Montalà-Flaquer, M., Bartrés-Faz, D., Vaqué-Alcázar, L., Peró-Cebollero, M., & Guàrdia-Olmos, J. (2019). Age-related changes in resting-state functional connectivity in older adults. *Neural Regeneration Research*, *14*(9), 1544. https://doi.org/10.4103/1673-5374.255976

Feng, R., Rolls, E. T., Cheng, W., & Feng, J. (2020). Hypertension is associated with reduced hippocampal connectivity and impaired memory. *EBioMedicine*, *61*, 103082. https://doi.org/10.1016/j.ebiom.2020.103082

Fischer, F., Malherbe, C., Schlemm, E., Schröder, J., Heinze, M., Cheng, B., Schulz, M., Fiehler, J., Larena-Avellaneda, A., Gerloff, C., & Thomalla, G. (2022). Intrinsic functional brain connectivity is resilient to chronic hypoperfusion caused by unilateral carotid artery stenosis. *NeuroImage: Clinical*, *34*, 103014. https://doi.org/10.1016/j.nicl.2022.103014

Fitzgerald, B., Yao, J. F., Talavage, T. M., Hocke, L. M., Frederick, B. deB, & Tong, Y. (2021). Using carpet plots to analyze transit times of low frequency oscillations in resting state fMRI. *Scientific Reports*, *11*(1), 7011. https://doi.org/10.1038/s41598-021-86402-z

Fox, M. D., & Raichle, M. E. (2007). Spontaneous fluctuations in brain activity observed with functional magnetic resonance imaging. *Nature Reviews Neuroscience*, *8*(9), 700–711. https://doi.org/10.1038/nrn2201

Fox, M. D., Snyder, A. Z., Vincent, J. L., Corbetta, M., Van Essen, D. C., & Raichle, M. E. (2005). The human brain is intrinsically organized into dynamic, anticorrelated functional networks. *Proceedings of the National Academy of Sciences*, *102*(27), 9673–9678. https://doi.org/10.1073/pnas.0504136102

Frederick, B. deB, Salo, T., & Drucker, D. M. (2022). *Bbfrederick/rapidtide: Version 2.2.8.1—8/29/22 deployment bug fix* (v2.2.8.1) [Computer software]. Zenodo. https://doi.org/10.5281/zenodo.7032879

Friston, K. J., Frith, C. D., Liddle, P. F., & Frackowiak, R. S. J. (1993). Functional Connectivity: The Principal-Component Analysis of Large (PET) Data Sets. *Journal of Cerebral Blood Flow & Metabolism*, *13*(1), 5–14. https://doi.org/10.1038/jcbfm.1993.4

Gao, L., Wang, T., Qian, T., Xiao, F., Bai, L., Zhang, J., & Xu, H. (2019). Severe asymptomatic carotid stenosis is associated with robust reductions in homotopic functional connectivity. *NeuroImage: Clinical*, *24*, 102101. https://doi.org/10.1016/j.nicl.2019.102101

Garcés, P., Pereda, E., Hernández-Tamames, J. A., Del-Pozo, F., Maestú, F., & Ángel Pineda-Pardo, J. (2016). Multimodal description of whole brain connectivity: *A comparison of resting state MEG, fMRI, and DWI*. *Human Brain Mapping*, *37*(1), 20–34. https://doi.org/10.1002/hbm.22995

Gawryluk, J. R., Mazerolle, E. L., & D'Arcy, R. C. N. (2014). Does functional MRI detect activation in white matter? A review of emerging evidence, issues, and future directions. *Frontiers in Neuroscience*, *8*. https://doi.org/10.3389/fnins.2014.00239

Gee, D. G., Biswal, B. B., Kelly, C., Stark, D. E., Margulies, D. S., Shehzad, Z., Uddin, L. Q., Klein, D. F., Banich, M. T., Castellanos, F. X., & Milham, M. P. (2011). Low frequency fluctuations reveal integrated and segregated processing among the cerebral hemispheres. *NeuroImage*, *54*(1), 517–527. https://doi.org/10.1016/j.neuroimage.2010.05.073

Glover, G. H., Li, T.-Q., & Ress, D. (2000). Image-based method for retrospective correction of physiological motion effects in fMRI: RETROICOR. *Magnetic Resonance in Medicine*, *44*(1), 162–167. https://doi.org/10.1002/1522-2594(200007)44:1<162::AID-MRM23>3.0.CO;2-E

Goense, J. B. M., & Logothetis, N. K. (2008). Neurophysiology of the BOLD fMRI Signal in Awake Monkeys. *Current Biology*, *18*(9), 631–640. https://doi.org/10.1016/j.cub.2008.03.054

Goense, J., Bohraus, Y., & Logothetis, N. K. (2016). fMRI at High Spatial Resolution: Implications for BOLD-Models. *Frontiers in Computational Neuroscience*, *10*. https://doi.org/10.3389/fncom.2016.00066

Göttler, J., Kaczmarz, S., Kallmayer, M., Wustrow, I., Eckstein, H.-H., Zimmer, C., Sorg, C., Preibisch, C., & Hyder, F. (2019). Flow-metabolism uncoupling in patients with asymptomatic unilateral carotid artery stenosis assessed by multi-modal magnetic resonance imaging. *Journal of Cerebral Blood Flow & Metabolism*, *39*(11), 2132–2143. https://doi.org/10.1177/0271678X18783369

Göttler, J., Kaczmarz, S., Nuttall, R., Griese, V., Napiórkowski, N., Kallmayer, M., Wustrow, I., Eckstein, H.-H., Zimmer, C., Preibisch, C., Finke, K., & Sorg, C. (2020). The stronger one-sided relative hypoperfusion, the more pronounced ipsilateral spatial attentional bias in patients with asymptomatic carotid stenosis. *Journal of Cerebral Blood Flow & Metabolism*, *40*(2), 314–327. https://doi.org/10.1177/0271678X18815790

Göttler, J., Preibisch, C., Riederer, I., Pasquini, L., Alexopoulos, P., Bohn, K. P., Yakushev, I., Beller, E., Kaczmarz, S., Zimmer, C., Grimmer, T., Drzezga, A., & Sorg, C. (2019). Reduced blood oxygenation level dependent connectivity is related to hypoperfusion in Alzheimer's disease. *Journal of Cerebral Blood Flow and Metabolism : Official Journal of the International Society of Cerebral Blood Flow and Metabolism*, *39*(7), 1314–1325. https://doi.org/10.1177/0271678X18759182

Gotts, S. J., Ramot, M., Jasmin, K., & Martin, A. (2019). Altered resting-state dynamics in autism spectrum disorder: Causal to the social impairment? *Progress in Neuro-Psychopharmacology and Biological Psychiatry*, *90*, 28–36. https://doi.org/10.1016/j.pnpbp.2018.11.002

Greicius, M. (2008). Resting-state functional connectivity in neuropsychiatric disorders. *Current Opinion in Neurology*, *21*(4), 424–430. https://doi.org/10.1097/WCO.0b013e328306f2c5

Greicius, M. D., Krasnow, B., Reiss, A. L., & Menon, V. (2003). Functional connectivity in the resting brain: A network analysis of the default mode hypothesis. *Proceedings of the National Academy of Sciences*, *100*(1), 253–258. https://doi.org/10.1073/pnas.0135058100

Greicius, M. D., Srivastava, G., Reiss, A. L., & Menon, V. (2004). Default-mode network activity distinguishes Alzheimer's disease from healthy aging: Evidence from functional MRI. *Proceedings of the National Academy of Sciences of the United States of America*, *101*(13), 4637–4642. https://doi.org/10.1073/pnas.0308627101

Gu, Y., Han, F., & Liu, X. (2019). Arousal Contributions to Resting-State fMRI Connectivity and Dynamics. *Frontiers in Neuroscience*, *13*, 1190. https://doi.org/10.3389/fnins.2019.01190

Guo, B., Zhou, F., Li, M., & Gore, J. C. (2022). Latency structure of BOLD signals within white matter in resting-state fMRI. *Magnetic Resonance Imaging*, *89*, 58–69. https://doi.org/10.1016/j.mri.2021.12.010

Hall, C. N., Howarth, C., Kurth-Nelson, Z., & Mishra, A. (2016). Interpreting BOLD: Towards a dialogue between cognitive and cellular neuroscience. *Philosophical Transactions of the Royal Society B: Biological Sciences*, *371*(1705), 20150348. https://doi.org/10.1098/rstb.2015.0348

Hara, S., Tanaka, Y., Ueda, Y., Hayashi, S., Inaji, M., Ishiwata, K., Ishii, K., Maehara, T., & Nariai, T. (2017). Noninvasive Evaluation of CBF and Perfusion Delay of Moyamoya Disease Using Arterial Spin-Labeling MRI with Multiple Postlabeling Delays: Comparison with ^{15}O-Gas PET and DSC-MRI. *American Journal of Neuroradiology*, *38*(4), 696–702. https://doi.org/10.3174/ajnr.A5068

Hedderich, D., Kluge, A., Pyka, T., Zimmer, C., Kirschke, J. S., Wiestler, B., & Preibisch, C. (2019). Consistency of normalized cerebral blood volume values in glioblastoma using different leakage correction algorithms on dynamic susceptibility contrast magnetic resonance imaging data without and with preload. *Journal of Neuroradiology = Journal de Neuroradiologie*, *46*(1), 44–51. https://doi.org/10.1016/j.neurad.2018.04.006

Hiltunen, T., Kantola, J., Abou Elseoud, A., Lepola, P., Suominen, K., Starck, T., Nikkinen, J., Remes, J., Tervonen, O., Palva, S., Kiviniemi, V., & Palva, J. M. (2014). Infra-Slow EEG Fluctuations Are Correlated with Resting-State Network Dynamics in fMRI. *The Journal of Neuroscience*, *34*(2), 356–362. https://doi.org/10.1523/JNEUROSCI.0276-13.2014

Hipp, J. F., & Siegel, M. (2015). BOLD fMRI Correlation Reflects Frequency-Specific Neuronal Correlation. *Current Biology*, *25*(10), 1368–1374. https://doi.org/10.1016/j.cub.2015.03.049

Hoirisch-Clapauch, S., Nardi, A. E., Gris, J.-C., & Brenner, B. (2014). Coagulation and Mental Disorders. *Rambam Maimonides Medical Journal*, *5*(4), e0036. https://doi.org/10.5041/RMMJ.10170

Honey, C. J., Sporns, O., Cammoun, L., Gigandet, X., Thiran, J. P., Meuli, R., & Hagmann, P. (2009). Predicting human resting-state functional connectivity from structural connectivity. *Proceedings of the National Academy of Sciences*, *106*(6), 2035–2040. https://doi.org/10.1073/pnas.0811168106

Huang, K.-L., Chang, T.-Y., Ho, M.-Y., Chen, W.-H., Yeh, M.-Y., Chang, Y.-J., Wong, H.-F., Chang, C.-H., Liu, C.-H., Lee, T.-H., & Wu, C. W. (2018). The correlation of asymmetrical functional connectivity with cognition and reperfusion in carotid stenosis patients. *NeuroImage: Clinical*, *20*, 476–484. https://doi.org/10.1016/j.nicl.2018.08.011

Huang, X., Long, Z., & Lei, X. (2019). Electrophysiological signatures of the resting-state fMRI global signal: A simultaneous EEG-fMRI study. *Journal of Neuroscience Methods*, *311*, 351–359. https://doi.org/10.1016/j.jneumeth.2018.09.017

Huang, Y., Wei, P.-H., Xu, L., Chen, D., Yang, Y., Song, W., Yi, Y., Jia, X., Wu, G., Fan, Q., Cui, Z., & Zhao, G. (2023). Intracranial electrophysiological and structural basis of BOLD functional connectivity in human brain white matter. *Nature Communications*, *14*(1), 3414. https://doi.org/10.1038/s41467-023-39067-3

Jahanian, H., Christen, T., Moseley, M. E., & Zaharchuk, G. (2018). Erroneous Resting-State fMRI Connectivity Maps Due to Prolonged Arterial Arrival Time and How to Fix Them. *Brain Connectivity*, *8*(6), 362–370. https://doi.org/10.1089/brain.2018.0610

Jaime, S., Gu, H., Sadacca, B. F., Stein, E. A., Cavazos, J. E., Yang, Y., & Lu, H. (2019). Delta Rhythm Orchestrates the Neural Activity Underlying the Resting State BOLD Signal via Phase–amplitude Coupling. *Cerebral Cortex*, *29*(1), 119–133. https://doi.org/10.1093/cercor/bhx310

Jann, K., Gee, D. G., Kilroy, E., Schwab, S., Smith, R. X., Cannon, T. D., & Wang, D. J. J. (2015). Functional connectivity in BOLD and CBF data: Similarity and reliability of resting brain networks. *NeuroImage*, *106*, 111–122. https://doi.org/10.1016/j.neuroimage.2014.11.028

Jespersen, S. N., & Østergaard, L. (2012). The Roles of Cerebral Blood Flow, Capillary Transit Time Heterogeneity, and Oxygen Tension in Brain Oxygenation and Metabolism. *Journal of Cerebral Blood Flow & Metabolism*, *32*(2), 264–277. https://doi.org/10.1038/jcbfm.2011.153

Johnston, J. M., Vaishnavi, S. N., Smyth, M. D., Zhang, D., He, B. J., Zempel, J. M., Shimony, J. S., Snyder, A. Z., & Raichle, M. E. (2008). Loss of Resting Interhemispheric Functional Connectivity after Complete Section of the Corpus Callosum. *Journal of Neuroscience*, *28*(25), 6453–6458. https://doi.org/10.1523/JNEUROSCI.0573-08.2008

Joliot, M., Jobard, G., Naveau, M., Delcroix, N., Petit, L., Zago, L., Crivello, F., Mellet, E., Mazoyer, B., & Tzourio-Mazoyer, N. (2015). AICHA: An atlas of intrinsic connectivity of homotopic areas. *Journal of Neuroscience Methods*, *254*, 46–59. https://doi.org/10.1016/j.jneumeth.2015.07.013

Kaczmarz, S., Göttler, J., Kooijman, H., van de Ven, K., Karampinos, D., Zimmer, C., & Preibisch, C. (2016). *Evaluation of pCASL sequences for CBF measures in healthy participants and patients with high- grade internal carotid artery stenosis*.

Kaczmarz, S., Göttler, J., Petr, J., Hansen, M. B., Mouridsen, K., Zimmer, C., Hyder, F., & Preibisch, C. (2021). Hemodynamic impairments within individual watershed areas in asymptomatic carotid artery stenosis by multimodal MRI. *Journal of Cerebral Blood Flow & Metabolism*, *41*(2), 380–396. https://doi.org/10.1177/0271678X20912364

Kaczmarz, S., Griese, V., Preibisch, C., Kallmayer, M., Helle, M., Wustrow, I., Petersen, E. T., Eckstein, H.-H., Zimmer, C., Sorg, C., & Göttler, J. (2018). Increased variability of watershed areas in patients with high-grade carotid stenosis. *Neuroradiology*, *60*(3), 311–323. https://doi.org/10.1007/s00234-017-1970-4

Kalisch, R., Elbel, G.-K., Gössl, C., Czisch, M., & Auer, D. P. (2001). Blood Pressure Changes Induced by Arterial Blood Withdrawal Influence Bold Signal in Anesthesized Rats at 7 Tesla: Implications for Pharmacologic MRI. *NeuroImage*, *14*(4), 891–898. https://doi.org/10.1006/nimg.2001.0890

Kanda, T., Fukusato, T., Matsuda, M., Toyoda, K., Oba, H., Kotoku, J., Haruyama, T., Kitajima, K., & Furui, S. (2015). Gadolinium-based Contrast Agent Accumulates in the Brain Even in Subjects without Severe Renal Dysfunction: Evaluation of Autopsy Brain Specimens with Inductively Coupled Plasma Mass Spectroscopy. *Radiology*, *276*(1), 228–232. https://doi.org/10.1148/radiol.2015142690

Katsel, P., Roussos, P., Pletnikov, M., & Haroutunian, V. (2017). Microvascular anomaly conditions in psychiatric disease. Schizophrenia – angiogenesis connection. *Neuroscience & Biobehavioral Reviews*, *77*, 327–339. https://doi.org/10.1016/j.neubiorev.2017.04.003

Khalil, A. A., Ostwaldt, A.-C., Nierhaus, T., Ganeshan, R., Audebert, H. J., Villringer, K., Villringer, A., & Fiebach, J. B. (2017). Relationship Between Changes in the Temporal Dynamics of the Blood-Oxygen-Level-Dependent Signal and Hypoperfusion in Acute Ischemic Stroke. *Stroke*, *48*(4), 925–931. https://doi.org/10.1161/STROKEAHA.116.015566

Khalil, A. A., Villringer, K., Filleböck, V., Hu, J.-Y., Rocco, A., Fiebach, J. B., & Villringer, A. (2020). Non-invasive monitoring of longitudinal changes in cerebral hemodynamics in acute ischemic stroke using BOLD signal delay. *Journal of Cerebral Blood Flow & Metabolism*, *40*(1), 12.

Khursheed, F., Tandon, N., Tertel, K., Pieters, T. A., Disano, M. A., & Ellmore, T. M. (2011). Frequency-specific electrocorticographic correlates of working memory delay period fMRI activity. *NeuroImage*, *56*(3), 1773–1782. https://doi.org/10.1016/j.neuroimage.2011.02.062

Kleinfeld, D., Mitra, P. P., Helmchen, F., & Denk, W. (1998). Fluctuations and stimulus-induced changes in blood flow observed in individual capillaries in layers 2 through 4 of rat neocortex. *Proceedings of the National Academy of Sciences*, *95*(26), 15741–15746. https://doi.org/10.1073/pnas.95.26.15741

Kluge, A., Lukas, M., Toth, V., Pyka, T., Zimmer, C., & Preibisch, C. (2016). Analysis of three leakage-correction methods for DSC-based measurement of relative cerebral blood volume with respect to heterogeneity in human gliomas. *Magnetic Resonance Imaging*, *34*(4), 410–421. https://doi.org/10.1016/j.mri.2015.12.015

Kolesar, T. A., Bilevicius, E., Wilson, A. D., & Kornelsen, J. (2019). Systematic review and meta-analyses of neural structural and functional differences in generalized anxiety disorder and healthy controls using magnetic resonance imaging. *NeuroImage: Clinical*, *24*, 102016. https://doi.org/10.1016/j.nicl.2019.102016

Kroll, H., Zaharchuk, G., Christen, T., Heit, J. J., & Iv, M. (2017). Resting-State BOLD MRI for Perfusion and Ischemia. *Topics in Magnetic Resonance Imaging*, *26*(2), 91–96. https://doi.org/10.1097/RMR.0000000000000119

Kuznetsova, A., Brockhoff, P. B., & Christensen, R. H. B. (2017). lmerTest Package: Tests in Linear Mixed Effects Models. *Journal of Statistical Software*, *82*(13), 1–26. https://doi.org/10.18637/jss.v082.i13

Kwong, K. K., Belliveau, J. W., Chesler, D. A., Goldberg, I. E., Weisskoff, R. M., Poncelet, B. P., Kennedy, D. N., Hoppel, B. E., Cohen, M. S., & Turner, R. (1992). Dynamic magnetic resonance imaging of human brain activity during primary sensory stimulation. *Proceedings of the National Academy of Sciences*, *89*(12), 5675–5679. https://doi.org/10.1073/pnas.89.12.5675

Lecrux, C., Bourourou, M., & Hamel, E. (2019). How reliable is cerebral blood flow to map changes in neuronal activity? *Autonomic Neuroscience*, *217*, 71–79. https://doi.org/10.1016/j.autneu.2019.01.005

Lee, D. S., Kang, H., Kim, H., Park, H., Oh, J. S., Lee, J. S., & Lee, M. C. (2008). Metabolic connectivity by interregional correlation analysis using statistical parametric mapping (SPM) and FDG brain PET; methodological development and patterns of metabolic connectivity in adults. *European Journal of Nuclear Medicine and Molecular Imaging*, *35*(9), 1681–1691. https://doi.org/10.1007/s00259-008-0808-z

Leenders, K. L. (1994). PET: blood flow and oxygen consumption in brain tumors. *Journal of Neuro-Oncology*, *22*(3), 269–273. https://doi.org/10.1007/BF01052932

Lewis, N., Lu, H., Liu, P., Hou, X., Damaraju, E., Iraji, A., & Calhoun, V. (2020). Static and dynamic functional connectivity analysis of cerebrovascular reactivity: An fMRI study. *Brain and Behavior*, *10*(6), e01516. https://doi.org/10.1002/brb3.1516

Li, S.-J., Biswal, B., Li, Z., Risinger, R., Rainey, C., Cho, J.-K., Salmeron, B. J., & Stein, E. A. (2000). Cocaine administration decreases functional connectivity in human primary visual and motor cortex as detected by functional MRI. *Magnetic Resonance in Medicine*, *43*(1), 45–51. https://doi.org/10.1002/(SICI)1522-2594(200001)43:1<45::AID-MRM6>3.0.CO;2-0

Li, Y., Zhang, H., Yu, M., Yu, W., Frederick, B. deB, & Tong, Y. (2018). Systemic low-frequency oscillations observed in the periphery of healthy human subjects. *Journal of Biomedical Optics*, *23*(05), 1. https://doi.org/10.1117/1.JBO.23.5.057001

Li, Z., Zhu, Y., Childress, A. R., Detre, J. A., & Wang, Z. (2012). Relations between BOLD fMRI-derived resting brain activity and cerebral blood flow. *PloS One*, *7*(9), e44556. https://doi.org/10.1371/journal.pone.0044556

Liang, X., Zou, Q., He, Y., & Yang, Y. (2013). Coupling of functional connectivity and regional cerebral blood flow reveals a physiological basis for network hubs of the human brain. *Proceedings of the National Academy of Sciences*, *110*(5), 1929–1934. https://doi.org/10.1073/pnas.1214900110

Lin, C.-J., Tu, P.-C., Chern, C.-M., Hsiao, F.-J., Chang, F.-C., Cheng, H.-L., Tang, C.-W., Lee, Y.-C., Chen, W.-T., & Lee, I.-H. (2014). Connectivity Features for Identifying Cognitive Impairment in Presymptomatic Carotid Stenosis. *PLoS ONE*, *9*(1), e85441. https://doi.org/10.1371/journal.pone.0085441

Lin, L., Xing, G., & Han, Y. (2018). Advances in Resting State Neuroimaging of Mild Cognitive Impairment. *Frontiers in Psychiatry*, *9*, 671. https://doi.org/10.3389/fpsyt.2018.00671

Liu, T. T., Nalci, A., & Falahpour, M. (2017). The global signal in fMRI: Nuisance or Information? *NeuroImage*, *150*, 213–229. https://doi.org/10.1016/j.neuroimage.2017.02.036

Logothetis, N. K., Pauls, J., Augath, M., Trinath, T., & Oeltermann, A. (2001). *Neurophysiological investigation of the basis of the fMRI signal*. *412*.

Logothetis, N. K., & Wandell, B. A. (2004). Interpreting the BOLD Signal. *Annual Review of Physiology*, *66*(1), 735–769. https://doi.org/10.1146/annurev.physiol.66.082602.092845

Love, S., & Miners, J. S. (2016). Cerebral Hypoperfusion and the Energy Deficit in Alzheimer's Disease: Hypoperfusion and energy deficit in Alzheimer's. *Brain Pathology*, *26*(5), 607–617. https://doi.org/10.1111/bpa.12401

Lowe, M. J., Phillips, M. D., Lurito, J. T., Mattson, D., Dzemidzic, M., & Mathews, V. P. (2002). Multiple Sclerosis: Low-Frequency Temporal Blood Oxygen Level–Dependent Fluctuations Indicate Reduced Functional Connectivity—Initial Results. *Radiology*, *224*(1), 184–192. https://doi.org/10.1148/radiol.2241011005

Lu, H., Jaime, S., & Yang, Y. (2019). Origins of the Resting-State Functional MRI Signal: Potential Limitations of the "Neurocentric" Model. *Frontiers in Neuroscience*, *13*, 1136. https://doi.org/10.3389/fnins.2019.01136

Lüdecke, D., Ben-Shachar, M. S., Patil, I., Waggoner, P., & Makowski, D. (2021). performance: An R Package for Assessment, Comparison and Testing of Statistical Models. *Journal of Open Source Software*, *6*(60), 3139. https://doi.org/10.21105/joss.03139

Lv, H., Wang, Z., Tong, E., Williams, L. M., Zaharchuk, G., Zeineh, M., Goldstein-Piekarski, A. N., Ball, T. M., Liao, C., & Wintermark, M. (2018). Resting-State Functional MRI: Everything That Nonexperts Have Always Wanted to Know. *American Journal of Neuroradiology*, ajnr;ajnr.A5527v1. https://doi.org/10.3174/ajnr.A5527

Lv, Y., Margulies, D. S., Cameron Craddock, R., Long, X., Winter, B., Gierhake, D., Endres, M., Villringer, K., Fiebach, J., & Villringer, A. (2013). Identifying the perfusion deficit in acute stroke with resting-state functional magnetic resonance imaging. *Annals of Neurology*, *73*(1), 136–140. https://doi.org/10.1002/ana.23763

Madsen, L. S., Nielsen, R. B., Parbo, P., Ismail, R., Mikkelsen, I. K., Gottrup, H., Østergaard, L., Brooks, D. J., & Eskildsen, S. F. (2022). Capillary function progressively deteriorates in prodromal Alzheimer's disease: A longitudinal MRI perfusion study. *Aging Brain*, *2*, 100035. https://doi.org/10.1016/j.nbas.2022.100035

Malhotra, K., Goyal, N., & Tsivgoulis, G. (2017). Internal Carotid Artery Occlusion: Pathophysiology, Diagnosis, and Management. *Current Atherosclerosis Reports*, *19*(10), 41. https://doi.org/10.1007/s11883-017-0677-7

Mancuso, L., Costa, T., Nani, A., Manuello, J., Liloia, D., Gelmini, G., Panero, M., Duca, S., & Cauda, F. (2019). The homotopic connectivity of the functional brain: A meta-analytic approach. *Scientific Reports*, *9*(1), 3346. https://doi.org/10.1038/s41598-019-40188-3

Manoliu, A., Riedl, V., Zherdin, A., Mühlau, M., Schwerthöffer, D., Scherr, M., Peters, H., Zimmer, C., Förstl, H., Bäuml, J., Wohlschläger, A. M., & Sorg, C. (2014). Aberrant Dependence of Default Mode/Central Executive Network Interactions on Anterior Insular Salience Network Activity in Schizophrenia. *Schizophrenia Bulletin*, *40*(2), 428–437. https://doi.org/10.1093/schbul/sbt037

Mark, C. I., Mazerolle, E. L., & Chen, J. J. (2015). Metabolic and vascular origins of the BOLD effect: Implications for imaging pathology and resting-state brain function: Understanding BOLD in

Disease and Rest. *Journal of Magnetic Resonance Imaging*, *42*(2), 231–246. https://doi.org/10.1002/jmri.24786

Mateo, C., Knutsen, P. M., Tsai, P. S., Shih, A. Y., & Kleinfeld, D. (2017). Entrainment of Arteriole Vasomotor Fluctuations by Neural Activity Is a Basis of Blood-Oxygenation-Level-Dependent "Resting-State" Connectivity. *Neuron*, *96*(4), 936-948.e3. https://doi.org/10.1016/j.neuron.2017.10.012

Merlini, M., Davalos, D., & Akassoglou, K. (2012). In vivo imaging of the neurovascular unit in CNS disease. *IntraVital*, *1*(2), 87–94. https://doi.org/10.4161/intv.22214

Mouridsen, K., Hansen, M. B., Østergaard, L., & Jespersen, S. N. (2014). Reliable estimation of capillary transit time distributions using DSC-MRI. *Journal of Cerebral Blood Flow and Metabolism : Official Journal of the International Society of Cerebral Blood Flow and Metabolism*, *34*(9), 1511–1521. PubMed. https://doi.org/10.1038/jcbfm.2014.111

Mueller, S., Wang, D., Fox, M. D., Yeo, B. T. T., Sepulcre, J., Sabuncu, M. R., Shafee, R., Lu, J., & Liu, H. (2013). Individual Variability in Functional Connectivity Architecture of the Human Brain. *Neuron*, *77*(3), 586–595. https://doi.org/10.1016/j.neuron.2012.12.028

Mulert, C., Leicht, G., Hepp, P., Kirsch, V., Karch, S., Pogarell, O., Reiser, M., Hegerl, U., Jäger, L., Moller, H. J., & McCarley, R. W. (2010). Single-trial coupling of the gamma-band response and the corresponding BOLD signal. *NeuroImage*, *49*(3), 2238–2247. https://doi.org/10.1016/j.neuroimage.2009.10.058

Mundiyanapurath, S., Ringleb, P. A., Diatschuk, S., Hansen, M. B., Mouridsen, K., Østergaard, L., Wick, W., Bendszus, M., & Radbruch, A. (2016). Capillary Transit Time Heterogeneity Is Associated with Modified Rankin Scale Score at Discharge in Patients with Bilateral High Grade Internal Carotid Artery Stenosis. *PLOS ONE*, *11*(6), e0158148. https://doi.org/10.1371/journal.pone.0158148

Murphy, K., & Fox, M. D. (2017). Towards a consensus regarding global signal regression for resting state functional connectivity MRI. *NeuroImage*, *154*, 169–173. https://doi.org/10.1016/j.neuroimage.2016.11.052

Najjar, S., Pahlajani, S., De Sanctis, V., Stern, J. N. H., Najjar, A., & Chong, D. (2017). Neurovascular Unit Dysfunction and Blood–Brain Barrier Hyperpermeability Contribute to Schizophrenia

Neurobiology: A Theoretical Integration of Clinical and Experimental Evidence. *Frontiers in Psychiatry*, *8*, 83. https://doi.org/10.3389/fpsyt.2017.00083

Nakagawa, S., Johnson, P. C. D., & Schielzeth, H. (2017). The coefficient of determination R(2) and intra-class correlation coefficient from generalized linear mixed-effects models revisited and expanded. *Journal of the Royal Society, Interface*, *14*(134). https://doi.org/10.1098/rsif.2017.0213

Nakagawa, S., & Schielzeth, H. (2013). A general and simple method for obtaining R^2 from generalized linear mixed-effects models. *Methods in Ecology and Evolution*, *4*(2), 133–142. https://doi.org/10.1111/j.2041-210x.2012.00261.x

NASCET SC. (1991). North American Symptomatic Carotid Endarterectomy Trial. Methods, patient characteristics, and progress. *Stroke*, *22*(6), 711–720. https://doi.org/10.1161/01.STR.22.6.711

Nielsen, R. B., Parbo, P., Ismail, R., Dalby, R., Tietze, A., Brændgaard, H., Gottrup, H., Brooks, D. J., Østergaard, L., & Eskildsen, S. F. (2020). Impaired perfusion and capillary dysfunction in prodromal Alzheimer's disease. *Alzheimer's & Dementia: Diagnosis, Assessment & Disease Monitoring*, *12*(1). https://doi.org/10.1002/dad2.12032

Nippert, A. R., Biesecker, K. R., & Newman, E. A. (2018). Mechanisms Mediating Functional Hyperemia in the Brain. *The Neuroscientist*, *24*(1), 73–83. https://doi.org/10.1177/1073858417703033

Nir, Y., Fisch, L., Mukamel, R., Gelbard-Sagiv, H., Arieli, A., Fried, I., & Malach, R. (2007). Coupling between Neuronal Firing Rate, Gamma LFP, and BOLD fMRI Is Related to Interneuronal Correlations. *Current Biology*, *17*(15), 1275–1285. https://doi.org/10.1016/j.cub.2007.06.066

Nir, Y., Mukamel, R., Dinstein, I., Privman, E., Harel, M., Fisch, L., Gelbard-Sagiv, H., Kipervasser, S., Andelman, F., Neufeld, M. Y., Kramer, U., Arieli, A., Fried, I., & Malach, R. (2008). Interhemispheric correlations of slow spontaneous neuronal fluctuations revealed in human sensory cortex. *Nature Neuroscience*, *11*(9), 1100–1108. https://doi.org/10.1038/nn.2177

Nishida, S., Aso, T., Takaya, S., Takahashi, Y., Kikuchi, T., Funaki, T., Yoshida, K., Okada, T., Kunieda, T., Togashi, K., Fukuyama, H., & Miyamoto, S. (2019). Resting-state Functional Magnetic Resonance Imaging Identifies Cerebrovascular Reactivity Impairment in Patients With Arterial Occlusive Diseases: A Pilot Study. *Neurosurgery*, *85*(5), 680–688. https://doi.org/10.1093/neuros/nyy434

Noordmans, H. J., van Blooijs, D., Siero, J. C. W., Zwanenburg, J. J. M., Klaessens, J. H. G. M., & Ramsey, N. F. (2018). Detailed view on slow sinusoidal, hemodynamic oscillations on the human brain cortex by F ourier transforming oxy/deoxy hyperspectral images. *Human Brain Mapping*, *39*(9), 3558–3573. https://doi.org/10.1002/hbm.24194

Nuttall, R., Pasquini, L., Scherr, M., Sorg, C., & Alzheimer's Disease Neuroimaging Initiative. (2016). Degradation in intrinsic connectivity networks across the Alzheimer's disease spectrum. *Alzheimer's & Dementia: Diagnosis, Assessment & Disease Monitoring*, *5*(1), 35–42. https://doi.org/10.1016/j.dadm.2016.11.006

Obata, T., Liu, T. T., Miller, K. L., Luh, W.-M., Wong, E. C., Frank, L. R., & Buxton, R. B. (2004). Discrepancies between BOLD and flow dynamics in primary and supplementary motor areas: Application of the balloon model to the interpretation of BOLD transients. *NeuroImage*, *21*(1), 144–153. https://doi.org/10.1016/j.neuroimage.2003.08.040

Ogawa, S., Lee, T. M., Kay, A. R., & Tank, D. W. (1990). Brain magnetic resonance imaging with contrast dependent on blood oxygenation. *Proceedings of the National Academy of Sciences*, *87*(24), 9868–9872. https://doi.org/10.1073/pnas.87.24.9868

Ogawa, S., & Lee, T.-M. (1990). Magnetic resonance imaging of blood vessels at high fields:In vivo andin vitro measurements and image simulation. *Magnetic Resonance in Medicine*, *16*(1), 9–18. https://doi.org/10.1002/mrm.1910160103

Ogawa, S., Lee, T.-M., Nayak, A. S., & Glynn, P. (1990). Oxygenation-sensitive contrast in magnetic resonance image of rodent brain at high magnetic fields. *Magnetic Resonance in Medicine*, *14*(1), 68–78. https://doi.org/10.1002/mrm.1910140108

Ogawa, S., Tank, D. W., Menon, R., Ellermann, J. M., Kim, S. G., Merkle, H., & Ugurbil, K. (1992). Intrinsic signal changes accompanying sensory stimulation: Functional brain mapping with

magnetic resonance imaging. *Proceedings of the National Academy of Sciences*, *89*(13), 5951–5955. https://doi.org/10.1073/pnas.89.13.5951

Østergaard, L. (2020). Blood flow, capillary transit times, and tissue oxygenation: The centennial of capillary recruitment. *Journal of Applied Physiology*, *129*(6), 1413–1421. https://doi.org/10.1152/japplphysiol.00537.2020

Østergaard, L., Aamand, R., Gutiérrez-Jiménez, E., Ho, Y.-C. L., Blicher, J. U., Madsen, S. M., Nagenthiraja, K., Dalby, R. B., Drasbek, K. R., Møller, A., Brændgaard, H., Mouridsen, K., Jespersen, S. N., Jensen, M. S., & West, M. J. (2013). The capillary dysfunction hypothesis of Alzheimer's disease. *Neurobiology of Aging*, *34*(4), 1018–1031. https://doi.org/10.1016/j.neurobiolaging.2012.09.011

Østergaard, L., Chesler, D. A., Weisskoff, R. M., Sorensen, A. G., & Rosen, B. R. (1999). Modeling Cerebral Blood Flow and Flow Heterogeneity from Magnetic Resonance Residue Data. *Journal of Cerebral Blood Flow & Metabolism*, *19*(6), 690–699. https://doi.org/10.1097/00004647-199906000-00013

Østergaard, L., Engedal, T. S., Moreton, F., Hansen, M. B., Wardlaw, J. M., Dalkara, T., Markus, H. S., & Muir, K. W. (2016). Cerebral small vessel disease: Capillary pathways to stroke and cognitive decline. *Journal of Cerebral Blood Flow and Metabolism : Official Journal of the International Society of Cerebral Blood Flow and Metabolism*, *36*(2), 302–325. https://doi.org/10.1177/0271678X15606723

Østergaard, L., Jespersen, S. N., Mouridsen, K., Mikkelsen, I. K., Jonsdottír, K. Ý., Tietze, A., Blicher, J. U., Aamand, R., Hjort, N., Iversen, N. K., Cai, C., Hougaard, K. D., Simonsen, C. Z., Von Weitzel-Mudersbach, P., Modrau, B., Nagenthiraja, K., Riisgaard Ribe, L., Hansen, M. B., Bekke, S. L., … Andersen, G. (2013). The role of the cerebral capillaries in acute ischemic stroke: The extended penumbra model. *Journal of Cerebral Blood Flow and Metabolism : Official Journal of the International Society of Cerebral Blood Flow and Metabolism*, *33*(5), 635–648. https://doi.org/10.1038/jcbfm.2013.18

Østergaard, L., Weisskoff, R. M., Chesler, D. A., Gyldensted, C., & Rosen, B. R. (1996). High resolution measurement of cerebral blood flow using intravascular tracer bolus passages.

Part I: Mathematical approach and statistical analysis. *Magnetic Resonance in Medicine*, *36*(5), 715–725. https://doi.org/10.1002/mrm.1910360510

Özbay, P. S., Chang, C., Picchioni, D., Mandelkow, H., Moehlman, T. M., Chappel-Farley, M. G., van Gelderen, P., de Zwart, J. A., & Duyn, J. H. (2018). Contribution of systemic vascular effects to fMRI activity in white matter. *NeuroImage*, *176*, 541–549. https://doi.org/10.1016/j.neuroimage.2018.04.045

Petcharunpaisan, S. (2010). Arterial spin labeling in neuroimaging. *World Journal of Radiology*, *2*(10), 384. https://doi.org/10.4329/wjr.v2.i10.384

Pfannmöller, J., & Lotze, M. (2019). Review on biomarkers in the resting-state networks of chronic pain patients. *Brain and Cognition*, *131*, 4–9. https://doi.org/10.1016/j.bandc.2018.06.005

Potreck, A., Loebel, S., Pfaff, J., Østergaard, L., Mouridsen, K., Radbruch, A., Bendszus, M., & Mundiyanapurath, S. (2019). Increased volumes of mildly elevated capillary transit time heterogeneity positively predict favorable outcome and negatively predict intracranial hemorrhage in acute ischemic stroke with large vessel occlusion. *European Radiology*, *29*(7), 3523–3532. https://doi.org/10.1007/s00330-019-06064-4

Power, J. D., Barnes, K. A., Snyder, A. Z., Schlaggar, B. L., & Petersen, S. E. (2012). Spurious but systematic correlations in functional connectivity MRI networks arise from subject motion. *NeuroImage*, *59*(3), 2142–2154. https://doi.org/10.1016/j.neuroimage.2011.10.018

Power, J. D., Schlaggar, B. L., & Petersen, S. E. (2014). Studying Brain Organization via Spontaneous fMRI Signal. *Neuron*, *84*(4), 681–696. https://doi.org/10.1016/j.neuron.2014.09.007

Powers, W. J. (1987). The Effect of Hemodynamically Significant Carotid Artery Disease on the Hemodynamic Status of the Cerebral Circulation. *Annals of Internal Medicine*, *106*(1), 27. https://doi.org/10.7326/0003-4819-106-1-27

Powers, W. J., Fox, P. T., & Raichle, M. E. (1988). The effect of carotid artery disease on the cerebrovascular response to physiologic stimulation. *Neurology*, *38*(9), 1475–1475. https://doi.org/10.1212/WNL.38.9.1475

Preibisch, C., Castrillón G., J. G., Bührer, M., & Riedl, V. (2015). Evaluation of Multiband EPI Acquisitions for Resting State fMRI. *PLOS ONE*, *10*(9), e0136961. https://doi.org/10.1371/journal.pone.0136961

Preibisch, C., Sorg, C., Förschler, A., Grimmer, T., Sax, I., Wohlschläger, A. M., Perneczky, R., Förstl, H., Kurz, A., Zimmer, C., & Alexopoulos, P. (2011). Age-related cerebral perfusion changes in the parietal and temporal lobes measured by pulsed arterial spin labeling. *Journal of Magnetic Resonance Imaging*, *34*(6), 1295–1302. https://doi.org/10.1002/jmri.22788

Qiu, M., Scheinost, D., Ramani, R., & Constable, R. T. (2017). Multi-modal analysis of functional connectivity and cerebral blood flow reveals shared and unique effects of propofol in large-scale brain networks. *NeuroImage*, *148*, 130–140. https://doi.org/10.1016/j.neuroimage.2016.12.080

R Core Team. (2020). *R: A Language and Environment for Statistical Computing*. R Foundation for Statistical Computing. https://www.R-project.org/

Ragland, J. D., Yoon, J., Minzenberg, M. J., & Carter, C. S. (2007). Neuroimaging of cognitive disability in schizophrenia: Search for a pathophysiological mechanism. *International Review of Psychiatry*, *19*(4), 417–427. https://doi.org/10.1080/09540260701486365

Raichle, M. E., MacLeod, A. M., Snyder, A. Z., Powers, W. J., Gusnard, D. A., & Shulman, G. L. (2001). A default mode of brain function. *Proceedings of the National Academy of Sciences*, *98*(2), 676–682. https://doi.org/10.1073/pnas.98.2.676

Rajagopalan, P., Krishnan, K. R., Passe, T. J., & Macfall, J. R. (1995). Magnetic resonance imaging using deoxyhemoglobin contrast versus positron emission tomography in the assessment of brain function. *Progress in Neuro-Psychopharmacology & Biological Psychiatry*, *19*(3), 351–366. https://doi.org/10.1016/0278-5846(95)00017-p

Rasmussen, P. M., Jespersen, S. N., & Østergaard, L. (2015). The Effects of Transit Time Heterogeneity on Brain Oxygenation during Rest and Functional Activation. *Journal of Cerebral Blood Flow & Metabolism*, *35*(3), 432–442. https://doi.org/10.1038/jcbfm.2014.213

Rayshubskiy, A., Wojtasiewicz, T. J., Mikell, C. B., Bouchard, M. B., Timerman, D., Youngerman, B. E., McGovern, R. A., Otten, M. L., Canoll, P., McKhann, G. M., & Hillman, E. M. C. (2014). Direct, intraoperative observation of ~0.1Hz hemodynamic oscillations in awake human cortex: Implications for fMRI. *NeuroImage*, *87*, 323–331. https://doi.org/10.1016/j.neuroimage.2013.10.044

Reimann, H. M., Todiras, M., Hodge, R., Huelnhagen, T., Millward, J. M., Turner, R., Seeliger, E., Bader, M., Pohlmann, A., & Niendorf, T. (2018). Somatosensory BOLD fMRI reveals close link between salient blood pressure changes and the murine neuromatrix. *NeuroImage*, *172*, 562–574. https://doi.org/10.1016/j.neuroimage.2018.02.002

Richter, V., Helle, M., van Osch, M. J. P., Lindner, T., Gersing, A. S., Tsantilas, P., Eckstein, H.-H., Preibisch, C., & Zimmer, C. (2017). MR Imaging of Individual Perfusion Reorganization Using Superselective Pseudocontinuous Arterial Spin-Labeling in Patients with Complex Extracranial Steno-Occlusive Disease. *AJNR. American Journal of Neuroradiology*, *38*(4), 703–711. https://doi.org/10.3174/ajnr.A5090

Risk, B. B., Murden, R. J., Wu, J., Nebel, M. B., Venkataraman, A., Zhang, Z., & Qiu, D. (2021). Which multiband factor should you choose for your resting-state fMRI study? *NeuroImage*, *234*, 117965. https://doi.org/10.1016/j.neuroimage.2021.117965

RStudio Team. (2019). *RStudio: Integrated Development Environment for R* [Computer software]. RStudio, Inc. http://www.rstudio.com/

Schneider, S. C., Archila-Meléndez, M. E., Göttler, J., Kaczmarz, S., Zott, B., Priller, J., Kallmayer, M., Zimmer, C., Sorg, C., & Preibisch, C. (2022). Resting-state BOLD functional connectivity depends on the heterogeneity of capillary transit times in the human brain A combined lesion and simulation study about the influence of blood flow response timing. *NeuroImage*, *255*, 119208. https://doi.org/10.1016/j.neuroimage.2022.119208

Schneider, S. C., Kaczmarz, S., Göttler, J., Kufer, J., Zott, B., Priller, J., Kallmayer, M., Zimmer, C., Sorg, C., & Preibisch, C. (2023). Stronger influence of systemic than local hemodynamic-vascular factors on resting-state BOLD functional connectivity. *NeuroImage*, *281*, 120380. https://doi.org/10.1016/j.neuroimage.2023.120380

Schölvinck, M. L., Leopold, D. A., Brookes, M. J., & Khader, P. H. (2013). The contribution of electrophysiology to functional connectivity mapping. *NeuroImage*, *80*, 297–306. https://doi.org/10.1016/j.neuroimage.2013.04.010

Schölvinck, M. L., Maier, A., Ye, F. Q., Duyn, J. H., & Leopold, D. A. (2010). Neural basis of global resting-state fMRI activity. *Proceedings of the National Academy of Sciences*, *107*(22), 10238–10243. https://doi.org/10.1073/pnas.0913110107

Schroeder, T. (1988). Hemodynamic significance of internal carotid artery disease. *Acta Neurologica Scandinavica*, *77*(5), 353–372. https://doi.org/10.1111/j.1600-0404.1988.tb05921.x

Schulte, M. L., Wood, J. D., & Hudetz, A. G. (2003). Cortical electrical stimulation alters erythrocyte perfusion pattern in the cerebral capillary network of the rat. *Brain Research*, *963*(1), 81–92. https://doi.org/10.1016/S0006-8993(02)03848-9

Shalev, H., Serlin, Y., & Friedman, A. (2009). Breaching the Blood-Brain Barrier as a Gate to Psychiatric Disorder. *Cardiovascular Psychiatry and Neurology*, *2009*, 1–7. https://doi.org/10.1155/2009/278531

Siegel, J. S., Power, J. D., Dubis, J. W., Vogel, A. C., Church, J. A., Schlaggar, B. L., & Petersen, S. E. (2014). Statistical improvements in functional magnetic resonance imaging analyses produced by censoring high-motion data points: Censoring High Motion Data in fMRI. *Human Brain Mapping*, *35*(5), 1981–1996. https://doi.org/10.1002/hbm.22307

Siegel, J. S., Snyder, A. Z., Ramsey, L., Shulman, G. L., & Corbetta, M. (2016). The effects of hemodynamic lag on functional connectivity and behavior after stroke. *Journal of Cerebral Blood Flow & Metabolism*, *36*(12), 2162–2176. https://doi.org/10.1177/0271678X15614846

Siero, J. C. W., Hartkamp, N. S., Donahue, M. J., Harteveld, A. A., Compter, A., Petersen, E. T., & Hendrikse, J. (2015). Neuronal activation induced BOLD and CBF responses upon acetazolamide administration in patients with steno-occlusive artery disease. *NeuroImage*, *105*, 276–285. https://doi.org/10.1016/j.neuroimage.2014.09.033

Simon, A. B., & Buxton, R. B. (2015). Understanding the dynamic relationship between cerebral blood flow and the BOLD signal: Implications for quantitative functional MRI. *NeuroImage*, *116*, 158–167. https://doi.org/10.1016/j.neuroimage.2015.03.080

Son, S. J., Kim, J., Lee, E., Park, J. Y., Namkoong, K., Hong, C. H., Ku, J., Kim, E., & Oh, B. H. (2015). Effect of hypertension on the resting-state functional connectivity in patients with Alzheimer's disease (AD). *Archives of Gerontology and Geriatrics*, *60*(1), 210–216. https://doi.org/10.1016/j.archger.2014.09.012

Sorg, C., Riedl, V., Mühlau, M., Calhoun, V. D., Eichele, T., Läer, L., Drzezga, A., Förstl, H., Kurz, A., Zimmer, C., & Wohlschläger, A. M. (2007). Selective changes of resting-state networks in individuals at risk for Alzheimer's disease. *Proceedings of the National Academy of Sciences*, *104*(47), 18760–18765. https://doi.org/10.1073/pnas.0708803104

Soto-Rojas, L. O., Pacheco-Herrero, M., Martínez-Gómez, P. A., Campa-Córdoba, B. B., Apátiga-Pérez, R., Villegas-Rojas, M. M., Harrington, C. R., de la Cruz, F., Garcés-Ramírez, L., & Luna-Muñoz, J. (2021). The Neurovascular Unit Dysfunction in Alzheimer's Disease. *International Journal of Molecular Sciences*, *22*(4), 2022. https://doi.org/10.3390/ijms22042022

Stark, D. E., Margulies, D. S., Shehzad, Z. E., Reiss, P., Kelly, A. M. C., Uddin, L. Q., Gee, D. G., Roy, A. K., Banich, M. T., Castellanos, F. X., & Milham, M. P. (2008). Regional Variation in Interhemispheric Coordination of Intrinsic Hemodynamic Fluctuations. *Journal of Neuroscience*, *28*(51), 13754–13764. https://doi.org/10.1523/JNEUROSCI.4544-08.2008

Stefanovic, B., Hutchinson, E., Yakovleva, V., Schram, V., Russell, J. T., Belluscio, L., Koretsky, A. P., & Silva, A. C. (2008). Functional Reactivity of Cerebral Capillaries. *Journal of Cerebral Blood Flow & Metabolism*, *28*(5), 961–972. https://doi.org/10.1038/sj.jcbfm.9600590

Tanrıtanır, A. C., Villringer, K., Galinovic, I., Grittner, U., Kirilina, E., Fiebach, J. B., Villringer, A., & Khalil, A. A. (2020). The Effect of Scan Length on the Assessment of BOLD Delay in Ischemic Stroke. *Frontiers in Neurology*, *11*, 381. https://doi.org/10.3389/fneur.2020.00381

Tessitore, A., Cirillo, M., & De Micco, R. (2019). Functional Connectivity Signatures of Parkinson's Disease. *Journal of Parkinson's Disease*, *9*(4), 637–652. https://doi.org/10.3233/JPD-191592

Thomas Yeo, B. T., Krienen, F. M., Sepulcre, J., Sabuncu, M. R., Lashkari, D., Hollinshead, M., Roffman, J. L., Smoller, J. W., Zöllei, L., Polimeni, J. R., Fischl, B., Liu, H., & Buckner, R. L. (2011). The organization of the human cerebral cortex estimated by intrinsic functional connectivity. *Journal of Neurophysiology*, *106*(3), 1125–1165. https://doi.org/10.1152/jn.00338.2011

Tong, Y., Bergethon, P. R., & Frederick, B. deB. (2011). An improved method for mapping cerebrovascular reserve using concurrent fMRI and near-infrared spectroscopy with Regressor Interpolation at Progressive Time Delays (RIPTiDe). *NeuroImage*, *56*(4), 2047–2057. https://doi.org/10.1016/j.neuroimage.2011.03.071

Tong, Y., & Frederick, B. deB. (2014). Tracking cerebral blood flow in BOLD fMRI using recursively generated regressors: Tracking Cerebral Blood Flow in BOLD fMRI. *Human Brain Mapping*, *35*(11), 5471–5485. https://doi.org/10.1002/hbm.22564

Tong, Y., Hocke, L. M., Fan, X., Janes, A. C., & Frederick, B. deB. (2015). Can apparent resting state connectivity arise from systemic fluctuations? *Frontiers in Human Neuroscience*, *9*. https://doi.org/10.3389/fnhum.2015.00285

Tong, Y., Hocke, L. M., & Frederick, B. B. (2019). Low Frequency Systemic Hemodynamic "Noise" in Resting State BOLD fMRI: Characteristics, Causes, Implications, Mitigation Strategies, and Applications. *Frontiers in Neuroscience*, *13*, 787. https://doi.org/10.3389/fnins.2019.00787

Tong, Y., Hocke, L. M., Licata, S. C., & Frederick, B. d. (2012). Low-frequency oscillations measured in the periphery with near-infrared spectroscopy are strongly correlated with blood oxygen level-dependent functional magnetic resonance imaging signals. *Journal of Biomedical Optics*, *17*(10), 1. https://doi.org/10.1117/1.JBO.17.10.106004

Tong, Y., Lindsey, K. P., Hocke, L. M., Vitaliano, G., Mintzopoulos, D., & Frederick, B. deB. (2017). Perfusion information extracted from resting state functional magnetic resonance imaging. *Journal of Cerebral Blood Flow & Metabolism*, *37*(2), 564–576. https://doi.org/10.1177/0271678X16631755

Tong, Y., Yao, J. (Fiona), Chen, J. J., & Frederick, B. B. (2019). The resting-state fMRI arterial signal predicts differential blood transit time through the brain. *Journal of Cerebral Blood Flow & Metabolism*, *39*(6), 1148–1160. https://doi.org/10.1177/0271678X17753329

Tsvetanov, K. A., Henson, R. N. A., & Rowe, J. B. (2021). Separating vascular and neuronal effects of age on fMRI BOLD signals. *Philosophical Transactions of the Royal Society B: Biological Sciences*, *376*(1815), 20190631. https://doi.org/10.1098/rstb.2019.0631

Turchi, J., Chang, C., Ye, F. Q., Russ, B. E., Yu, D. K., Cortes, C. R., Monosov, I. E., Duyn, J. H., & Leopold, D. A. (2018). The Basal Forebrain Regulates Global Resting-State fMRI Fluctuations. *Neuron*, *97*(4), 940-952.e4. https://doi.org/10.1016/j.neuron.2018.01.032

Uludag, K., Ugurbil, K., & Berliner, L. (Eds.). (2015). *fMRI: From Nuclear Spins to Brain Functions* (Vol. 30). Springer US. https://doi.org/10.1007/978-1-4899-7591-1

Van Den Heuvel, M. P., Mandl, R. C. W., Kahn, R. S., & Hulshoff Pol, H. E. (2009). Functionally linked resting-state networks reflect the underlying structural connectivity architecture of the human brain. *Human Brain Mapping*, *30*(10), 3127–3141. https://doi.org/10.1002/hbm.20737

van Niftrik, C. H. B., Piccirelli, M., Muscas, G., Sebök, M., Fisher, J. A., Bozinov, O., Stippich, C., Valavanis, A., Regli, L., & Fierstra, J. (2019). The voxel-wise analysis of false negative fMRI activation in regions of provoked impaired cerebrovascular reactivity. *PLOS ONE*, *14*(5), e0215294. https://doi.org/10.1371/journal.pone.0215294

VanGilder, R. L., Rosen, C. L., Barr, T. L., & Huber, J. D. (2011). Targeting the neurovascular unit for treatment of neurological disorders. *Pharmacology & Therapeutics*, *130*(3), 239–247. https://doi.org/10.1016/j.pharmthera.2010.12.004

Varangis, E., Habeck, C. G., Razlighi, Q. R., & Stern, Y. (2019). The Effect of Aging on Resting State Connectivity of Predefined Networks in the Brain. *Frontiers in Aging Neuroscience*, *11*, 234. https://doi.org/10.3389/fnagi.2019.00234

Vincent, J. L., Patel, G. H., Fox, M. D., Snyder, A. Z., Baker, J. T., Van Essen, D. C., Zempel, J. M., Snyder, L. H., Corbetta, M., & Raichle, M. E. (2007). Intrinsic functional architecture in the anaesthetized monkey brain. *Nature*, *447*(7140), 83–86. https://doi.org/10.1038/nature05758

Viticchi, G., Falsetti, L., Potente, E., Bartolini, M., & Silvestrini, M. (2021). Impact of carotid stenosis on cerebral hemodynamic failure and cognitive impairment progression: A narrative review. *Annals of Translational Medicine*, *9*(14), 1209–1209. https://doi.org/10.21037/atm-20-7226

Wang, L., Xiong, X., Zhang, L., & Shen, J. (2021). Neurovascular Unit: A critical role in ischemic stroke. *CNS Neuroscience & Therapeutics*, *27*(1), 7–16. https://doi.org/10.1111/cns.13561

Wang, T., Xiao, F., Wu, G., Fang, J., Sun, Z., Feng, H., Zhang, J., & Xu, H. (2017). Impairments in Brain Perfusion, Metabolites, Functional Connectivity, and Cognition in Severe Asymptomatic Carotid Stenosis Patients: An Integrated MRI Study. *Neural Plasticity*, *2017*, 1–7. https://doi.org/10.1155/2017/8738714

Wanger, T. J., Janes, A. C., & Frederick, B. B. (2022). Spatial variation of changes in test–retest reliability of functional connectivity after global signal regression: The effect of considering

hemodynamic delay. *Human Brain Mapping*, hbm.26091. https://doi.org/10.1002/hbm.26091

Ward, P. G. D., Orchard, E. R., Oldham, S., Arnatkevičiūtė, A., Sforazzini, F., Fornito, A., Storey, E., Egan, G. F., & Jamadar, S. D. (2020). Individual differences in haemoglobin concentration influence bold fMRI functional connectivity and its correlation with cognition. *NeuroImage*, *221*, 117196. https://doi.org/10.1016/j.neuroimage.2020.117196

Weissenbacher, A., Kasess, C., Gerstl, F., Lanzenberger, R., Moser, E., & Windischberger, C. (2009). Correlations and anticorrelations in resting-state functional connectivity MRI: A quantitative comparison of preprocessing strategies. *NeuroImage*, *47*(4), 1408–1416. https://doi.org/10.1016/j.neuroimage.2009.05.005

West, K. L., Zuppichini, M. D., Turner, M. P., Sivakolundu, D. K., Zhao, Y., Abdelkarim, D., Spence, J. S., & Rypma, B. (2019). BOLD hemodynamic response function changes significantly with healthy aging. *NeuroImage*, *188*, 198–207. https://doi.org/10.1016/j.neuroimage.2018.12.012

Wilcox, C. E., Abbott, C. C., & Calhoun, V. D. (2019). Alterations in resting-state functional connectivity in substance use disorders and treatment implications. *Progress in Neuro-Psychopharmacology and Biological Psychiatry*, *91*, 79–93. https://doi.org/10.1016/j.pnpbp.2018.06.011

Winder, A. T., Echagarruga, C., Zhang, Q., & Drew, P. J. (2017). Weak correlations between hemodynamic signals and ongoing neural activity during the resting state. *Nature Neuroscience*, *20*(12), 1761–1769. https://doi.org/10.1038/s41593-017-0007-y

Wouters, A., Christensen, S., Straka, M., Mlynash, M., Liggins, J., Bammer, R., Thijs, V., Lemmens, R., Albers, G. W., & Lansberg, M. G. (2017). A Comparison of Relative Time to Peak and Tmax for Mismatch-Based Patient Selection. *Frontiers in Neurology*, *8*, 539. https://doi.org/10.3389/fneur.2017.00539

Yan, C.G. & Zang, Y.F. (2010). DPARSF: A MATLAB toolbox for “pipeline” data analysis of resting-state fMRI. *Frontiers in System Neuroscience*. https://doi.org/10.3389/fnsys.2010.00013

Yao, J. (Fiona), Wang, J. H., Yang, H. (Shawn), Liang, Z., Cohen-Gadol, A. A., Rayz, V. L., & Tong, Y. (2019). Cerebral circulation time derived from fMRI signals in large blood vessels. *Journal of Magnetic Resonance Imaging*, *50*(5), 1504–1513. https://doi.org/10.1002/jmri.26765

Yoshikawa, A., Masaoka, Y., Yoshida, M., Koiwa, N., Honma, M., Watanabe, K., Kubota, S., Natsuko, I., Ida, M., & Izumizaki, M. (2020). Heart Rate and Respiration Affect the Functional Connectivity of Default Mode Network in Resting-State Functional Magnetic Resonance Imaging. *Frontiers in Neuroscience*, *14*, 631. https://doi.org/10.3389/fnins.2020.00631

Yu, X., Ji, C., & Shao, A. (2020). Neurovascular Unit Dysfunction and Neurodegenerative Disorders. *Frontiers in Neuroscience*, *14*, 334. https://doi.org/10.3389/fnins.2020.00334

Zhou, J., Greicius, M. D., Gennatas, E. D., Growdon, M. E., Jang, J. Y., Rabinovici, G. D., Kramer, J. H., Weiner, M., Miller, B. L., & Seeley, W. W. (2010). Divergent network connectivity changes in behavioural variant frontotemporal dementia and Alzheimer's disease. *Brain*, *133*(5), 1352–1367. https://doi.org/10.1093/brain/awq075

Zhou, J., & Seeley, W. W. (2014). Network Dysfunction in Alzheimer's Disease and Frontotemporal Dementia: Implications for Psychiatry. *Biological Psychiatry*, *75*(7), 565–573. https://doi.org/10.1016/j.biopsych.2014.01.020

Zlokovic, B. V. (2011). Neurovascular pathways to neurodegeneration in Alzheimer's disease and other disorders. *Nature Reviews Neuroscience*, *12*(12), 723–738. https://doi.org/10.1038/nrn3114

Zou, X., Yuan, Y., Liao, Y., Jiang, C., Zhao, F., Ding, D., Gu, Y., Chen, L., Chu, Y., Hsu, Y., Liebig, P. A., Xu, B., & Mao, Y. (2022). Moyamoya disease: A human model for chronic hypoperfusion and intervention in Alzheimer's disease. *Alzheimer's & Dementia: Translational Research & Clinical Interventions*, *8*(1). https://doi.org/10.1002/trc2.12285

Zuo, X.-N., Kelly, C., Di Martino, A., Mennes, M., Margulies, D. S., Bangaru, S., Grzadzinski, R., Evans, A. C., Zang, Y.-F., Castellanos, F. X., & Milham, M. P. (2010). Growing Together and Growing Apart: Regional and Sex Differences in the Lifespan Developmental Trajectories of Functional Homotopy. *The Journal of Neuroscience*, *30*(45), 15034–15043. https://doi.org/10.1523/JNEUROSCI.2612-10.2010

List of publications

- **Schneider, S. C.**, Archila-Meléndez, M. E., Göttler, J., Kaczmarz, S., Zott, B., Priller, J., Kallmayer, M., Zimmer, C., Sorg, C., & Preibisch, C. (2022). Resting-state BOLD functional connectivity depends on the heterogeneity of capillary transit times in the human brain. A combined lesion and simulation study about the influence of blood flow response timing. *NeuroImage*, *255*, 119208. https://doi.org/10.1016/j.neuroimage.2022.119208
- **Schneider, S. C.,** Kaczmarz, S., Göttler, J., Kufer, J., Zott, B., Priller, J., Kallmayer, M., Zimmer, C., Sorg, C., & Preibisch, C. (2023). Stronger influence of systemic than local hemodynamic-vascular factors on resting-state BOLD functional connectivity. *NeuroImage*, *281*, 120380. https://doi.org/10.1016/j.neuroimage.2023.120380

List of presentations

- **Schneider, Sebastian,** Archila-Meléndez, Mario, Göttler, Jens, Kaczmarz, Stephan, Kufer, Jan, Zott, Benedikt, Priller, Josef, Kallmayer, Michael, Zimmer, Claus, Sorg, Christian, & Preibisch, Christine. (2022, May 12). Impact of capillary transit time heterogeneity on resting-state BOLD-FC in patients with unilateral asymptomatic carotid artery stenosis. *Proceedings of the Joint Annual Meeting ISMRM-ESMRMB 2022 & ISMRT Annual Meeting*. Joint Annual Meeting ISMRM-ESMRMB & ISMRT 31st Annual Meeting, London, UK.